The study of a past interglacial vegetation change as a tool to understand the human role in hydrological changes

Pablo Vera Polo

PhD in Earth Sciences
Curriculum: Geosciences
XXXVII Cycle
International Joint PhD with University of Granada

Tutors:
Laura Sadori
Gonzalo Jiménez Moreno

Programa Doctorado
Ciencias de la Tierra

PhD in Earth Sciences

Curriculum: Geosciences

XXVII Cycle

The study of a past interglacial vegetation change as a tool to understand the human role in hydrological changes

Pablo Vera Polo

PhD Thesis 2025

Tutors:

Laura Sadori

Gonzalo Jiménez Moreno

Programa Doctorado
Ciencias de la Tierra

Editor: Universidad de Granada. Tesis Doctorales
Autor: Pablo Vera Polo
ISBN: 978-84-1195-781-6
URI: https://hdl.handle.net/10481/103608

La borsa di dottorato è stata cofinanziata con risorse del
Programma Operativo Nazionale Ricerca e Innovazione 2014-2020, risorse FSE REACT-EU
Azione IV.4 “Dottorati e contratti di ricerca su tematiche dell’innovazione”
e Azione IV.5 “Dottorati su tematiche Green”

The study of a Past interglacial vegetation change as a tool to understand the human role in hydrological changes

PhD thesis. Sapienza University of Rome & University of Granada

Author's email: pablo.verapolo@uniroma1.it

UNIVERSIDAD
DE GRANADA

Escuela
Internacional
de Posgrado

ACEPTACION Y RENUNCIA DE LOS COAUTORES DE LA PUBLICACION

Publicación/artículo: Climate, vegetation, and environmental change during the MIS 12-MIS 11 glacial-interglacial transition inferred from a high-resolution pollen record from the Fucino Basin of central Italy (doi.org/10.1016/j.palaeo.2024.112486)

Los coautores:

D.	Pablo Vera-Polo
Dª.	Laura Sadori
D.	Gonzalo Jiménez-Moreno
Dª.	Alessia Masi
D.	Biagio Giaccio
D.	Giovanni Zanchetta
D.	P. Chronis Tzedakis
D.	Bernd Wagner

declaran que:

ACEPTAN y AUTORIZAN la utilización de dicha publicación/artículo como parte de la documentación de depósito y defensa de la tesis doctoral de D. Pablo Vera Polo titulada The study of a past interglacial vegetation change as a tool to understand the human role in hydrological changes,

Abstract (ENG)

Examining sedimentary records from previous interglacial periods provides valuable insights into past climate variability and ecosystem responses to warmer conditions. This research addresses important gaps in our understanding of the global water cycle and ecological adaptations of vegetation to past climate changes that could be directly compared to changes during current global warming.

This PhD thesis analysed pollen samples from the carbonated sediments from Fucino Basin in the Central Apennines, which is an ideal location to study vegetation dynamics within a mountainous and Mediterranean climate during the interglacial period corresponding to Marine Isotope Stage (MIS) 11 (ca. 424-367 ka). The first stage of MIS 11 interglacial complex (MIS 11c; ca. 426–396 ka) is particularly interesting due to the fact that it represents one of the longest and warmest interglacial phases within the last 800 ka, with approximate mean global temperatures 0.5–0.7°C higher and sea level around 6–13 meters above pre-industrial Holocene ones, respectively. In absence of anthropogenic influences, MIS 11c, being an orbital analogue of the late Holocene (MIS 1), facilitates the examination of ecosystem responses to naturally warmer climates. High-resolution palynological analyses conducted on Fucino Basin sediments reveal millennial-scale climatic oscillations spanning from 430 ka to 388 ka, including the latter phase of MIS 12 glacial period, the Glacial Termination V (T-V), and most of MIS 11. The Fucino F4-F5 composite record provides one of the few independent radiometrically constrained chronologies for MIS 11, allowing direct comparisons to other regional and global climatic and palynological datasets.

The T-V was one of the most pronounced climatic transitions of the Pleistocene, forming part of the major climatic reorganisation known as the Mid-Brunhes Event (MBE). This event, recorded at 424.5 ± 4.0 ka in Fucino, reflects a substantial shift from a cold, arid phase, with a dominance of herbaceous and xerophytic taxa including Poaceae, *Artemisia*, Amaranthaceae, *Ephedra*, and *Hippophäe* and siliciclastic-dominated sedimentation, to a warm, humid phase marked by increased *Abies* and a deciduous arboreal assemblage including *Quercus*, *Carpinus*, *Corylus*, and *Ulmus*, and dominated by a calcareous sedimentation, more organic than in the glacial. The warm and humid conditions recorded throughout MIS 11c in Fucino are consistent with climate reconstructions from other lakes in the Mediterranean region, such as Lake Ohrid and Ioannina, where similarly humid conditions are recorded. Notably, *Abies* dominated the surrounding vegetation in the Fucino Basin, evidencing high regional humidity.

The Fucino Basin pollen record reveals the sensitivity of mesothermic and altitudinal taxa to insolation fluctuations. A significant arid event occurred between 415 ka and 413 ka, dividing the two precessional cycles that formed the MIS 11c interglacial. This event, described in the palynological record for the first time, may correspond to a global climate signal, as it aligns with lower sea surface temperatures and drier conditions in other records from marine context.

This study also calculated pollen-based quantitative paleoclimatic reconstructions using weighted averaging partial least squares (WA-PLS) regression. These reconstructions allow for direct comparisons with current

climate parameters, elucidating the impact of natural climatic oscillations on vegetation dynamics during MIS 11c. The results show that vegetation dynamics in the Fucino Basin was highly influenced by insolation-driven climate variability, which contributes to a better understanding of past climate dynamics and vegetation responses.

This PhD thesis provides both qualitative and quantitative data that are important for contextualising current anthropogenic impacts on ecosystems by contrasting them with natural climatic and ecological trends observed in the orbital interglacial analogue MIS 11c. These findings highlight the relevance of paleoclimatic studies in improving our understanding of natural climate variability and its implications for future climate responses.

Abstract (IT)

Lo studio de gli archivi documenti sedimentari dei periodi interglaciali passati fornisce importanti indicazioni sulla variabilità climatica del passato e sulle possibili risposte degli ecosistemi a condizioni più calde. Questa ricerca affronta importanti lacune nella comprensione del ciclo globale dell'acqua e degli adattamenti ecologici della vegetazione ai cambiamenti climatici del passato, che potrebbero essere direttamente confrontati con i cambiamenti durante l'attuale riscaldamento globale.

Questa tesi di dottorato ha analizzato campioni di pollini provenienti da sedimenti carbonatici del bacino del Fucino nell'Appennino centrale, un sito ideale per la definizione delle dinamiche della vegetazione in un ambiente montuoso mediterraneo durante il periodo interglaciale corrispondente allo Stadio Isotopico Marino (MIS) 11 (ca. 424-367 ka). La prima fase del MIS 11 (MIS 11c; circa 426-396 ka) è particolarmente interessante poichè rappresenta una delle fasi interglaciali più lunghe e calde degli ultimi 800 ka, con temperature medie globali superiori di 0.5-0.7 °C rispetto all'attuale e livello del mare di circa 6-13 m più elevato rispetto ai valori dell'Olocene preindustriale. Il MIS 11c è considerato un analogo orbitale dell'Olocene e consente lo studio delle risposte degli ecosistemi a climi naturalmente più caldi, non essendo interessato dall'impatto antropico.

Le analisi palinologiche ad alta risoluzione dei sedimenti del bacino del Fucino rivelano oscillazioni climatiche millenarie tra 430 ka e 388 ka, nell'intervallo compreso tra l'ultima fase del periodo glaciale MIS 12, la Terminazione Glaciale V (T-V), e gran parte del MIS 11. L'indagine della carota Fucino F4-F5 offre una delle rare cronologie indipendenti con datazione radiometrica per il MIS 11, permettendo confronti diretti con i dati climatici e palinologici provenienti da registri regionali e globali.

La T-V è stata una delle transizioni climatiche più marcate del Pleistocene e parte di una delle maggiori riorganizzazioni climatiche note come Mid-Brunhes Event (MBE). Questa transizione, datata a 424.5 ± 4.0 ka nel Fucino, evidenzia un sostanziale passaggio da una fase fredda e arida - caratterizzata dalla dominanza di taxa erbacei e steppici come Poaceae, *Artemisia*, Amaranthaceae*, Ephedra* e *Hippophäe* e da sedimentazione prevalentemente siliciclastica - a una fase calda e umida, contraddistinta dalla presenza di *Abies* e da un'associazione di alberi decidui (*Quercus*, *Carpinus*, *Corylus*, e *Ulmus)*, con sedimentazione prevalentemente organica e calcarea. Le condizioni calde e umide registrate lungo il MIS 11c nel Fucino trovano riscontro nelle ricostruzioni climatiche di altri altri laghi della regione mediterranea, come i laghi di Ohrid e Ioannina. In particolare, la dominanza di *Abies* nella vegetazione circostante nel bacino del Fucino testimonia un'elevata umidità regionale.

Il record pollinico del bacino nel Fucino rivela la sensibilità dei taxa mesotermici e altitudinali alle variazioni dell'insolazione. Un significativo evento arido, identificato tra 415 ka e 413 ka, separa i due cicli precessionali dell'interglaciale MIS 11c. Questo evento, documentato per la prima volta in un record palinologico, potrebbe rappresentare un segnale climatico globale, correlandosi con temperature superficiali marine inferiori e condizioni più aride in altri record del contesto marino.

Le ricostruzioni paleoclimatiche quantitative, basate su analisi polliniche mediante regressione dei minimi quadrati parziali medi ponderati (WA-PLS), consentono un confronto diretto con i parametri climatici attuali, chiarendo l'impatto delle oscillazioni climatiche naturali sulle dinamiche della vegetazione durante il MIS 11c. I risultati mostrano che le dinamiche della vegetazione nel bacino del Fucino sono state fortemente influenzate dalla variabilità climatica dovuta all'insolazione, contribuendo a una migliore comprensione delle dinamiche climatiche passate e delle risposte della vegetazione.

In conclusione, questa tesi di dottorato fornisce importanti dati qualitativi e quantitativi per contestualizzare gli attuali impatti antropici sugli ecosistemi, confrontandoli con le tendenze climatiche ed ecologiche naturali osservate nell'analogo interglaciale MIS 11c. I risultati sottolineano l'importanza degli studi paleoclimatici per la comprensione della variabilità climatica naturale e le sue implicazioni per le risposte climatiche future.

Abstract (SP)

El estudio de los registros sedimentarios de los periodos interglaciares pasados proporciona datos importantes sobre la variabilidad climática en el pasado y las posibles respuestas de los ecosistemas ante condiciones más cálidas. Esta investigación aborda importantes lagunas en nuestra comprensión sobre el ciclo global del agua y las adaptaciones ecológicas de la vegetación ante cambios climáticos pasados que podrían compararse directamente con los cambios producidos durante el calentamiento global actual.

Esta tesis doctoral investiga muestras de polen de los sedimentos carbonatados provenientes de la cuenca del Fucino en los Apeninos Centrales, el cual es un lugar ideal para estudiar la dinámica de la vegetación dentro de un clima montañoso y Mediterráneo durante el periodo interglaciar correspondiente al estadio isotópico marino (MIS) 11 (ca. 424-367 ka). La primera etapa del complejo interglaciar MIS 11 (MIS 11c; ca. 426-396 ka) es particularmente interesante, debido a que representa una de las fases interglaciares más largas y cálidas dentro de los últimos 800 ka, registrando temperaturas globales medias de aproximadamente 0.5-0.7°C más altas y niveles del mar alrededor de 6-13 metros por encima de los respectivos valores del Holoceno preindustrial. En ausencia de la influencia antropogénica, el MIS 11c al ser un análogo orbital del Holoceno, facilita el estudio de las respuestas de los ecosistemas a climas naturalmente más cálidos. El análisis palinológico realizado a alta resolución temporal en los sedimentos de la cuenca del Fucino revelan oscilaciones climáticas a escala milenaria que abarcan el periodo comprendido entre 430 ka hasta 388 ka, incluyendo la última fase del periodo glaciar MIS 12, la Terminación Glaciar V (T-V), y la mayor parte del MIS 11. El sondeo Fucino F4-F5 posee una de las pocas cronologías independientes radiométricamente constreñidas para el MIS 11, permitiendo realizar comparaciones directas con datos climáticos y palinológicos de registros regionales y globales.

La T-V fue una de las transiciones climáticas más pronunciadas ocurridas durante el Pleistoceno, formando parte de una de las principales reorganizaciones climáticas conocida como Evento de Mid-Brunhes (MBE). Este acontecimiento, registrado en 424.5 ± 4. 0 ka en Fucino, refleja un cambio sustancial de una fase fría y árida, caracterizada por la dominancia de taxones herbáceos y esteparios como Poaceae, *Artemisia*, Amaranthaceae, *Ephedra*, e *Hippophäe* y por una sedimentación dominada por material siliciclástico, a una fase cálida y húmeda, marcada por una mayor representación de *Abies* y un conjunto arbóreo caducifolio *Quercus Carpinus*, *Corylus*, y *Ulmus*, y dominada por una sedimentación más orgánica y calcárea. Las condiciones cálidas y húmedas registradas a lo largo del MIS 11c en Fucino concuerdan con las reconstrucciones climáticas de otros lagos del de la región mediterránea, como el lago Ohrid y Ioannina, donde se registraron condiciones húmedas similares. En particular, *Abies* dominaba la vegetación circundante en la cuenca de Fucino, lo que evidencia una elevada humedad regional.

El registro polínico de la Cuenca de Fucino revela la sensibilidad de los taxones mesotérmicos y altitudinales a las fluctuaciones de la insolación. Un evento árido significativo se registra en la cuenca entre 415 ka y 413 ka, dividiendo los dos ciclos precesionales que formaron parte del interglaciar MIS 11c. Este evento, el cual este estudio lo describe por primera vez en un registro palinológico, puede corresponder a una señal climática global,

ya que se alinea con temperaturas superficiales del mar más bajas y condiciones más secas en otros registros marinos.

También se han realizado reconstrucciones paleoclimáticas cuantitativas basadas en el polen utilizando la regresión de mínimos cuadrados parciales con promedio ponderado (WA-PLS). Estas reconstrucciones permiten comparaciones directas con los parámetros climáticos actuales, dilucidando el impacto de las oscilaciones climáticas naturales en la dinámica de la vegetación durante el MIS 11c. Los resultados muestran que la dinámica de la vegetación en la cuenca del Fucino estuvo muy influenciada por la variabilidad climática debida a la insolación, lo que contribuye a una mejor comprensión de la dinámica climática del pasado y de las respuestas de la vegetación.

Esta tesis doctoral proporciona datos cualitativos y cuantitativos importantes para contextualizar los impactos antropogénicos actuales sobre los ecosistemas, los cuales se pueden contrastar con las tendencias climáticas y ecológicas naturales observadas en el análogo interglaciar orbital MIS 11c. Estos resultados ponen de relieve la relevancia de los estudios paleoclimáticos para mejorar nuestra comprensión de la variabilidad natural del clima y sus implicaciones para las respuestas climáticas futuras.

Index

Introduction

For more than a decade, scientists have argued regarding the warmth of the current interglacial period and its drivers. A key question remains: was the preindustrial late Holocene climate, particularly its warmth, a natural consequence of orbital dynamics that had not yet tipped Earth into another glacial state, or did it result largely from anthropogenic influence through early agricultural greenhouse gas emissions? (Ruddiman et al., 2016). Understanding the importance of these factors has become increasingly crucial as the world faces with the accelerating modern climate warming and its various effects on ecosystems, economies, and society. In particular, the Mediterranean region is expected to experience significant warming and drying trends in the upcoming decades (IPCC, 2013). However, there are still significant uncertainties in the understanding how the water cycle and ecosystems will respond to global warming. In this context, paleoecological and fossil sedimentary records can provide valuable information about climate system dynamics under different natural conditions, revealing variability of ecosystems in response to climatic shifts.

The study of past interglacial periods serves as a valuable fossil reference for a better understanding of our current climate change and its underlying mechanisms, identifying key factors that influence the climate system without the human activity influence. Studying temporally long paleoecological records is crucial for understanding recurrent climatic and paleoenvironmental changes, but also for exploring unique aspects among them (Tzedakis and Bennett, 1995; Tzedakis, 2007; Tzedakis et al., 2009)

The Quaternary climate is distinctive by its marked cyclicity (led by the change of the Earth's orbital parameters; Hays et al., 1976) alternating glacial and interglacial stages. To better understand the Holocene and the current interglacial conditions may continue to evolve, it is essential to compare it to a similar interglacial whose climate system responded to insolation and greenhouse gases with similar trends. Marine Isotope Stage (MIS) 11 had those conditions (with greenhouse gases (GHG) slightly bigger than nowadays) at the beginning of the interglacial period (Berger et al., 2012; Tzedakis et al., 2022). MIS 11's comparable orbital configurations, particularly in terms of obliquity and eccentricity, underscore the value of this period as an analogue for the MIS 1, with MIS 11c in particular providing insights into climate behaviour without anthropogenic impact (Berger et al., 2012; Vavrus et al., 2018).

The MIS 11 interglacial period is divided into three climatic substages, comprising two warm phases (MIS 11a and MIS 11c) separated by a cooler interval (MIS 11b) (Hrynowiecka et al., 2019). The nomenclature, used to define these divisions, is employed in the present study, as well as in the majority of the Mediterranean palynological research (e.g. Oliveira et al., 2016; Kousis et al., 2018; Koutsodendris et al., 2023a; Sassoon et al., 2023). Determining the precise timing and duration of these substages in terrestrial pollen records remains challenging due to the intrinsic difficulties associated with dating continental sedimentary sequences. Consequently, comparisons with marine isotopic records involve a high level of uncertainty and speculation.

This challenge is increased by increased by inconsistencies in the chronological framework of marine records. (Tzedakis et al., 1997; Koutsodendris et al., 2014).

MIS 11c (~426-396 ka; Tzedakis et al., 2022), is characterised for being an extremely long interglacial period, during ~30 kyrs and spanning two precessional cycles and was marked by high sea levels (~6-13 m above present; Spratt and Lisiecki, 2016) and high atmospheric CO_2 concentrations (~265-280 ppm; Brandon et al., 2020; Nehrbass-Ahles et al., 2020). Its low-amplitude precessional changes and subdued insolation variations, a result of the 400-kyr eccentricity cycle (marked by low present eccentricity values; Loutre, 2003; Tzedakis, 2010).

Due to its long duration, MIS 11 climate and ecosystem variability can provide a reference scenario of how the current interglacial could evolve in absence of human perturbations. The comparable orbital configurations (obliquity and, mainly, eccentricity) of MIS 11 and MIS 1 motivated modelling of the Earth's climate changes. Both periods show a similar latitudinal and seasonal distribution of the incoming solar radiation (Berger et al., 2012; Vavrus et al., 2018). However, there are some limitations to the MIS 1-11c analogy (e.g. MIS 11c registered two precessional cycles while MIS 1 registered only one). This discrepancy limits the direct comparability between the two periods but underscores the importance of examining interglacial phases individually in the context of their orbital and environmental conditions.

At the onset of the MIS 11c, was registered one of the largest ranges of climate variation during the Pleistocene. This abrupt climatic change is globally associated with the MIS 12-11 transition, a horizon recognised in marine records (e.g. Naafs et al., 2014), Antarctic ice cores (e.g. Bouchet et al., 2023), and terrestrial climate records across the world (Bouchet et al., 2024). The Mid-Brunhes Event (MBE) marks the limit from the previous low-amplitude to later high-amplitude glacial-interglacial cycles, with MIS 11c being the first high-amplitude interglacial since that event. Despite relatively low levels of incoming insolation and eccentricity (Laskar et al., 2004; Rodrigues et al., 2011; Cheng et al., 2016), MIS 11c is considered an exceptionally warm interglacial within the last million years (Rodrigues et al., 2011). The discrepancy between the strong deglacial warming at the onset of MIS 11c and the weak astronomical forcing is referred to in the literature as the "Stage 11 problem" (Imbrie et al., 1993), fundamentally challenging the orbital theory of Pleistocene glacial-interglacial cycles (Paillard, 2001; Berger and Wefer, 2003; Tzedakis et al., 2017, 2022). The apparent mismatch between modest insolation forcing and the significant climatic response during this transition needs for further inquiry to better understand the mechanisms underlying these climatic complexities (Huybers, 2006; Tzedakis et al., 2022).

Tzedakis et al., (2022) suggested that the weak forcing led to a slow deglaciation that continued well into MIS 11c. Independently dated records are crucial for assessing these paleoclimatic questions and identifying short- and long-term paleoclimatic changes and their drivers (e.g. Bakker et al., 2017; Leicher et al., 2024) and could be helpful to solve this "Stage 11 problem".

Comparison of data from the continent/sea/ice is essential to unveil the mechanisms of interaction and feedback between the atmosphere, cryosphere and hydrosphere and thus elucidate the causes of the millennial-scale, Dangaard-Oeschger or NAO-like variability, or the long-term, glacial-interglacial cycles or the role of the variation in atmospheric CO_2. Likewise, these studies are very important for assessing the timing and the regional propagation of the climate change in the northern hemisphere during certain climatic events. The study of temporally long paleoecological records is also necessary to have the resolution necessary to understand recurrent climatic or paleoenvironmental changes, produced with a certain periodicity (e.g., glacial-interglacial cycles) (Tzedakis and Bennett, 1995; Tzedakis, 2007).

Fossil pollen records have been used as a source to develop quantitative paleoclimatic reconstructions during Pleistocene (e.g. Fawcett et al., 2011; Kousis et al., 2018; Ardenghi et al., 2019; Sinopoli et al., 2019). Several transfer functions have been employed to obtain quantitative values of temperature and precipitation from pollen data, comparing the fossil pollen assemblages with the modern pollen distributions. The two most widely employed techniques are the modern analogue technique (MAT; Guiot, 1990) and the weighted averaging partial least squares (WA-PLS; Ter Braak and Juggins, 1993). The paleoclimatic quantitative reconstruction derived from these techniques facilitate the assessment of interglacial climatic changes and their implications for understanding natural dynamics in the context of the Quaternary climate cycles without the influence of human impact (Ruddiman, 2003; Kleinen et al., 2014).

Mediterranean region provide a unique framework for studying glacial-interglacial cycle dynamics, due to the intricate interaction between tectonics, volcanism, climate variability and continental lacustrine sedimentation (Tzedakis et al., 1997). Mediterranean pollen records offer significant insights into the region's vegetation and climatic history, demonstrating considerable variability throughout time that reflects changes in vegetation ecosystems due to climate oscillations (e.g. Bertini, 2010; Valsecchi et al., 2012; Desprat et al., 2013; Peyron et al., 2013; Donders et al., 2021). The proximity of previously examined Mediterranean pollen sites (e.g. Balkan Peninsula; Koutsodendris et al., 2019, 2023a; Donders et al., 2021) to refugial zones where climate-sensitive plant taxa endured during cold stages (Bennett et al., 1991) makes them especially useful for climate and environmental variability research, as migrational lags have minimal effect (Magri and Tzedakis, 2000). Previous studies in this region have demonstrated that glacial periods were distinguished by a reduction in tree populations and the dominance of open steppe vegetation, whereas warm and humid interglacial phases were characterised by more wooded landscapes (Cheddadi et al., 2005; Kousis et al., 2018; Hu et al., 2024).

The Fucino Basin at ~650m above sea level, in central Italy, is the largest and, possibly, oldest and long-lived basin of the Central Apennines intermountain tectonic depressions system (e.g. Cavinato et al., 2002), whilst the entire lacustrine sedimentary succession of the Fucino Basin could continuously span back to 2 Ma (Giaccio et al., 2015). The Fucino Basin contains a unique sedimentary record which contains the richest and most continuous Mediterranean succession of well-documented and radioisotopically dated Middle to Upper Pleistocene volcanic layers (tephras), enabling an accurate and precise age model for the last 424 ka (Giaccio

et al., 2017, 2019; Monaco et al., 2021, 2022; Leicher et al., 2023, 2024), and may span the last 430 ka, recording important climate periods as the end of MIS 12 glacial, the Termination V and most of the MIS 11.

The Fucino paleolake record (Giaccio et al., 2015) should add a nodal point between other Middle Pleistocene paleoclimatic records like Lake Ohrid and the Tenaghi Philippon. For this study the F4-F5 composite core was used (with an overlap of 0.75m between both cores, with the objective of avoiding any gap in the sequence), obtaining a total of 87.75m of continuous sediment accumulation (Giaccio et al., 2019).

This PhD project focusses on the palynological analysis of MIS 11c, being a valuable reference for understanding natural climate dynamics. The Fucino Basin, with its well-preserved lacustrine sediments and high-resolution pollen data, offers an ideal opportunity to study vegetation dynamics and millennial- to sub-millennial-scale hydrological variability during MIS 11c. By comparing these data to both regional and contemporary climate parameters, this research aims to clarify natural trends in climate variability, providing context for assessing human impacts on current climate systems. The overall objective of this study is to know and understand the natural trend of climate change to have a better comprehension of human influence on present hydrological changes. With the aim to reach this main objective this PhD characterised the vegetation dynamics in response to MIS 11 climate change through a high-resolution pollen analysis of samples obtained from Fucino Basin. This pollen characterisation together with other available proxies from the Fucino record provided us a reconstruction of millennial to sub-millennial scale hydrological variability. Those changes could be directly compared with regional changed occurred at the same time and today current climatic parameters.

To achieves these described objectives, this PhD thesis is sub-divided into three main chapters:

- Chapter 1 (Vera-Polo et al., 2024) is a detailed study of the T-V and glacial-interglacial boundary, that is considered one of the biggest climatic shifts in the past 800 ka. This chapter focussed in the palynological analysis of Fucino record, comparing the pollen-based reconstructions from this climatic shift with other Mediterranean record, examining the MIS 12-MIS 11c boundary in a regional context.
- Chapter 2 focused on the study of vegetation dynamics during MIS 11c, providing millennial-scale variability that could be related with regional to global climatic changes. This chapter includes the entire detailed pollen record and identifies some important events that give us insights about the evolution of the climate parameters during MIS 11. The paper will be shortly submitted to Quaternary Science Reviews (Vera-Polo et al., submitted soon).
- Chapter 3 takes the results of chapter 2 and developed a paleoclimatic quantitative reconstruction, which was directly compared with our current climatic parameters such us temperature and precipitation. This reconstruction was also compared with other global climatic reconstructions, providing us more information about the general trends that affected the ecosystems, and which could indicate only regional variability. A short paper will be submitted to Climate of the Past.

Chapter 1: Climate and vegetation variability during Termination V in Fucino Basin

- Vera-Polo, P., Sadori, L., Jiménez-Moreno, G., Masi, A., Giaccio, B., Zanchetta, G., Tzedakis, P.C., Wagner, B., 2024. Climate, vegetation, and environmental change during the MIS 12-MIS 11 glacial-interglacial transition inferred from a high-resolution pollen record from the Fucino Basin of central Italy. Palaeogeography, Palaeoclimatology, Palaeoecology 655, 112486. https://doi.org/10.1016/j.palaeo.2024.112486

Palaeogeography, Palaeoclimatology, Palaeoecology 655 (2024) 112486

Contents lists available at ScienceDirect

Palaeogeography, Palaeoclimatology, Palaeoecology

journal homepage: www.elsevier.com/locate/palaeo

Climate, vegetation, and environmental change during the MIS 12-MIS 11 glacial-interglacial transition inferred from a high-resolution pollen record from the Fucino Basin of central Italy

Vera-Polo, P.* [a, b], Sadori, L.[a], Jiménez-Moreno G.[b], Masi, A.[a], Giaccio, B.[c d], Zanchetta, G.[e], Tzedakis, P.C.[f], Wagner, B.[g]

a Dipartimento di Biologia Ambientale, University of Rome "La Sapienza", Rome, Italy, 00185

b Departamento de Estratigrafía y Paleontología, Universidad de Granada, Granada, Spain, 18071

c Istituto di Geologia Ambientale e Geoingegneria, CNR-IGAG, Monterotondo, Rome, Italy, 00015

d Istituto Nazionale di Geofisica e Vulcanologia, INGV, Rome, Italy, 00143

e Dipartimento di Scienze della Terra, University of Pisa, Pisa, Italy, 56126

f Environmental Change Research Centre, Department of Geography, University College London, London, UK, WC1E6BT

g Institute of Geology and Mineralogy, University of Cologne, Cologne, Germany, 50939

* Corresponding author: pablo.verapolo@uniroma1.it

Abstract

Glacial Termination V (T-V) comprised a relatively rapid shift from glacial to interglacial conditions (MIS 12 glacial to the MIS 11c); it was one of the greatest climatic changes of the Pleistocene, and forms part of the major climatic reorganization known as the Mid-Brunhes Event (MBE). The Fucino Basin, located in the Central Apennine chain of central Italy, contains a continuous and well-preserved lacustrine sedimentary record of T-V and MIS 11, dated using tephrochronology. In this paper, we report a high-resolution palynological analysis, supported by geochemical proxies, from the lowermost section of the F4-F5 composite record, to improve understanding of T-V in this region. This record reveals a substantial transition between MIS 12 and MIS 11c at 424.5 ± 4.0 ka, from a very cold and dry environment indicated by the herbaceous and xerophytic association of Poaceae, *Artemisia*, Amaranthaceae, *Ephedra*, and *Hippophäe*, and sedimentation dominated by inorganic siliciclastic sediments, to a warm and humid period characterised by a significant increase in *Abies* and a deciduous tree association mainly formed by *Betula, Carpinus*, *Corylus, Quercus*, *Ulmus,* and dominated by more organic calcareous sediments. This transition was correlated with a significant lake-level rise, with an enhanced nutrient input into the lake between 425.0 ± 4.5 ka and 424.0 ± 3.9 ka, as inferred from the variance between algae, aquatic plants, and terrestrial herbaceous taxa. Following the MIS 11c temperature maximum at 424.2 ± 3.9 ka, a reduction in summer insolation occurred, provoking a significant increase in humidity that

produced the widespread development of *Abies*. The results from this study suggest that, at Fucino, fluctuations in humidity are predominantly responsible for the vegetation changes observed during T-V.

Key words: pollen analysis, Mediterranean region, central Italy, glacial-interglacial cycles, MIS 12, Termination V, MIS 11c, climate change, Mid-Brunhes Event

1.1 Introduction

The Quaternary climate is characterised by a marked periodical alternation of glacial and interglacial (G/I) cycles, paced by Earth's orbital parameters changes (Hays et al., 1976). Studying temporally long paleoecological records is crucial for understanding recurrent climatic and paleoenvironmental changes, such as G/I cycles, but also for exploring unique aspects among them (Tzedakis and Bennett, 1995; Tzedakis, 2007; Tzedakis et al., 2009).

One notably long interglacial was MIS 11c (~426-396 ka) (Tzedakis et al., 2022), which spanned two precessional cycles and was marked by high sea levels (6-13 m above present; (Spratt and Lisiecki, 2016) and high atmospheric greenhouse gases concentration (hovering around 265-280 CO_2 ppm for ~30 kyr; Brandon et al., 2020; Nehrbass-Ahles et al., 2020). Its low-amplitude precessional changes and subdued insolation variations, a result of the 400-kyr eccentricity cycle (marked by low present eccentricity values), make it a partial astronomical analogue for the Holocene (Loutre and Berger, 2000; Tzedakis, 2010).

MIS 12 was characterised by one of the largest glaciations registered in Europe (Ehlers and Gibbard, 2008). The end of this glacial period (Termination V) seems to occur when the insolation values began to rise, coinciding with a large volume of ice covering the Earth surface (Raymo, 1997). Glacial Termination V (T-V), which occurred between 430.5 ± 1.5 and 426.0 ± 2.0 ka (Cheng et al., 2016), is consequently recognised as one of the most extreme climatic shifts in the last 900 ka of the Earth system, despite minimal astronomical forcing (Napier et al., 2018; Giaccio et al., 2021; Sassoon et al., 2023). This large climatic change is also known as the Mid Brunhes Event (MBE), which marks the definitive establishment of the long, high-amplitude, and saw-tooth structured G/I cycles (Berger and Wefer, 2003). While the insolation forcing during T-V was relatively weak (Loutre and Berger, 2000), it was associated with one of the highest-amplitude deglacial warmings (Berger and Wefer, 2003; Rodrigues et al., 2011). This rapid climate warming provoked one of the biggest increases in global biosphere productivity, reaching values of 10-30% higher than present-day (according to pollen data and total organic carbon; Brandon et al., 2020). The disparity between the modest insolation forcing and the pronounced climatic response is known as the "Stage 11 problem" (Imbrie et al., 1993). Tzedakis et al. (2022) suggested that the weak forcing led to a slow deglaciation that continued well into MIS 11c, but constraining the rate of the sea-level rise is challenging (Rohling et al., 2010; Vázquez Riveiros et al., 2013; Barker et al., 2015). Independently dated records are crucial for assessing these paleoclimatic questions and identifying short- and long-term paleoclimatic changes and their drivers (e.g. Bakker et al., 2017; Li et al., 2023; Leicher et al., 2024) and could be helpful to solve this “Stage 11 problem”.

The Mediterranean region, with its complex interplay of tectonics, volcanism, and thick lacustrine sedimentary sequences provides a unique setting to investigate the dynamics of G/I cycles (Tzedakis et al., 1997). Mediterranean pollen records provide valuable insights into the region's vegetation and climatic history.

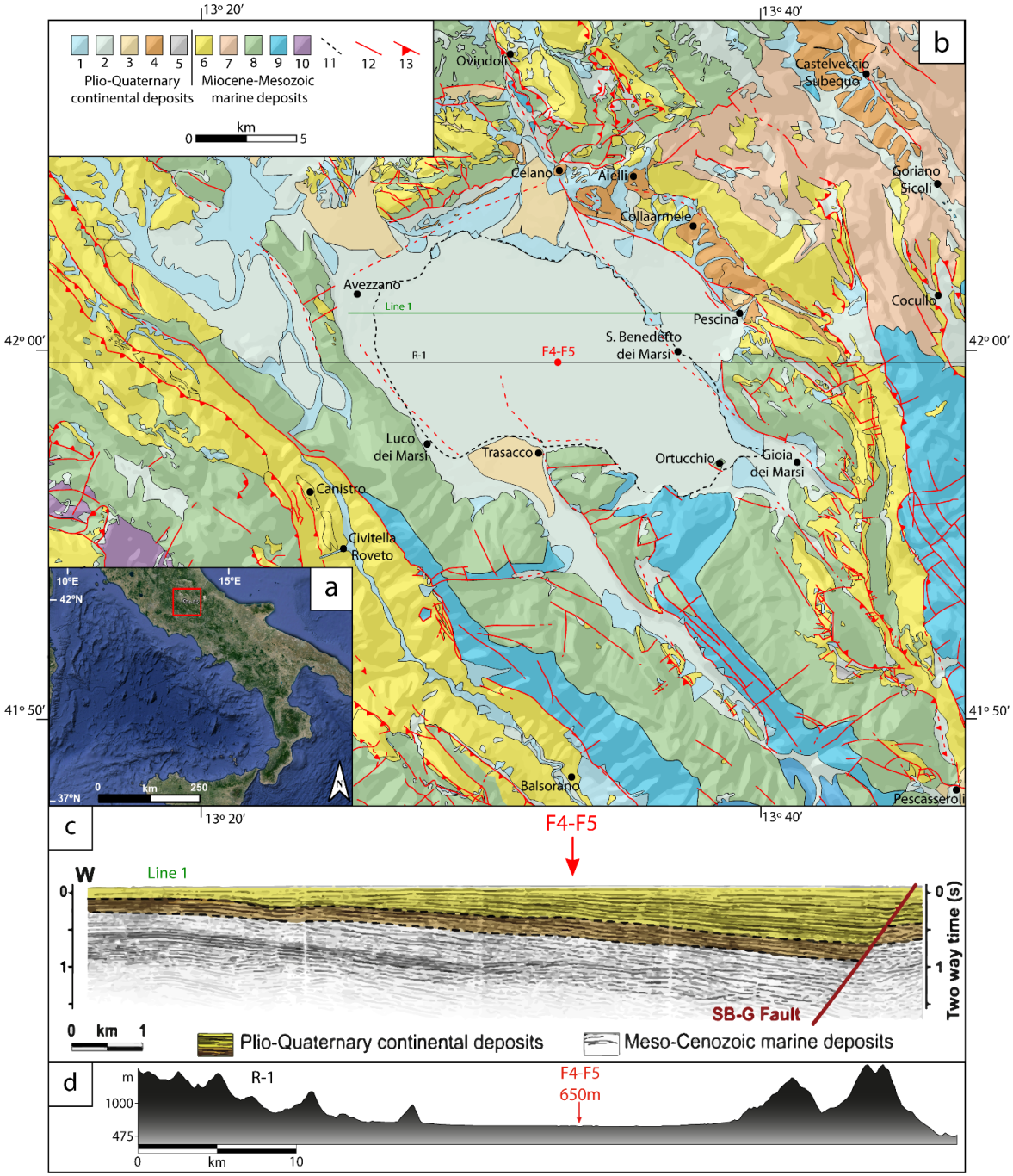

Fig. 1.1.- *a) Geographical location of the Fucino basin (red square) in Italy. Image obtained from Google Earth. b) Simplified geological map of the basin area. Modified from ISPRA, 1934, 1939, 1942, 1967 and Caielli et al., 2023. 1) Holocene-Upper Pleistocene calcareous debris fans and fluvio-lacustrine conglomerates; 2) Holocene fluvio-lacustrine deposits; 3) Middle-Upper Pleistocene talus and alluvial fans; 4) Middle Pleistocene calcareous lacustrine deposits. 5) Pleistocene moraine deposits; 6) Miocene brackish marls, sandstones, conglomerates and calcarenites from carbonate ramp; 7) Eocene stratified limestones with Nummulites; 8) Cretaceous well-stratified calcareous and dolomitic series from platform and margin; 9) Jurassic calcareous dolomitic banks with gastropods and brachiopods; 10) Triassic dolomitic series. 11) Historical lake margin (Holocene); 12) Fault and normal faults 13) Thrust faults. Simplified shaded relief is used as basemap to highlight the morphological configuration of the basin. c) Seismic Line 1 (see green trace in panel b) depicting the architecture of Plio-Quaternary continental deposits in the Fucino Basin along a W-E orientated profile, from Giaccio et al., 2019. d) Relief around the Fucino Basin following the black trace R-1 from the panel b). Altitude in m.a.s.l.*

In addition, due to the proximity of the studied Mediterranean pollen sites (e.g., in Balkan Peninsula, Koutsodendris et al., 2019, 2023a; Donders et al., 2021) to refugial areas (any area of any size in which a taxon persisted at any population density during a cold stage; Bennett et al., 1991) it is postulated that there are no significant migrational lags in the Mediterranean pollen records (Magri and Tzedakis, 2000). Because of this, the Mediterranean region is characterised by a wide variety of landscapes, including treeless areas, woodland and several types of forests, with the occurrence of typically Mediterranean adapted plants or mesophilous trees. This vegetational variability allowed us to find representations of diverse climatic associations in relatively small areas and study their response to climate changes throughout time.

The Fucino Basin, in central Italy (Fig. 1.1), is the largest and, possibly, oldest and long-lived basin of the Central Apennines intermountain tectonic depressions system (e.g. Cavinato et al., 2002), whilst the entire lacustrine sedimentary succession of the Fucino Basin could continuously span back to 2 Ma (Giaccio et al., 2015). The hitherto well investigated uppermost interval contains the richest and most continuous Mediterranean succession of well-documented and radioisotopically dated Middle to Upper Pleistocene volcanic layers (tephras), enabling an accurate and precise age model for the last 424 ka (Giaccio et al., 2017, 2019; Monaco et al., 2021, 2022; Leicher et al., 2023, 2024), and may span the last 430 ka (e.g. Giaccio et al., 2019).

In this study, we present a detailed pollen record from the lowermost portion of this record, spanning the end of MIS 12 and the beginning of MIS 11. The high-resolution pollen data allow us to study millennial-scale vegetation changes and to gain insight into the significant environmental change and climatic fluctuations that occurred during the MBE.

1.2 Study Site: geology, climate, and vegetation

The Fucino Basin (42º 00' N; 13º 30' E) is situated approximately at 650 m a.s.l. within the Central Apennine Chain (Abruzzo) and is bounded by mountain peaks such as Monte Velino (2486 m a.s.l.) and Monte Sirente (2348 m a.s.l.). It is the largest (~900 km^2) Central Apennine intermountain tectonic basin, hosting thick and continuous Plio-Quaternary alluvial and lacustrine deposits (Cavinato et al., 2002; Giaccio et al., 2019) (Fig. 1.1). The basin opened during the post-orogenic tectonic extensional phase along the Fucino Fault System (FFS), which has been active since the Pliocene and consists of three principal segments oriented along a 110º-140 ºN axis (Galadini and Galli, 2000; Cavinato et al., 2002; Galadini and Messina, 2004; Mondati et al., 2021). The FFS activity and configuration, consequence of the general regional uplift, resulted in the formation of a half-graben basin with a steep topographic slope on the basin floor (Giaccio et al., 2015; Caielli et al., 2023). Lake Fucino formed at the lowermost part of the basin during the Early Pleistocene, occupying an area of ~140 km^2 and reaching a maximum water depth of 20 m, being the Italy's third largest lake (Mannella et al., 2019), before its artificial drainage in 1875 for agricultural purposes (Giaccio et al., 2017). The interaction between the lake and the differential movements along the FFS controlled the sedimentary infilling of the basin. This resulted

in a presumably continuous deposition, with a variable sedimentation rate, and influenced by the wedge-shape sedimentary infilling forced by the basin's half-graben geometry (Giaccio et al., 2017, 2019; Mannella et al., 2019), of fine-grained lacustrine calcareous marls, fluvio-glacial sediments from the surrounding relief, and several tephra layers from peri-Tyrrhenian magmatic provinces (Giaccio et al., 2017, 2019; Monaco et al., 2021, 2022; Leicher et al., 2023, 2024). As a result, Quaternary deposits of ~900 m accumulated in the depocenter, with increasing sedimentation rates from west to east.

At present, the Fucino Basin is characterised by a Mediterranean climate with warm and dry summers (e.g. Lionello et al., 2006) and continental characteristics, according to historical data from the regional meteorological network (Peyron et al., 2013) and from data recollected from the nearby Borgo Ottomila meteorological station (652 m a.s.l.). From April to October, monthly average temperatures are over 10 ºC, peaking in July and August (18 to 21 ºC). From November to March, monthly average temperatures are below 10 ºC, with January being the coldest month recording minimum daily temperatures from -5 to -2 ºC (Mannella et al., 2019). The WorldClim v2.1 database (Fick and Hijmans, 2017) recorded present-day mean annual temperatures of ~10.0 ºC, however, according to the information from meteorological stations, the mean annual temperature for Fucino Basin is ~12.5 ºC. The average annual precipitation ranges from 600 to 750 mm in the plains to 900 to 1200 mm in the piedmont zone.

Due to the unique lithological and geomorphological setting of the Fucino Basin, mountain and Mediterranean climates are represented in the same region, controlling the vegetation distribution. This makes the central Apennines a region with a rich and diverse vegetation, characterised by a complex mosaic of vegetation zones (Fig. S1.1) and different from that of central Europe, being more related to the vegetation of south-eastern Europe (Blasi and Del Vico, 2012). The present-day potential natural vegetation in the area is difficult to identify because of significant human impact and agricultural use (Frate et al., 2018). The vegetation in the Fucino Basin is currently dominated by grasslands on the lower and flatter areas of the basin and extends to the western side of the surrounding reliefs, due to the pluviometric shading caused by the predominantly westerly winds (Tomassetti et al., 2003). The potential natural vegetation in this area is dominated by hygrophilous and hydrophytic freshwater vegetation (Blasi et al., 2017) at the lowermost part of the basin. At lower elevations at the base of the surroundings reliefs, oak forest with *Quercus pubescens* dominates. Mixed woods of *Ostrya carpinofolia*, *Quercus cerris*, and *Acer* spp. spread in cooler and higher elevation areas (Fig. S1.1). Communities of evergreen scrubs dominated by *Quercus ilex* are established in thermally favourable areas and on lithoid outcrops. At the lower limit of the mountain plain, in the valleys and ravines, grows a mixed forest linked to particularly riparian conditions, with *Acer pseudoplatanus, Ulmus glabra, Tilia platyphyllos* and *Fraxinus excelsior*. The mountain bioclimatic vegetation belt is dominated by *Fagus sylvatica*, flanked, in some locations as isolated stands, by *Abies alba*. The rich floral array of beech forests differs, depending on the type of substrate and climatic conditions, giving the development of various plant associations (Fig. S1.1). Small forest patches of *Betula pendula,* a glacial relic, complement the vegetation panorama and confirm the importance of the basin for conservation of biodiversity. Above 2000 m forests give way to less dense

formations, with herbaceous plants becoming the undisputed protagonist of the high mountain vegetation, which is rich in endemic taxa and glacial relics. The alpine meadows, rocky slopes, and scree fields with a vegetation dominated by Poaceae, Cyperaceae, and alpine herbs are adapted to alpine mountainous conditions (Blasi, 2010; Blasi et al., 2017) (Fig. S1.1).

1.3 Materials and methods

1.3.1 The composite F4-F5 core

Two parallel holes, F4 and F5, taken approximately 3 m apart, were drilled in June 2017 in the central area of the basin (42º00'07'' N, 13º32'19'' E; Fig. 1.1; Giaccio et al., 2019) with a 1.5-m-long core barrel and 0.75 m overlap between succeeding runs in both holes to continuously recover the entire sedimentary succession. Cores F4 and F5 reached depths of 87.00 m and 87.75 m, respectively. The composite F4-F5 record was built by establishing correlations between the lithological and physical properties of the individual cores from parallel holes. This overlap minimized any potential gap that could have occurred between subsequent core sections from the two holes (Giaccio et al., 2019). This study is restricted to the bottommost part of the record and includes only the sediment succession recovered in the lowermost core barrel of the F5 hole, without the possibility of establishing a direct correlation with the F4 core (Fig. 1.2).

1.3.2 Geochronology and age-depth modelling

The F4-F5 composite record contains at least 130 tephra layers (Giaccio et al., 2019), which allow a precise geochronological analysis for different stratigraphical intervals spanning the last ~430 ka (Giaccio et al., 2017; Monaco et al., 2021, 2022; Leicher et al., 2023, 2024).

The analytical details of the chronological control for the investigated interval were previously described by Monaco et al. (2021). Specifically, the age model for the ~365-430 ka interval and related 95%-confidence interval were both generated using the open-source statistical environment R (R Core Team, 2017) and the Bacon programme (Blaauw and Christen, 2011), which was constrained by 9 tephra layers dated directly or indirectly with the $^{40}Ar/^{39}Ar$ method (Monaco et al., 2021; Fig. 1.2).

The age model provided by Monaco et al. (2021) extrapolated the sedimentation rate between the lowermost two tephra layers (TF-125, 414.8 ± 2.2 ka and TF-126, 424.3 ± 3.2 ka) towards the bottom of the sediment succession. However, a distinct lithological change, clearly documented by the XRF Ca data (Fig. S1.2; Monaco et al., 2021) at 97.30 m composite depth, ~5.6 cm below TF-126 marks the transition from MIS 12 glacial sedimentation below to MIS 11c interglacial sedimentation above (Monaco et al., 2021). As the average sedimentation rates in the F4-F5 core during the following glacial periods MIS 10, MIS 8, MIS 6, and MIS 4-2 range between 0.12 and 0.28 mm/yr (Giaccio et al., 2019; Monaco et al., 2021, 2022; Leicher et al., 2023, 2024), we here extrapolated a mean sedimentation rate of 0.20 mm/yr for the section below 97.30 m, with a propagated

uncertainty of 3.5 ka to 5.0 ka, which also accounts for the range of variability of sedimentation rate (Fig. 1.2). Overall, the resulting age-depth model provided age constraints with an overall uncertainty of ± 4.2 ka, ranging from 3.6 ka to 5.0 ka. As a result, samples ages encompassing an age range between 429.0 ± 5.0 ka to 418.5 ± 3.6 ka in the record are derived from this extrapolation.

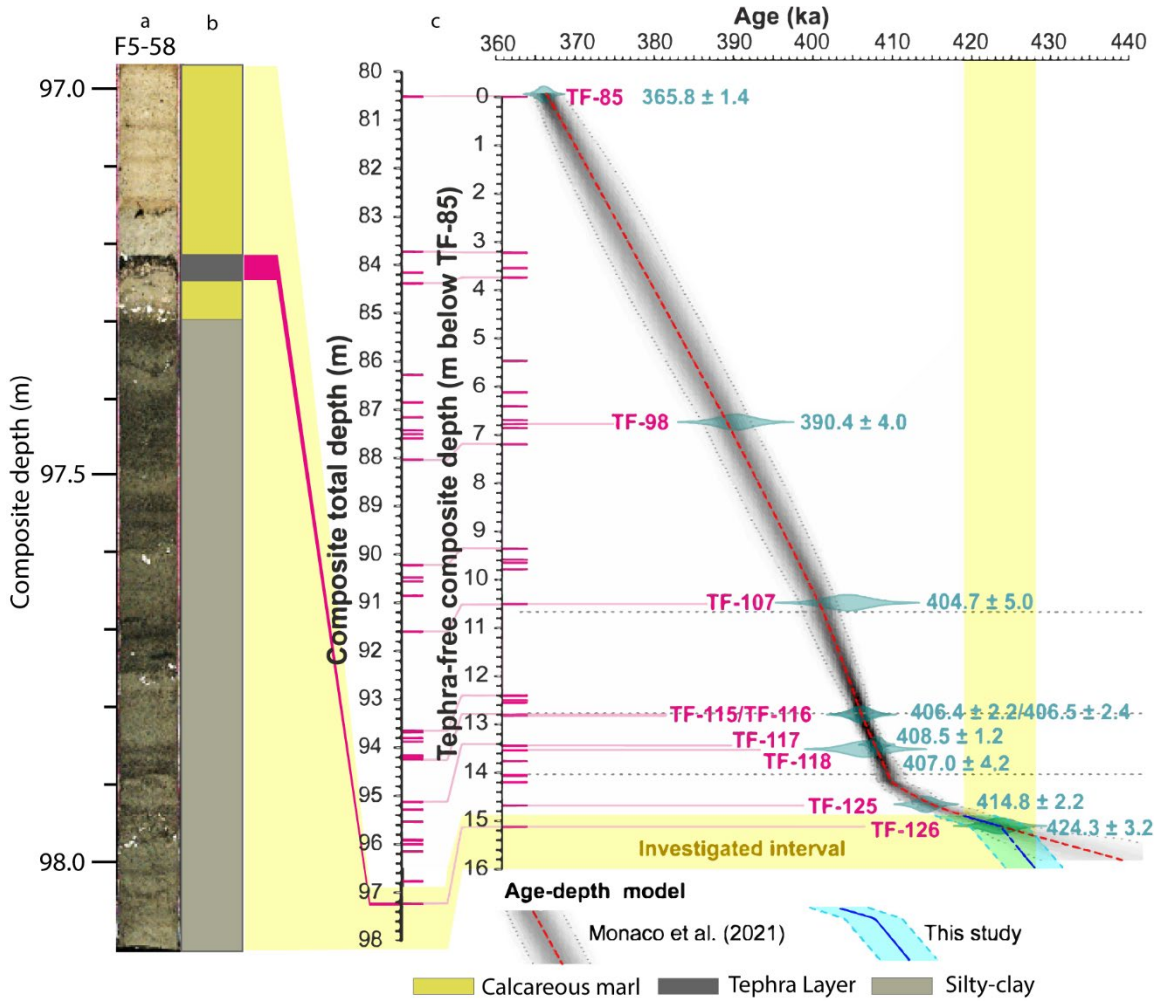

Fig. 1.2*.- a) Core-scanner image of the core-section F5-58; b) Simplified lithology of the core section F5-58. c) Bayesian age-depth model modified after Monaco et al. (2021) for the 18 m of the composite core interval. The yellow rectangle represents the interval investigated here (418-428 cal. ka). The pink marks are the tephra layers identified along the core. From 424.3 (TF-126) to the base the age model for this study was changed in comparison to the previous age extrapolation (Monaco et al., 2021; see text for details).*

1.3.3 XRF

X-ray fluorescence (XRF) scanning was conducted on the split core halves of the F4-F5 sediment cores using an ITRAX XRF scanner (Cox Analytical Systems, Sweden) with a line-scan camera mounted and a chromium tube set at 55 kV and 30 mA, a dwell time of 10 seconds and a step-size of 2.5 mm. The resulting data were processed using the QSpec 6.5 software (Cox Analytical, Sweden), and the values are presented in counts per second, averaged at 25 cm intervals. So far, only Ca counts from the analysis were published (Giaccio et al., 2019). The optical information obtained from the high-resolution line-scan imaging and XRF data were used to correlate the individual overlapping core segments from F4 and F5 sites (see Giaccio et al., 2019 for details).

To gain more information about the past environmental and sedimentary conditions, 13 elements of the XRF data were used, including calculation of the following ratios, which proved to be useful for Fucino Basin.

- Zr/K: It determines grain size changes (Cuven et al., 2011). Zr is very resistant to weathering and transport and is usually enriched in coarse sediment fractions (Wang et al., 2011; Croudace and Rothwell, 2015), whereas K is associated with illite clays and feldspar, and is more common in fine grained sediments (Kuhlmann et al., 2004). So, higher values of this proxy represent a coarser grain size composition.
- Ca/Ti: We adopted this ratio because the origin of Ca, in the Fucino Basin, is ambiguous and can be the result of in situ endogenic carbonate precipitation, or, to a minor extent, of biogenic shell calcification such as in ostracods, or of detrital influx from the large outcrops of marine limestones (Mannella et al., 2019). Endogenic carbonates precipitate due to the decrease of dissolved CO_2 from warmer water temperatures or photosynthesis (Freytet and Verrecchia, 2002). In this context, Ca/Ti would then mostly express authigenic carbonate precipitation without detrital input, being Ti only of clastic origin.
- Si/Ti: It is used as a proxy to determine siliceous productivity (biogenic silica) (e.g. Stansell et al., 2010; Brown, 2011; Melles et al., 2012).

The Log ratios were used to address and minimize any core scanner detector drifts, dilution effects and sources of irritation, providing the most robust record of relative chemical changes in the sedimentary record and reducing interpretation risks (Croudace and Rothwell, 2015).

A Principal Components Analysis (PCA) was performed on the XRF data using the Past4 software (Hammer et al., 2001), removing the data that corresponds with the tephra layer, in order to avoid that the geochemical associations connected to specific sedimentation processes (e.g., erosion and productivity) may be affected (Fig. S1.2). The PCA allows for the identification of variables (components) that capture the majority of variance within multivariate data (Hammer et al., 2001).

1.3.4 Geochemical analyses on discrete samples

Discrete samples taken from the top of each core catcher and every 4 cm were processed for total carbon (TC) and total inorganic carbon (TIC), and stable carbon and oxygen isotopes (see Mannella et al., 2018 for details). TOC was calculated from the difference of TC and TIC and used for this study, along with $\delta^{18}O$ for the paleoclimatic interpretations.

1.3.5 Pollen analysis

The palynological study focuses on T-V and the G/I transition within the deepest part of the F4-F5 record (drive F5-58). The age model modified from Monaco et al. (2021) (Fig. 1.2) was taken into consideration when selecting samples for this study. The sampling strategy involved three distinct intervals: 4-cm intervals (the bottommost 44 cm), 2-cm intervals (the overlying 28 cm), and 1-cm intervals (the uppermost 35 cm), excluding

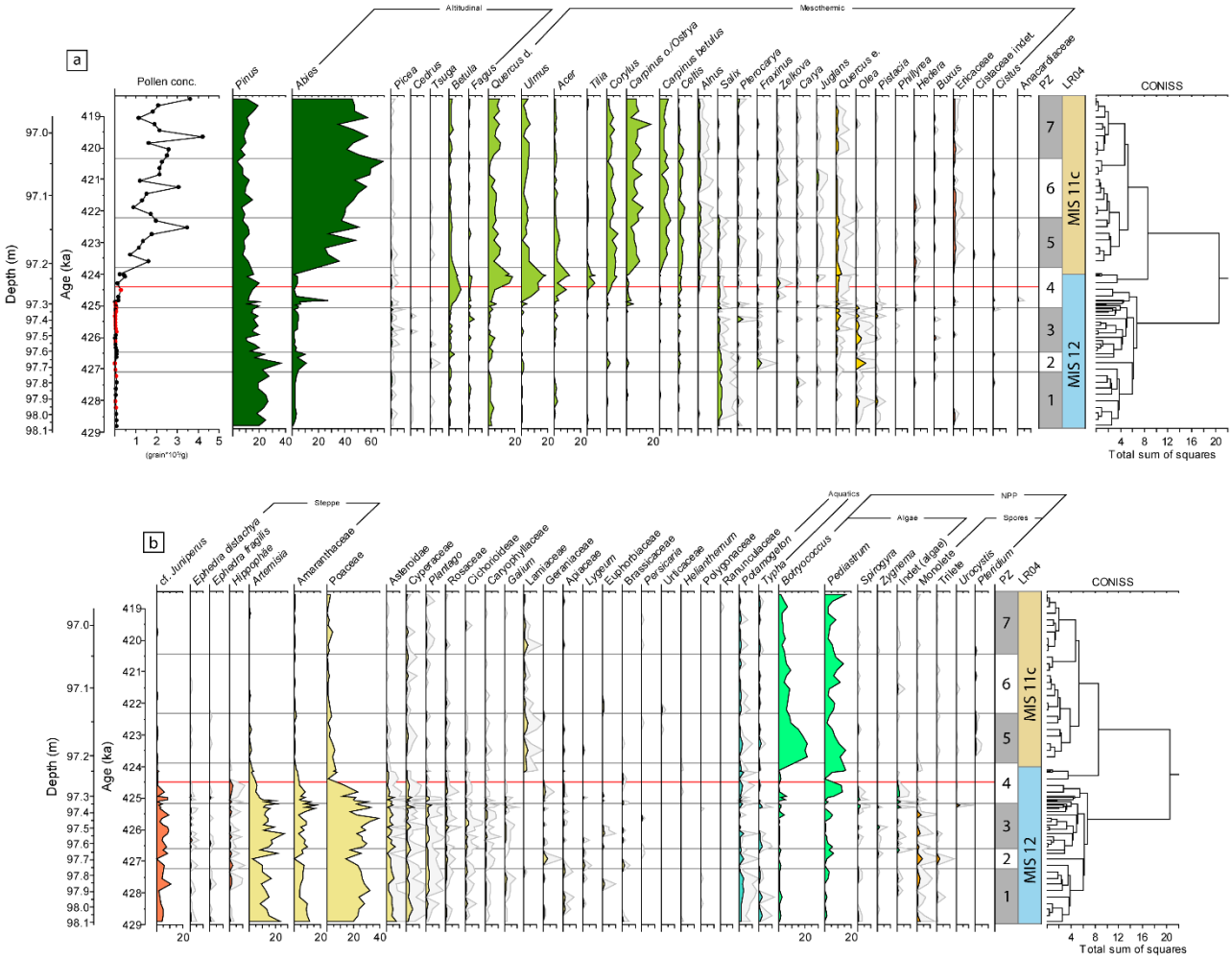

Fig. 1.3.- *Detailed percentage pollen diagram from the F4-F5 record. Total pollen concentration is shown in the first curve of the uppermost diagram (3a) followed by trees and shrubs. Red dots in pollen concentration curve indicates the samples that didn't reached the 300 pollen grains counts. Dark-green: coniferous trees; yellow-green: deciduous trees; yellow: sclerophyllous trees; orange-red: shrubs. In the lowermost diagram (3b) are displayed: herbaceous: pale-yellow; aquatic: turquoise; algae: light-green; spores: orange; other Non-Pollen Palynomorphs (NPP): black and the cluster analysis done by CONISS (Grimm, 1987). The boundary between MIS 12 and MIS 11 suggested by Lisiecki and Raymo (2005) is shown by the blue and beige boxes at ~424 ka. The red line indicates the Glacial-Interglacial boundary suggested by pollen zones (PZ) and CONISS analysis for the F4-F5 composite record. The light grey shading in the pollen percentages represents an exaggeration of the abundance x5.*

the tephra layers. This approach was used to compensate the presumed changes in sedimentation rates, with the aim of achieving a high-resolution record for the studied period. Consequently, a total of 66 samples were obtained, with a range of temporal spacing between samples of ~50 and ~215 years, resulting in an average temporal resolution of ~200 years between individual samples. After freeze drying, the samples were treated with hydrochloric acid (HCl, 37%) to remove carbonates, hydrofluoric acid (HF, 48%) to remove silicates, and sodium hydroxide (NaOH, 10%) to eliminate the cellulose fraction with the goal of concentrating the organic matter. A tablet of *Lycopodium* spores was added to each sample to calculate pollen concentrations. Subsequently, the samples were sieved using a 10 µm nylon sieve to remove particles smaller than pollen grains, including clays. The remaining material was mounted on microscope slides using glycerine. Palynomorph identification was performed under transmitted light microscopy at 400x magnification. Most of the samples showed abundant pollen grain concentrations, allowing the identification of a total of 300 terrestrial and aquatic pollen grains per sample. However, eighteen samples, from the lowermost interval (between 98.02-97.27 m

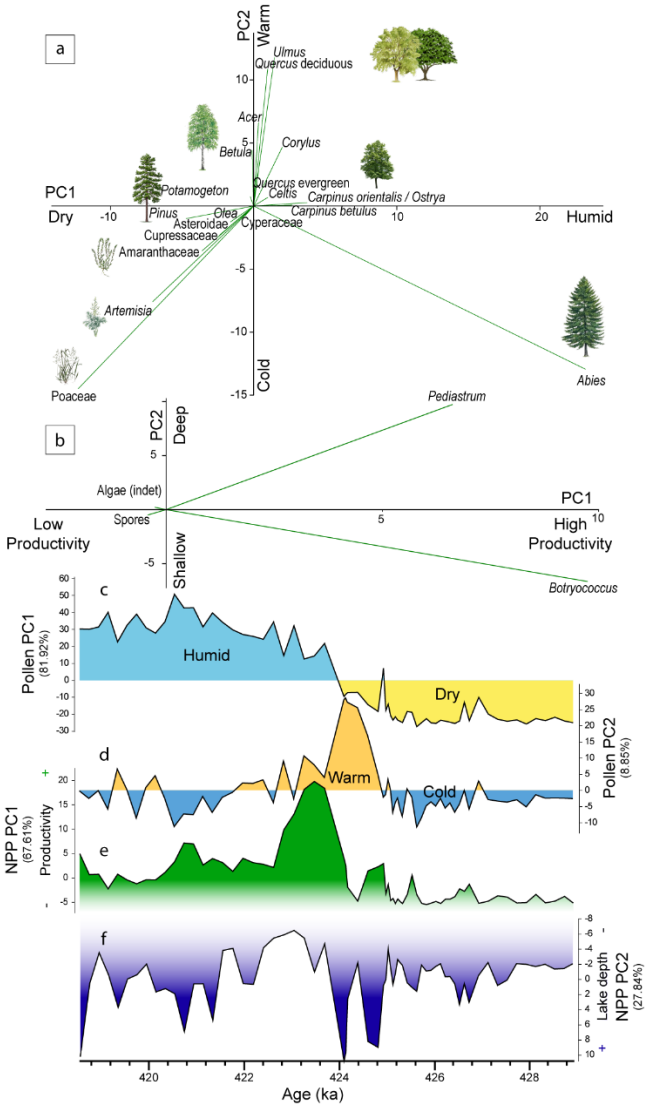

Fig. 1.4.- *Principal Component Analysis (PCA) of pollen percentage and Non-Pollen Palynomorphs (NPP) results. (a) Pollen scatter biplot using the PC1 and PC2 with its paleoclimatic interpretation. (b) NPP scatter biplot using the NPP-PC1 and NPP-PC2 with its interpretation. (c) Pollen PC1 is interpreted as the variation in humidity with yellow colour representing the drier period and blue colour the humid one. (d) Pollen PC2 is interpreted as the change in temperature with orange colour (representing the warmest periods) and blue colour (for the colder ones). (e) NPP-PC1 interpreted as the productivity in the lake during the studied period. f) NPP-PC2 inverted interpreted as the lake depth. The analyses were carried out using PAST 4.11 (Hammer et al., 2001). Pollen and NPP taxa with an abundance lower than 1% and with loadings lower than 0.025 were removed from (a) and (b) diagrams in order to enhance readability.*

composite depth; Fig. 1.3a), were characterised by such low pollen concentrations that counts of 300 pollen grains were not possible. These samples provided between 170 and 266 pollen grains, being mostly above 200. Overall, the pollen quantities proved to be sufficient for making a broadly environmental interpretation (Djamali and Cilleros, 2020).

Pollen grains identified as cf. *Juniperus* (Fig. 1.3) may include some grains of other Cupressaceae such as *Cupressus*, as well as those of *Taxus*. The last two were not observed in the samples, but we cannot exclude their presence in some of the pollen samples, considering the poor state of preservation of those pollen grains, primarily in the MIS 12 glacial samples, when *Juniperus* ss. was rather abundant.

The percentages of the different pollen taxa were calculated and represented using the Tilia Software, version 2.6.1 and an objective zonation of the pollen data was performed using CONISS cluster analysis (Grimm, 1987; Fig. 1.3). This software was used to compute the concentration of pollen grains in samples (Fig. 1.3a), considering the mass quantity (~2 g per sample) and the number of *Lycopodium* spores added and counted for each sample. The percentage of Non-Pollen Palynomorph (NPP) was calculated in relation of the total sum of the total pollen amount plus the total NPP.

In addition, a PCA was performed on both pollen and NPP percentage data. For comparison, the PCA was conducted to reduce the dataset to two variables (the first two components) (Fig. 1.4).

According to former studies (e.g. Joannin et al., 2011; Bertini et al., 2015; Camuera et al., 2019) and to PCA results (Fig. 1.4), pollen grains were grouped into ecologically-significant specific vegetation categories such as xerophyte/steppe taxa (*Artemisia,* Amaranthaceae*, Ephedra, Hippophaë*), altitudinal taxa (*Abies, Betula, Cedrus, Fagus, Picea, Tsuga*), and mesothermic taxa (*Acer*, *Alnus*, *Buxus, Carpinus betulus*, *Carpinus*

orientalis/Ostrya, *Carya*, *Celtis,* Cistaceae, *Corylus*, Ericaceae, *Fraxinus*, *Hedera*, *Juglans*, *Olea*, *Pistacia*, *Phillyrea*, *Pterocarya*, *Quercus* total*, Salix, Tilia, Ulmus, Zelkova*) (Figs. 1.3 and 1.5). Due to their low abundance, the correlation analysis, and according to PCA results (Fig. 1.4a), the Mediterranean/sclerophyllous taxa (Cistaceae, *Fraxinus*, *Olea*, *Pistacia*, *Phillyrea* and *Quercus* evergreen) were included in the group of mesothermic taxa (Fig. 1.5). The aquatic plants were excluded from the total sum of pollen. These categories have been shown to be successful as trustworthy climatic proxy indicators in the Mediterranean region (Altolaguirre et al., 2020).

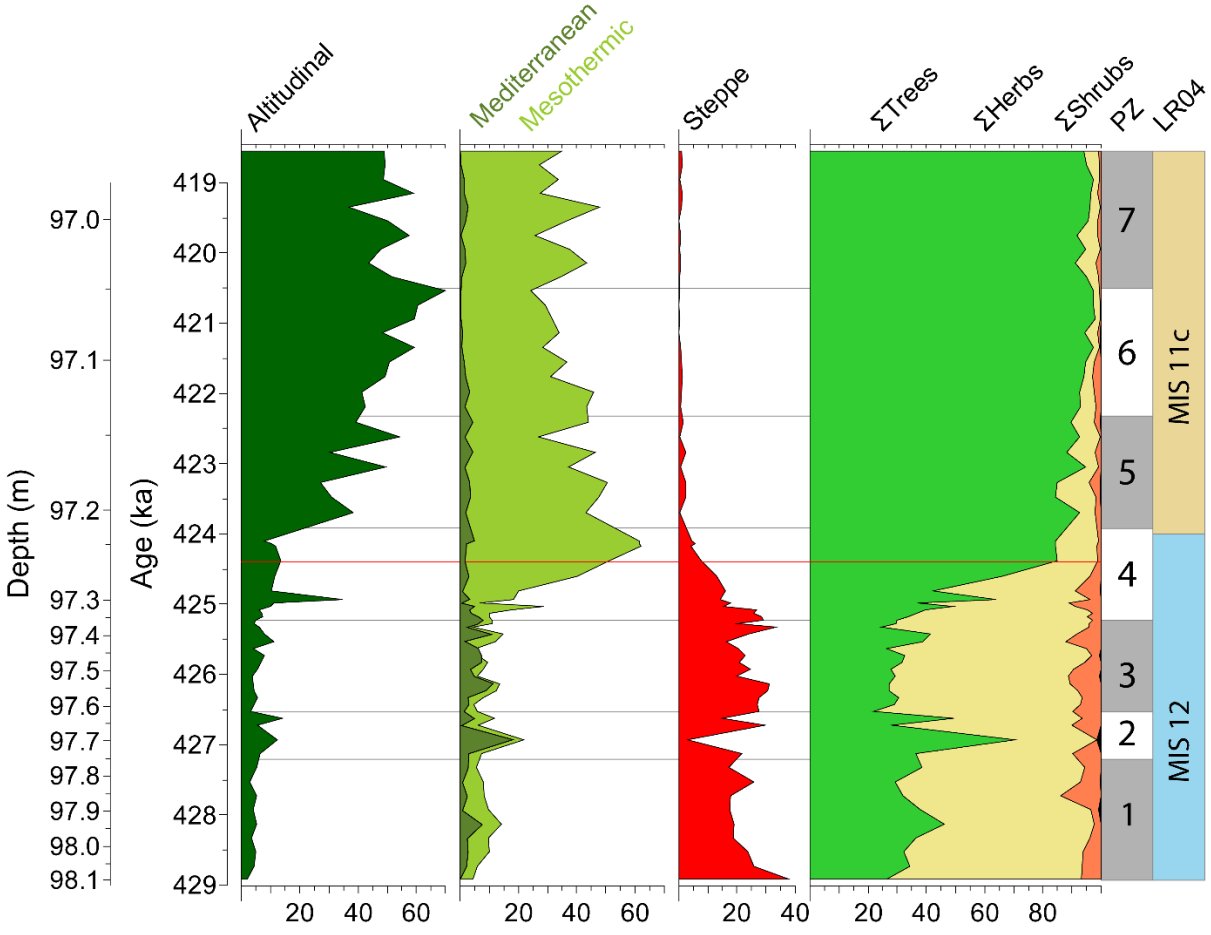

Fig. 1.5.- *Terrestrial pollen data grouped into the different paleoecological associations and the different Pollen Zones (PZ) and Glacial-Interglacial F4-F5 boundary (red line) as reference. The boundary between MIS 12 and MIS 11 suggested by Lisiecki and Raymo (2005) (LR04) is shown by the blue and beige boxes at ~424 ka. The taxa lists are reported in the text.*

1.3.6 Quantitative paleoclimatic reconstruction

A paleoclimatic quantitative reconstruction (mean annual precipitation and temperature) of the Fucino Basin pollen data was done using the C2 software (Juggins, 2007), integrating the Eurasian Modern Pollen Database (EMPDv2) and the paleoclimatic parameters from WorldClim v2.1 database (Fick and Hijmans, 2017) (Figs. 1.6, S1.3, S1.4 and S1.5). This comparison was made using a non-linear unimodal technique, Weighted-Averaging Partial-Least Squares (WA-PLS) regression. This type of model assumes that plant species have their maximum abundances in different climate niches and that niche breadth drives the species environmental

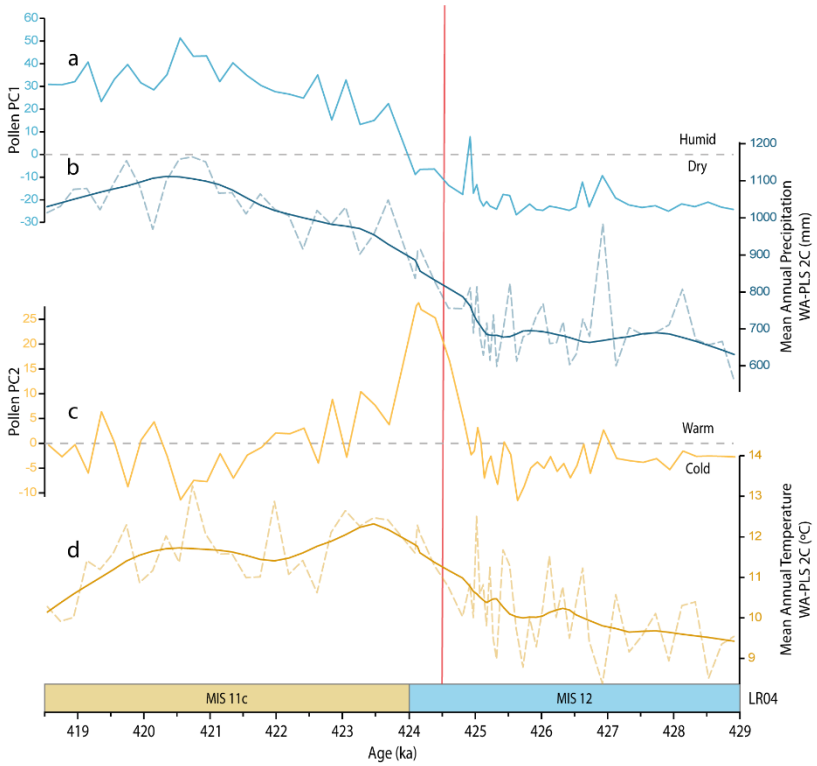

Fig. 1.6.- *Comparison of the pollen Principal Component Analysis (PCA) interpretation and the Weighted-Averaging Partial-Least Squares (WA-PLS) 2C reconstruction. a) Humidity reconstruction from Pollen PC1. The dashed line separates the positive (humid) and the negative (dry) values. b) Precipitation reconstruction from the WA-PLS method. c) Temperature variation from Pollen PC2. The dashed line separates the positive (warm) and negative (cold) values. d) Temperature reconstruction from the WA-PLS method. The dashed lines of b and d are the absolute values estimated by the WA-PLS reconstruction and the continuous smooth line represent the mean values calculated by the LOESS modelling with a value of 0.2. Glacial-Interglacial F4-F5 pollen boundary (red line) and the boundary between MIS 12 and MIS 11 suggested by Lisiecki and Raymo (2005) (LR04)) is shown by the blue and beige boxes at ~424 ka.*

tolerance (Chevalier et al., 2020). To reduce noise, the square-root species transformation was applied to the pollen training set for the pollen-based transfer function. For the construction of WA-PLS regressions, a total of five components were run, however, we used the second component (2C) WA-PLS model under the leave-one-out cross-validation method. Increasing the number of components reduces the root mean squared error, but it can also result in overfitting the data, resulting in a drop of the model predictive value (Ter Braak and Juggins, 1993; Camuera et al., 2022). After this analysis, the results of the coefficient of determination (R^2) were obtained, which determines the reliability of each of the reconstructions (Fig. S1.3). The closer this value is to 1, the more reliable it is (Ter Braak and Juggins, 1993). One difference between the quantitative WA-PLS and the qualitative PCA is that the WA-PLS assumes that the parameters to be estimated are fixed and the data are random observations from some population (Ilvonen et al., 2022), whereas the PCA uses arbitrary initial site scores without environmental parameters (Ter Braak and Juggins, 1993).

We also estimated the relative lake-level changes (Fig. 1.7) taking the formula used in Camuera et al. (2019): Algae total/(Algae total + Aquatic plants + Poaceae). However, this "lake level" qualitative estimation, primarily based on the amount of algae, also depends on trophic conditions of the lake waters and changes in lake bottom morphology.

The Past4 software (Hammer et al., 2001) was employed to determine the correlation between the reconstructions and the pollen data by an univariate correlation analysis, resulting in two statistical values for each pollen and reconstruction, the correlation value (R; a value between 1 and -1 representing a positive or an inverse correlation between the variables) and the statistical significance (p; a value near 0 means that the correlation between the variables is statistically significative, being negligible values higher than 0.05). Every

value of R shown in this study has statistical significance. This software was used also for smoothing the reconstructed precipitation and temperature signals (Fig. 1.6) by LOESS modelling with a value of 0.2.

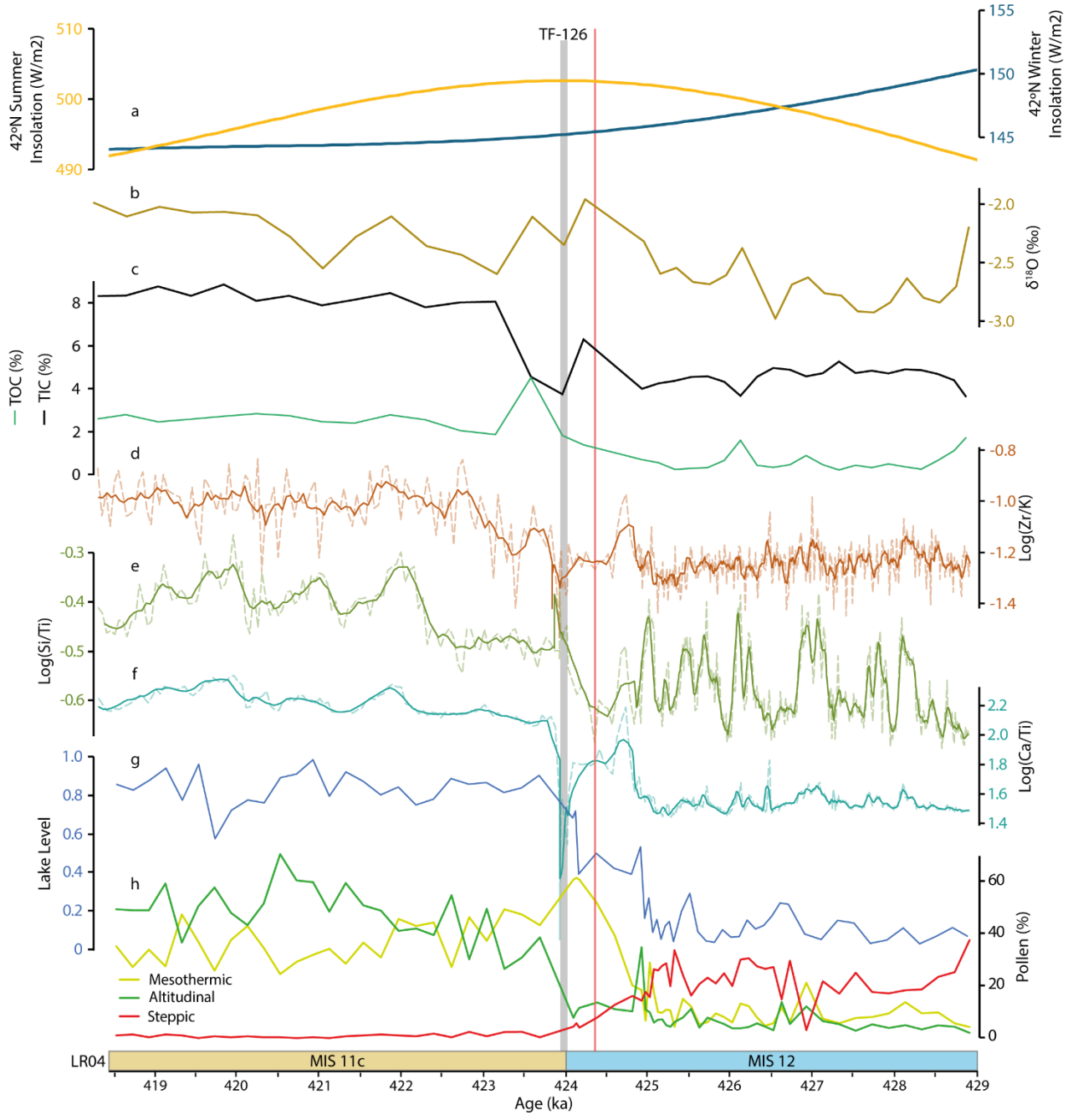

Fig. 1.7.- *Comparison of (a) summer and winter insolation at 42°N (Laskar et al., 2004) (b) δ18O from discrete samples, (c) Total Inorganic Carbon (TIC) (black) and Total Organic Carbon (TOC) (green) from discrete samples, (d) Zr/K, (e) Si/Ti, (f) Ca/Ti geochemical log-ratios from XRF scanning (dashed lines depict the actual values, while the continuous lines represent the mean average value for every 5 data points), (g) lake level according to Camuera et al. (2019) formula and (h) pollen associations percentages of the F5-58. Glacial-Interglacial F4-F5 pollen boundary is marked by the red line and the boundary between MIS 12 and MIS 11 suggested by Lisiecki and Raymo (2005) (LR04) is shown by the blue and beige boxes at ~424 ka. The TF-126 is indicated by the light-grey box.*

1.4 Results

1.4.1 Geochemistry

The XRF analysis provided 462 data points showing substantial changes at the T-V (Fig. S1.2). The age-related fluctuations of the elements can be separated into three intervals:

1) Prior to 424.9 ± 4.4 ka: Si, K, Ti, Fe, Rb and Zr have high constant values, whereas Ca has lower values (Fig. S1.2). The Log(Si/Ti) follows the same pattern as the Log(Ca/Ti) but the fluctuations have a higher amplitude (Fig. 1.7).

2) Between 424.9 ± 4.4 and 423.8 ± 3.8 ka: A transition occurs in which the high values of Si, K, Ti, Fe, Rb and Zr decrease (reverse trend in Ca). During this period, the minimum in Ca and maxima in siliciclastic elements (Fig. S1.2) is caused by the deposition of tephra TF-126 (Monaco et al., 2021).

3) After 423.8 ± 3.8 ka: the concentrations of Ca persist at elevated levels, exhibiting a slight upward trend, whereas Si, K, Ti, Fe, Rb, and Zr demonstrate a marked decline reaching their respective minima. The Log(Zr/K) increased, maintaining relative constant values along this period (Fig. 1.7).

The PCA separated the XRF data into two groups. Positive PCA values correspond to Ca and negative values to siliciclastics (Fig. S1.2). From ~429 to ~425 ka the siliciclastic input increases with respect to the rest of the studied MIS 12. During MIS 11c, the terrigenous input was substituted for Ca-rich sediments.

The TIC from the discrete samples shows an increase between 424.9 ± 4.5 and 423.8 ± 3.8 ka very similar to the XRF Ca data (Fig. 1.7). During the glacial period (before ~424.5 ± 4.0 ka), TIC values are around 5% and increase after G/I transition to 8-9%, which corresponds to ~70% calcite. TOC shows a similar trend, with values below 1%, during the glacial and values exceeding 2% after the transition This patter is also shown in $\delta^{18}O$, with more negative values until ~425 ka and less negative but fluctuating values after the transition (Fig. 1.7).

1.4.2 Pollen analysis

Microscopic examination of the samples from the F4-F5 sedimentary record revealed the good preservation of palynomorphs, with the identification of 58 pollen and 13 NPP taxa. The lower 34 samples (corresponding to MIS 12) are characterised by a high detrital content and have much lower pollen concentrations (~5300 pollen grains/g as average concentration value) than the upper 32, carbonate-rich samples (corresponding to MIS 11c, with ~168000 pollen grains/g as average concentration value) (Fig. 1.3a).

Herbs such as Poaceae, *Artemisia*, Amaranthaceae, and Asteraceae (mainly Asteroideae) dominated the terrestrial landscape during MIS 12 (Fig. 1.3). The rare forest taxa that characterised the surroundings of the Fucino Basin during the MIS 12 glaciation were primarily *Pinus* and cf. *Juniperus*, with some deciduous species such as *Quercus* and *Salix*. After T-V, open vegetation was completely replaced by forest species, primarily

deciduous trees, such as *Quercus*, *Betula*, *Carpinus*, *Corylus*, *Ulmus*, *Acer* and *Abies*. Within the lake, *Pediastrum* and *Botryococcus* algae also increased during the beginning of MIS 11c (Fig. 1.3).

The PCA of the pollen data shows that PC1 represents 81.9% of the total variance of the data, whereas PC2 represents 8.9%. Most taxa have low loadings (less than ± 0.05) except for *Abies*, *Carpinus orientalis/Ostrya*, *Carpinus betulus*, *Corylus*, *Ulmus*, Asteroideae, cf. *Juniperus*, Amaranthaceae, *Pinus*, *Artemisia,* and Poaceae. The positive scores from PC1 correspond to deciduous forest, warm-temperate taxa and *Abies*, and the negative ones corresponds to herbaceous taxa, *Pinus* and aquatics (Fig. 1.4a). Positive values of pollen PC1 mostly occurred after ~425 ka (Fig. 1.4c). The negative pollen PC2 group included herbaceous taxa and *Abies.* Positive pollen PC2 groups the deciduous forest (Fig. 1.4a). Most of the values for PC2 were negative, but positive values showed a distinct maximum between ~425 and ~422 ka (Fig. 1.4d).

In addition, a PCA was performed on the NPPs. The NPP-PC1 represents 67.6% and the NPP-PC2, 27.8% of the variances. The analysis separates three main groups defined by *Pediastrum* (positive NPP-PC1 and positive NPP-PC2), *Botryococcus* (positive NPP-PC1 and negative NPP-PC2) and the third group dominated by spores (negative NPP-PC1) (Fig. 1.4b). The evolution of NPP-PC1 over time seems to be related to pollen PC2 with a centennial-scale delay between their maxima and minima (Fig. 1.4e). The NPP-PC2 shows two main different periods, more stable values, and more abrupt changes, with a boundary at 424.5 ± 4.0 ka.

According to CONISS analysis on pollen data, the pollen diagram was divided into 7 pollen zones (PZ) (Figs. 1.3 and 1.5).

1.4.2.1 PZ-1 (between 428.9 ± 5.0 ka and 427.2 ± 5.0 ka; 98.10-97.76 m)

Herbaceous plants were mainly represented by Poaceae (19.3-31.5%). Steppic taxa predominated, mainly represented by *Artemisia* (8.6-23.5%) and Amaranthaceae (3.4-11.1%). Conifer taxa were dominated by *Pinus* (17.7-27.1%) and cf. *Juniperus* (1.7-10.4%). Deciduous tree forest was composed of *Quercus* deciduous type (1.1-4.1%) and *Salix* (0.3-3.4%), including some small peaks of *Acer* (0.0-2.3%) and *Ulmus* (0.0-1.0%). This subzone had the major representation of aquatic and hygrophilous taxa of all the samples analysed in this study (Cyperaceae: 1.0-4.9%; *Potamogeton*: 0.8-3.0%; *Typha*: 0.0-2.3%).

NPPs rarely occur during this zone.

1.4.2.2 PZ-2 (between 427.2 ± 5.0 ka and 426.6 ± 5.0 ka; 97.76-97.63 m)

During this period, the steppe taxa decreased drastically and mesothermic taxa colonised the area. There was also an increase in altitudinal taxa, mainly dominated by *Abies* (3.8-10.5%). The tree forest, dominated by *Pinus* (16.5-35.3%), *Olea* (0.0-7.5%), *Salix* (1.9-3.0%) and *Corylus* (0.0-3.0%), was more abundant than the herbaceous vegetation. The highest spore concentration occurred in this zone (0.6-6.7%).

1.4.2.3 PZ-3 (between 426.6 ± 5.0 ka and 425.1 ± 4.5 ka; 97.63-97.33 m)

Among herbs, Poaceae dominated this period (17.4-38.9%), followed by the steppe plants *Artemisia* (10.9-26.2%) and Amaranthaceae (2.6-15.7%). The tree population was dominated by *Pinus* (9.3-20.0%) and *Abies* (1.3-5.1%). The abundance of algae increased. *Quercus* deciduous type decreased during the second half of the zone. There were some levels, mainly at the end of the zone, where dinoflagellate cysts occurred.

During PZ-2 and PZ-3 a surprising increase in grains of *Olea* and *Quercus* evergreen type was found (Fig. 1.3). We cannot exclude the possibility of reworked pollen for these zones.

1.4.2.4 PZ-4 (between 425.1 ± 4.5 ka and 423.9 ± 3.8 ka; 97.33-97.22 m)

PZ-4 characterises a transitional period, with the substitution of the steppic (4.0-26.2%) by mesothermic (6.7-61.0%) plants, composed by *Ulmus* (0.0-18.0%), *Quercus* deciduous type (1.2-17.3%), *Acer* (0.3-12.0%), *Corylus* (0.0-7.7%) and *Tilia* (0.0-6.0%). Whereas the deciduous forest increased substantially, the herbs started to disappear in a more gradual way. The change was marked in terrestrial vegetation by a peak of *Abies* (27.6%) and, in the aquatic environment¸ by an increase in *Pediastrum*.

The demarcation between the glacial MIS 12 and the interglacial MIS 11c pollen boundary was established in the middle of this PZ at 424.5 ± 4.0 ka and using a value higher than 75% Arboreal Pollen (AP) according to Allen et al. (2000) and to the Fucino terrestrial pollen CONISS results.

1.4.2.5 PZ-5 (between 423.9 ± 3.8 ka and 422.3 ± 4.0 ka; 97.22-97.14 m)

PZ-5 shows a significant increase in pollen concentration. Altitudinal taxa (26.3-54.3%) dominated by *Abies* (24.7-51.3%) were the most representative, followed by mesothermic taxa (27.0-49.0%). *Carpinus* is abundant in this zone as well as in the following PZ-6 and PZ-7, maintaining constant values through time (~8-10%).

Algae were very abundant with *Botryococcus* peaking slightly later than *Pediastrum*.

1.4.2.6 PZ-6 (between 422.3 ± 4.0 ka and 420.4 ± 3.7 ka; 97.14-97.05 m)

The forest was dominated by *Abies* (39.7-69.0%), which further increased in this zone. The deciduous forest, represented by *Carpinus orientalis*/*Ostrya* (4.7-13%), *Corylus* (1.3-6.7%), *Ulmus* (1.3-5.0%), and *Quercus* deciduous (0.7-5.7%), was also an important component. Steppic taxa were almost absent (0.0-1.3%).

Algae suffered a decrease compared with the previous PZ-5, but they were still abundant.

1.4.2.7 PZ-7 (between 420.4 ± 3.7 ka and 418.6 ±3.6 ka; 97.05-96.95 m)

The *Abies* population remained domain in the forest (34.7-57.8%), however, it experienced a decrease compared with PZ-6. The highest value of *Carpinus orientalis*/*Ostrya* was reached (3.7-18.3%), followed in abundance by *Quercus* deciduous (3.7-9.0%), *Carpinus betulus* (3.3-7.3%), *Corylus* (1.7-6.3%), and *Ulmus* (1.3-6.3%). In this zone, *Botryococcus* (1.6-6.4%) and *Pediastrum* (2.2-15.8%) alternate.

1.4.3 Temperature and precipitation reconstructions

The mean annual precipitation and temperature reconstructions, with coefficients of determination (R^2) of 0.51 and 0.81, respectively, were obtained with the WA-PLS method (Fig. S1.3). The annual precipitation began to rise at 425.2 ± 4.6 ka from ~650 mm and peaked with a short interruption around 420.0 ± 3.6 ka, with estimated values near 1200 mm (Fig. 1.6). The same patterns are observed through time with pollen PC1 (interpreted as a variation in humidity; Fig. 1.4c), but with two main differences, (1) the peak observed by the PCA at 424.9 ± 4.4 ka is not that obvious in the quantitative precipitation reconstruction and (2) the peak at 426.9 ± 5.0 ka is overrepresented in the quantitative reconstruction, due to the low pollen concentration and the appearance of *Abies* in this sample. Both reconstructions are highly correlated with *Abies* population (R_{PCA}=0.98; $R_{WA\text{-}PLS}$=0.91), and *Alnus* (R_{PCA}=0.74; $R_{WA\text{-}PLS}$=0.71), *Carpinus* (R_{PCA}=0.87; $R_{WA\text{-}PLS}$=0.80) and *Corylus* (R_{PCA}=0.67; $R_{WA\text{-}PLS}$=0.74) association and inversely correlated with the steppe taxa (R_{PCA}=-0.89; $R_{WA\text{-}PLS}$=-0.93).

Several drawbacks of the temperature reconstructions could result in unreliable estimations. PC2 explains a very low variance value (8.9%) of pollen data and the positive values correlate with the species forming the deciduous forests, although they do not show the same trend on the graphic representation. PC2 shows a distinct maximum at 424.2 ± 3.9 ka, which corresponds with the beginning of the interglacial. However, PC2 values decreased after this maximum, inferring temperatures similar to those of the glacial period during the rest of MIS 11c (Fig. 1.6). Regarding the WA-PLS temperature reconstruction, it exhibits a positive correlation with groups such as *Alnus* ($R_{WA\text{-}PLS}$=0.59), *Corylus* ($R_{WA\text{-}PLS}$=0.66), *Celtis* ($R_{WA\text{-}PLS}$=0.63), and *Ulmus* ($R_{WA\text{-}PLS}$=0.46), and a negative correlation with steppe ($R_{WA\text{-}PLS}$=-0.59) and herbaceous groups. Moreover, the low concentration of pollen during MIS 12 (~429-425 ka; Fig. 1.3a) hampers reliable quantitative reconstruction. After the onset of the interglacial period, WA-PLS reconstructed temperatures show an opposite trend compared with the precipitation. A first increase in temperatures occurred at around 425.4 ± 4.9 ka from a mean estimated value of ~10 ºC to a maximum of ~13 ºC at 420.7 ± 3.6 ka, but the mean values decreased when estimated precipitation values increased (Fig. 1.6).

1.5 Discussion: Climate and lake level reconstruction in the Fucino area

1.5.1 General remarks

The tephrochronologically independently dated high-resolution Fucino pollen record provides significant regional information about vegetation and climate variations during the interval 429.0 ± 5.0 ka to 418.5 ± 3.6 ka, encompassing the T-V (430.5 ± 1.5 ka to 426.0 ± 2.0 ka; Cheng et al., 2016) and the MIS 12-MIS 11 boundary (424.0 ± 4.0 ka; Lisiecki and Raymo, 2005) and the early stage of the MIS 11c interglacial. At present, the Fucino basin (with an altitude of 650-680 m a.s.l.) is located in an area dominated by grasslands and deciduous forest with old-growth beech forest near the timberline and some conifer patches isolated at higher altitudes. Currently, the Fucino Basin is subjected to intense anthropogenic activity, particularly agriculture, which has significantly altered the composition of the natural/potential vegetation.

Previous studies (e.g. Joannin et al., 2011; Bertini et al., 2015; Camuera et al., 2019) have demonstrated that the abundance of temperate forest taxa serves as a valuable indicator of temperature and precipitation changes over time. In our study, we utilised deciduous and temperate-adapted forest species, such as *Quercus*, *Ulmus*, *Acer*, *Corylus*, and *Pterocarya*, as proxies for temperature (Fig. 1.4a) (e.g. Joannin et al., 2008). Notably, *Quercus* species have proven to be excellent proxies for distinguishing warm-humid from cold-arid paleoclimate phases (e.g. Denk et al., 2001; Joannin et al., 2008). *Abies* can also serve as proxy for precipitation and humidity (Alba-Sánchez et al., 2010), although disentangling temperature from precipitation signals can be challenging for certain species (Fig. S1.4). Previous palynological investigations indicate that increases in *Abies* abundance typically occur after the thermal maximum of interglacial periods and during a post-temperate phase, often associated with decreased summer insolation resulting in cooler conditions within overall still humid conditions (e.g. Tzedakis, 2007). Additionally, the abundance of herbaceous and steppic xerophytic plants (such as *Artemisia*, *Ephedra*, *Hippophäe*, and Amaranthaceae) can be utilised as indicators of cold and arid conditions (e.g. Fauquette et al., 1998; Tzedakis, 2007).

The XRF Ca values follow the same trend as the altitudinal taxa and estimated lake-level changes, whereas siliciclastic elements show variations similar to xerophytes (Figs. 1.7 and S1.2). The altitudinal taxa show some delay with respect to the Ca values, because Ca seems to be related with the lake productivity and the increase in the lake level. The lake productivity started to increase at the same time deduced by the rise in mesothermic taxa indicating the increase in temperature and, as consequence, enhanced eutrophication of the lake waters. At ~424.3 ± 4.0 ka, the altitudinal taxa indicate an increase in precipitation, which is also shown in the quantitative precipitation reconstruction (Figs. 1.6 and 1.7).

The abundance of algae (*Botryococcus, Pediastrum, Spirogyra, Zygnema*) is conditioned by lake level and shore surface area (Jiménez-Moreno et al., 2023), providing information about lake depth, availability of nutrients in the lake, and productivity. *Pediastrum* is a colonial green alga that indicates, for example, deeper lake water conditions (Fig. 1.4b and f; Nielsen and Sørensen, 1992; Anderson et al., 2020; Jiménez-Moreno et al., 2023) or eutrophication of the lake waters (Xiang et al., 2021). *Botryococcus* is a colonial green microalga

growing in shallower water but is also affected by nutrient conditions (Fig. 1.4b and e; (Guy-Ohlson, 1992; Jiménez-Moreno et al., 2023). The Log(Si/Ti) and Log(Ca/Ti) help to corroborate the productivity data provided by the algae community, as they are mostly the product of the activity and abundance of siliceous algae and calcite precipitation in the lake related to water temperatures, nutrient availability, and lake productivity, showing similar variations through time. During the dry and cold glacial MIS 12, the algae abundance was very low (Fig. 1.4). With the beginning of the interglacial period, the occurrence of algae increased, which matches with increasing TOC and TIC values, representing organic matter and authigenic calcite precipitation due to increasing lake productivity and temperatures. Strong variations in *Pediastrum* and *Botryococcus* values may indicate lake-level fluctuations, which are probably relatively low in magnitude (few meters only) but have a distinct impact on algae occurrences and nutrient conditions.

1.5.2 MIS 12 glaciation, T-V and beginning of MIS 11c (PZ-1 – PZ-5)

The full MIS 12 glacial condition are documented in Fucino F4-F5 sediment core between 429.0 ± 5.0 ka to 427.0 ± 5.0 ka, when vegetation was dominated by xerophytic and herbaceous taxa and *Pinus*, indicating cold and dry climate conditions, as confirmed by the steppic taxa association (Figs. 1.4a and 1.5). The mean temperature value reconstructed for this period in Fucino Basin was less than 10 ºC with a mean annual precipitation between 600 and 700 mm (Fig. 1.6). The Fucino estimated temperature and precipitation values show similar trends compared to Lake Ohrid mean annual temperature and precipitation (Kousis et al., 2018)

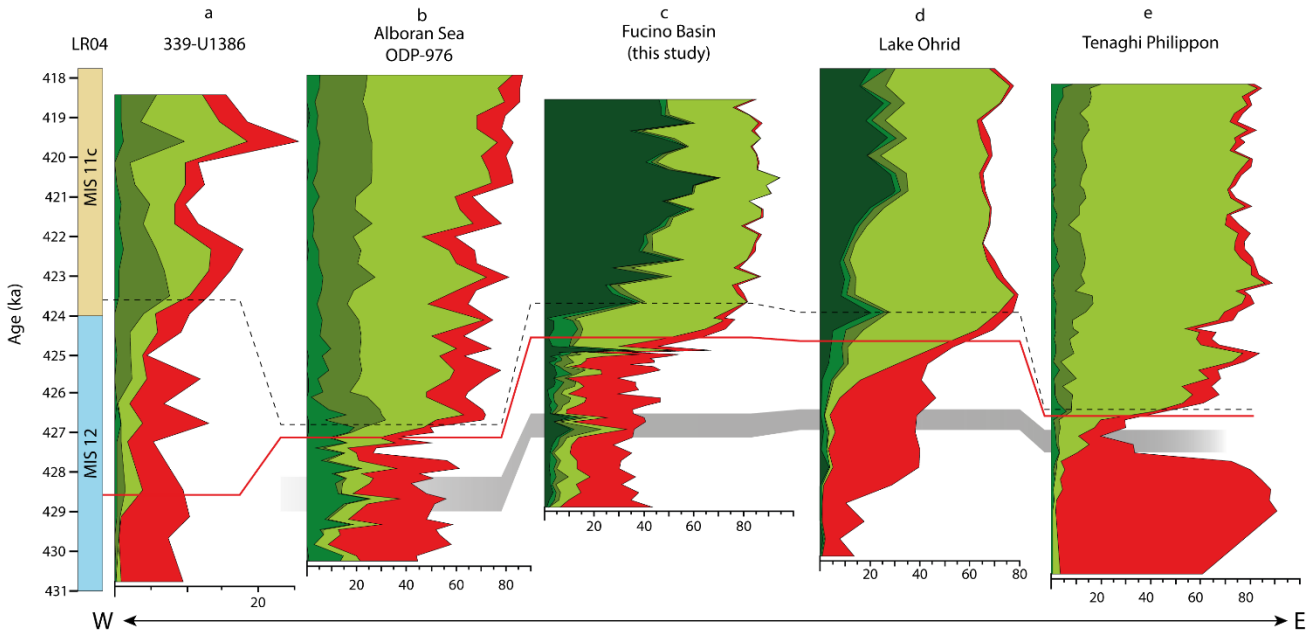

Fig. 1.8.- *Comparison of pollen records from (a) Iberian Margin (U1386 site; Hes et al., 2022), (b) Alboran Sea (ODP-976 site; Sassoon et al., 2023), (c) Fucino Basin (F4-F5 record; this study), (d) Lake Ohrid (Kousis et al., 2018; Koutsodendris et al., 2020), and (e) Tenaghi Philippon (Koutsodendris et al., 2023a, 2023b). Dark-green: Abies population; Green: altitudinal taxa without Abies; Brownish-green: Mediterranean taxa; Yellow-green: mesothermic taxa; Red: steppic taxa. The red line indicates the MIS 12-11c limit defined by their respective studies. The grey box correlates the PZ-2 defined in Fucino Basin. The dashed line correlates the beginning of the altitudinal taxa increase (for the continental eastern records) and the beginning of the Mediterranean taxa increase (for the marine western records).*

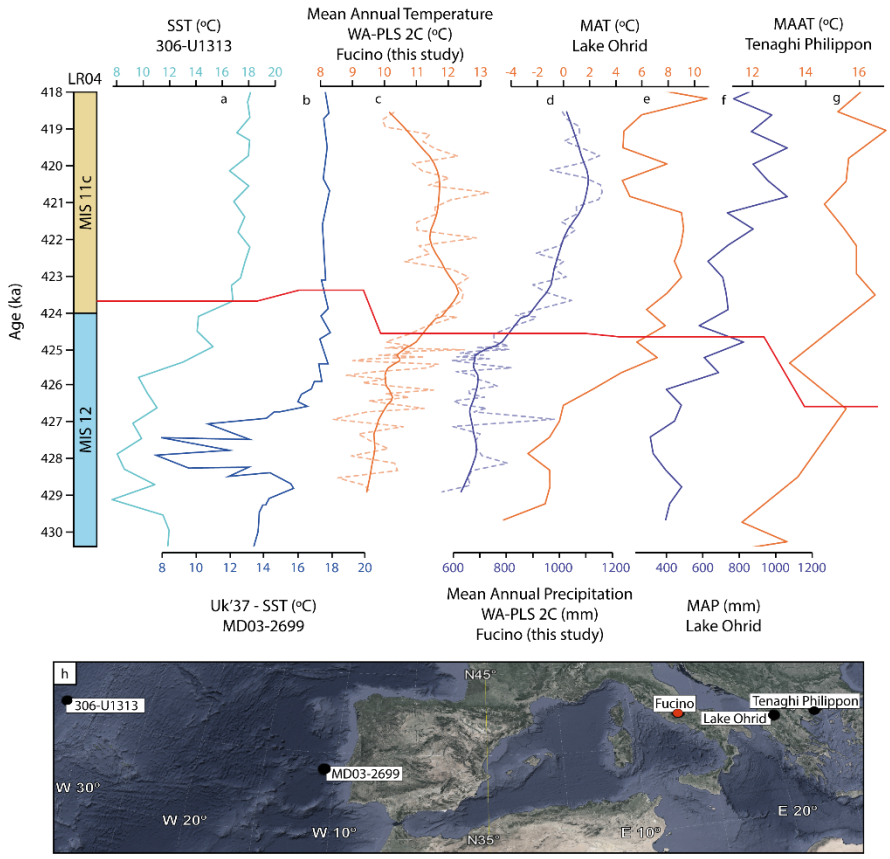

Fig. 1.9.- *Comparison of quantitative reconstructions of Sea Surface Temperature (SST) and continental temperatures and precipitation. a) North Atlantic SST from an alkenone based reconstruction (Naafs et al., 2013, 2014). b) Iberian margin SST from alkenones ($U^{k'}_{37}$ index) (Rodrigues et al., 2011). c) Mean Annual Temperature from Fucino Basin using the WA-PLS method from pollen data (Fig. 1.6; this study). d) Mean Annual Precipitation from Fucino Basin using the Weighted-Averaging Partial-Least Squares (WA-PLS) method from pollen data (Fig. 6; this study). e) Lake Ohrid Mean Annual Temperature (MAT) using the Modern Analogue Technique from pollen data (Koutsodendris, 2020). f) Lake Ohrid Mean Annual Precipitation (MAP) using the Modern Analogue Technique from pollen data (Koutsodendris, 2020). g) Tenaghi Mean Annual Air Temperature (MAAT) calculated by GDGTs (Ardenghi et al., 2019). h) Location of the sites. The red line marks the MIS 12-MIS 11c boundary defined in the different studies.*

and Tenaghi Philippon mean annual air temperature (Ardenghi et al., 2019), being the Lake Ohrid the coldest reconstruction because of its slightly higher altitude and continentality (Fig. 1.9).

Throughout the glacial period, the lake level and lake productivity were at a minimum (Fig. 1.7). Low Log(Zr/K) and siliciclastic elements during this period (Fig. 1.7 and S1.2) indicate restricted erosion of fine-grained materials and inflow into the lake, which matches with high abundances of steppic taxa and implies moderate to low precipitation.

The transition from MIS 12 to MIS 11c, involved an increase in global temperatures as summer insolation levels raised (Laskar et al., 2004; Bouchet et al., 2023). This rapid climatic shift drove one of the biggest increases in global biosphere productivity (Brandon et al., 2020), changing dramatically the terrestrial vegetation cover, leading to the replacement of the steppic landscape by a dominant forest all along the Mediterranean region. This can be observed in the pollen data from the Iberian Margin (Hes et al., 2022), Alboran Sea (Sassoon et al., 2023), Lake Ohrid (Kousis et al., 2018) and Tenaghi Philippon (Koutsodendris et al., 2023a) (Figs. 1.8 and 1.9).

At Fucino, a humid event (PZ-2) occurred between 427.0 ± 5.0 ka and 426.6 ± 5.0 ka, indicated by a tree forest increase and steppic taxa decrease (Fig. 1.5). Also, the Log(Si/Ti) and Log(Ca/Ti) values increased, indicating higher temperatures and more rainfall. The peaks would correspond with an increase in lake productivity (more algae) and calcite precipitation triggered by warmer temperatures, more nutrients and more Ca ion supply for the catchment (e.g. Wagner et al., 2019). This humid event seems also to have occurred in the Alboran Sea pollen record and is shown by an increase in altitudinal taxa and a slight reduction of steppic taxa (Sassoon et al., 2023) and at Lake Ohrid (Kousis et al., 2018; Koutsodendris et al., 2019; Donders et al., 2021)

(Fig. 1.8), and could point to a wider regional climatic event. Following this event, the *Olea* percentage increased. This species is associated with warmer conditions, but in our study, it appears at the end of the glacial period, which could be the result of reworking and their percentage exaggeration due to low pollen concentration. Other mesothermic taxa increased during this event, but mostly due to enhanced humidity (Figs. 1.6 and S1.2). This is interpreted from the composition of the vegetation, mainly composed of deciduous taxa, with greater needs for water. Therefore, this record confirms the importance of relative humidity (precipitation *versus* evapotranspiration) in shaping the vegetation in the Mediterranean region, where climate is primarily influenced by temporal and seasonal precipitation variability (Ilvonen et al., 2022). The minimum temperature value reconstructed may correspond to the highest percentage of *Pinus* (*Pinus* total) during this zone (according to EMPDv2; Davis et al., 2020), which occurs in areas with mean annual temperatures below 10°C (Fig. S1.4). These cold conditions may have influenced the relationship between evapotranspiration and precipitation, favouring the increase in humidity. The Log(Zr/K) value increases during this time as well as those "warm" pollen occurrences in the record, indicating an increase in erosion (Fig. 1.7), which agrees with the high precipitation values estimated from the quantitative reconstruction (Figs. 1.6 and 1.9).

The steppe taxa resume their dominance in the area following this event ending at 426.8 ± 5.0 ka, indicating further cold and arid conditions during the end of T-V (Fig. 1.5). Analysing the variation of xerophytic taxa during the end of the glacial period, some variability can be elucidated, with a slightly warmer and wetter period between two colder periods (with higher values of steppic taxa) following a "W" pattern characteristic of the Heinrich type events (Ht) (Singh et al., 2023). This Ht could correspond with the Ht4 identified by Rodrigues et al. (2011) at Iberian Margin with low Sea Surface Temperature (SST) values registered for this time (Fig. 1.9). The Ht are associated with SST cooling and reduction in Atlantic Meridional Overturning Circulation (AMOC), favouring the southward displacement of the Polar Front to the mid-latitudes of the North Atlantic (López-Martínez et al., 2006; Rodrigues et al., 2011, 2017; Singh et al., 2023) and they are associated within the beginning of terminations stages (e.g. Cheng et al., 2009). However, it is unclear if these terminal Ht are 'required' to start a termination, or if they are the result of the deglacial collapse of glacial ice sheets, and as such, consequences rather than causes of the glacial–interglacial changes (Hodell et al., 2008; Vázquez Riveiros et al., 2013). The Ht4 was the most extreme cold event registered in the SST at the Iberian Margin (Rodrigues et al., 2011), indicating the beginning of the T-V. This event has also been identified in the North Atlantic (Naafs et al., 2014), showing that it is of global importance (Hodell et al., 2008). We observe those temperature-humidity changes in the pollen record being able to define the duration of T-V just after the PZ-2 until the initial part of the PZ-4 (Figs. 1.3 and 1.5) for the Fucino pollen record.

After the T-V there was an initial succession when the steppe percentage began to decrease, a peak of mesothermic taxa was reached at 425.0 ± 4.5 ka, followed by a peak of altitudinal taxa (primarily *Abies*; Fig. 1.5). With a higher amplitude, the same transition can be observed between 424.2 ± 3.9 ka and 420.6 ± 3.9 ka, with mesothermic vegetation increasing and reaching a peak related to the increase and maxima in summer insolation (Fig. 1.7), the xerophytes then reached their minimum, and finally, the mesothermic vegetation was

replaced by altitudinal taxa, which became dominant. The duration of the warmer period could be evidenced by the pollen PC2 maxima but is not reliable in intensity (Fig. 1.4d and Fig. 1.6c). The increase in the Log(Zr/K) indicates sedimentation of coarser material, which means a higher transport energy, probably related to more rainfall and higher activity of the inlet streams. This detrital influx increased in a opposite pattern compared to xerophytes, whereas the lake level and its productivity (Log(Ca/Ti), Log(Si/Ti) and NPP PC1) increased abruptly (Figs. 1.4e and 1.7).

During this climatic transition, the mesothermic taxa occurring at Fucino were mainly composed by *Quercus* deciduous, *Ulmus*, *Acer,* and *Tilia,* which are more related to warmer and more humid conditions than the previous steppic taxa. Subsequently, those deciduous taxa were replaced by *Carpinus*, *Carpinus orientalis/Ostrya*, *Corylus*, *Celtis* and *Alnus*, which are related to more humid conditions (according to the PCA) (Fig. 1.4a) (Denk et al., 2001). A similar substitution of the deciduous taxa occurred in Lake Kopais (Southeeast Greece; Okuda et al., 2001) and at Lake Ohrid (Kousis et al., 2018). This confirms the typical G/I cycle described by Tzedakis, (2007) and Jiménez-Moreno et al. (2013), where the transition period into the interglacial is warmer and drier, followed by a more humid forest in the temperate phase of the interglacial. Lake Ohrid seems to exhibit a more similar vegetation evolution to Fucino than to other Mediterranean records, with a similar beginning of the T-V with the decline of the steppic taxa and their replacement by mesothermic taxa (Fig. 1.8). The quantitative reconstructions for this transition estimated an increase in precipitation values, corroborating the wetter climate for Fucino Basin and Lake Ohrid than other Mediterranean pollen records, such as Tenaghi Philippon and Alboran Sea, where the altitudinal taxa did not have enough representation. The rise in Fucino lake´s level, the increase in humidity and great abundance of altitudinal taxa may have been caused by the deglaciation of the mountain glaciers around the Fucino basin (Cheddadi et al., 2005; Giaccio et al., 2019). The comparison of the mean annual temperatures estimations with other Mediterranean records shows that Lake Ohrid temperatures were lower than at Fucino during the glacial period, but after the T-V both regions reached similar temperature values (Fig. 1.9).

1.5.3 MIS 11c (PZ-6, PZ-7)

Compared with other paleoclimatic estimations following the T-V, such as the SST from Iberian Margin (Rodrigues et al., 2011) or North Atlantic SST (Naafs et al., 2014), where temperatures increased from ~13 ºC to ~17 ºC (Fig. 1.9) relatively abruptly the estimated temperatures in the Fucino Basin continental record increased more gradually from ~9.5 ºC to a maximum of 13.0 ºC (Fig. 1.6). Estimated temperatures in Lake Ohrid (Kousis et al., 2018) increased from ~1.5 ºC to a 10 ºC at around 423 ka (Fig. 1.9), showing a more drastic change in temperatures during this time. The temperatures reconstructed from Tenaghi Philippon (Ardenghi et al., 2019) did not experience such an abrupt change, depicting a temperature difference from the beginning to the end of T-V of ~2.5 ºC, a temperature range similar to the Fucino Basin reconstructions. Precipitation during MIS 11c in Fucino Basin increased gradually reaching annual values near 1200 mm at around 421.0 ± 4.2 ka

(Fig. 1.6). This increase in precipitation to similar values is also observed in Sulmona Basin (Italy; Regattieri et al., 2016). It could be explained by the orographic effect, reaching higher precipitation values at the summit areas of the mountain's drainage basins (Regattieri et al., 2016). The records form Fucino Basin and Lake Ohrid also indicate similar estimated precipitation patterns (Fig. 1.9), with MIS 11c being one of the highest estimated values recorded in Lake Ohrid over the last 800 ka (Wagner et al., 2019). An increase in the pollen concentration, with *Abies* being the dominant pollen taxon, occurred during this interglacial (e.g. Brandon et al., 2020), coupled with an elevated sedimentation rate and diminished terrigenous input.

The altitudinal taxa during MIS 11c in Fucino Basin exhibit a consistent increase, culminating in a peak of *Abies* of about 69% at 420.5 ± 3.8 ka. This trend follows, with some delay due to the vegetation response to the external climatic parameters, the summer insolation through time (Fig. 1.7) and can also be observed at Lake Ohrid (Fig. 1.8). *Abies* populations are in general restricted to moist mountainous habitats (Alba-Sánchez et al., 2010), but such a high percentage of *Abies* has never been observed previously in other pollen records from in Europe during an interglacial. The increase of *Abies* at the beginning of the interglacial is less than 20% and 30% at Tenaghi Philippon (Pross et al., 2015) and at Lake Ohrid (Kousis et al., 2018) respectively, as *Abies* pollen grains cannot be transported for long distances by the wind due to their large pollen size, and hence their occurrence in the fossil record indicates proximity to the pollen source (Erdtman, 1969; Moreno-Amat et al., 2017). This means that *Abies* constituted the main forest species up to high altitudes in Fucino Basin during the MIS 11c interglacial. Previous studies on the present-day *Abies* ecology show that *Abies* growing at lower elevations has a much broader ecological amplitude (including pioneer characteristics and drought tolerance) than those growing at higher elevations (Dobrowolska, 1998; Burga and Hussendörfer, 2001; Schmidl et al., 2005; Kozáková et al., 2011), which could explain why *Abies* is so abundant in the Fucino Basin during the MIS 11c interglacial. However, *Abies* is less abundant in other records, which could indicate that the abundance is strongly influenced by the local orography and less by precipitation.

The comparison of the central Mediterranean pollen records shows an abrupt increase of Mediterranean taxa just after the T-V, which is only marginally represented at Fucino Basin and Lake Ohrid (Fig. 1.8). We can conclude from this observation that the Mediterranean region experienced an increase in temperatures and an abrupt change in vegetation during the G/I transition, but the central longitudinal Mediterranean area was more influenced by the balance of precipitation and evapotranspiration, with high precipitation values at that time (Figs. 1.8 and 1.9).

1.6 Conclusions

The palynological record from the Fucino F4-F5 sediment core interval, independently dated between 429.0 ± 5.0 ka to 418.5 ± 3.6 ka, permitted us to reconstruct vegetation and environmental changes over the late MIS 12 glacial, the glacial Termination V (T-V), and the early MIS 11c interglacial, one of the major changes of Quaternary Earth's climatic system history.

The MIS 12 in Fucino Basin was characterised by a very dry and cold climate evidenced by the abundant steppic taxa.

Centennial-scale variability seems to characterise the Fucino pollen record in glacial MIS 12, with Heinrich-type events identified withing the course of the T-V and highly variable mean-annual temperature and precipitations, which were 10.0-9.5 ºC and 700-650 mm, in average. In comparison with other Mediterranean pollen records, this reveals a large regional variability.

A relative humid event occurred between 427.0 ± 5.0 ka and 426.6 ± 5.0 ka and led, to a decrease in steppic taxa and an increase in tree forest from less than 20% to almost 90%, despite minimal astronomical forcing.

The onset of warmest, interglacial conditions at Fucino, demarcated by the increase in mesothermic taxa, is independently-dated to 424.5 ± 4.0 ka, which corresponds with the MIS 12/11 transition at 424 ± 4.0 ka in the benthic $\delta^{18}O$ record.

During the MIS 11c interglacial, the mean-annual temperatures and precipitations were lesser variable, compared with MIS 12 glacial period. The temperatures reached their maximum of ~12.5 ºC during the early stage of the MIS 11c interglacial at 423.5 ± 3.8 ka, to then gradually decreased to ~10.0 ºC at 418.5 ± 3.6 ka, while precipitations increased more gradually from ~800 mm/yr at the very beginning of the MIS 11c to a maximum of 1200 mm/yr at 421.0 ± 4.2 ka.

Overall, during the studied interval, the observed variability of the vegetation of the Mediterranean region was mainly controlled by a change in the hydrological regime and balance, which, in turn, was led by oceanic-atmospheric and precipitation/evaporation dynamics, despite minimal astronomical forcing.

Chapter 2: Vegetation dynamics during MIS 11 in Fucino Basin

- Vera-Polo, P., Sadori, L., Jiménez-Moreno, G., Masi, A., Giaccio, B., Zanchetta, G., Tzedakis, P.C., Wagner, B.. Vegetation and climatic evolution during the MIS 11 interglacial deduced from the first high-resolution and independently dated pollen record of the Fucino Basin, central Italy.

Vegetation and climatic evolution during the MIS 11 interglacial deduced from the first high-resolution and independently dated pollen record of the Fucino Basin, central Italy.

Vera-Polo, P.[a b], Sadori, L.[a], Jiménez-Moreno, G.[b], Masi, A[a], Giaccio, B.[c d], Zanchetta, G.[e], Tzedakis, C[f], Wagner, B[g]

a Dipartimento di Biologia Ambientale, University of Rome "La Sapienza", Rome, Italy

b Departamento de Estratigrafía y Paleontología, Universidad de Granada, Granada, Spain

c Istituto di Geologia Ambientale e Geoingegneria, CNR-IGAG, Monterotondo, Rome, Italy

d Istituto Nazionale di Geofisica e Vulcanologia, INGV, Rome, Italy

e Dipartimento di Scienze della Terra, University of Pisa, Pisa, Italy

f Environmental Change Research Centre, Department of Geography, University College London, London, UK

g Institute of Geology and Mineralogy, University of Cologne, Cologne, Germany

Abstract

The period between 426 ka and 396 ka, which is part of the Marine Isotope Stage 11 (MIS 11, ca. 424-367), is considered an orbital analogue to the Holocene without human-induced impacts and is designated as MIS 11c in marine records. Here, we present high-resolution pollen and geochemical data from the tephrochronologically constrained Fucino record, Central Apennines, allowing a detailed characterization of local and regional paleoenvironmental and paleoclimatic changes between 427-389 ka, covering the latest part of MIS 12 and most of MIS 11. This record is characterised for having one of the few radiometrically constrained chronologies of MIS 11. The abrupt climatic transition from cold and dry conditions of MIS 12 to a warm and humid interglacial climate occurred at ~424.5 ka at Fucino. It is evidenced by a shift from herbaceous and steppe vegetation to mesothermic and altitudinal forests. Notably, *Abies* species dominated the vegetation of the surroundings of the Fucino Basin during MIS 11c, indicating humid conditions, corroborated by a relatively high lake level estimation. Similar humid conditions for the MIS 11c interglacial have been documented in other central Mediterranean sites at similar altitudes, such as Lake Ohrid and Ioannina. The Fucino Basin high-resolution pollen record shows that the mesothermic and altitudinal taxa were highly influenced by insolation fluctuations, allowing to distinguish regional- from global-scale climate changes during MIS 11c interglacial, which was periodically interrupted by drier and colder events. One of those drier evets happened in Fucino between 415 ka and 413 ka. This event, firstly described in lacustrine pollen records, separates the two MIS 11c precessional cycles and could be globally correlated with a decrease in sea surface temperatures and drier periods identified in other lacustrine pollen records.

Key words: Pollen record, Central Italy, Climatic change, MIS 11, Mediterranean region, Glacial-Interglacial cycle

2.1 Introduction

The study of past interglacial periods serves as a valuable fossil reference for a better understanding of our current climate change and its underlying mechanisms, identifying key factors that influence the climate system without the human activity influence.

The interglacial period MIS 11 (ca. 426-367 ka; Ardenghi et al., 2019) with its substage (MIS 11c, ~426-396 ka) is suggested to be the most appropriate climate analogue for the past 500 kyr of the Holocene period (Tzedakis, 2010; Candy et al., 2014), due to its similar orbital configurations (McManus et al., 2003; Ardenghi et al., 2019), its weak precessional variations (Berger and Loutre, 2003) and large magnitude glacial terminations (EPICA Community Members, 2004; Tzedakis, 2010), but without human induced impacts (Loutre and Berger, 2000; Cheddadi et al., 2005; Tzedakis et al., 2022; Sassoon et al., 2023). It stands out in comparison with other Quaternary interglacials because it occurred after one of the most extreme climate changes, known as the Mid-Brunhes Event (MBE) (Rodrigues et al., 2011; Tzedakis et al., 2022), following one of the most severe cold and arid glacial periods (MIS 12) of the last 800 ka (Hu et al., 2024), with a significant expansion of the ice sheet and the deposition of till deposits across northern Europe (Ehlers and Gibbard, 2008; Ardenghi et al., 2019; Tzedakis et al., 2022).

MIS 11 is traditionally subdivided into three climatic substages, two warm stages (MIS 11a and MIS 11c) separated by a colder one (MIS 11b) (Hrynowiecka et al., 2019). This nomenclature is adopted by this study and most of the palynological studies in the Mediterranean region (e.g. Oliveira et al., 2016; Kousis et al., 2018; Sassoon et al., 2023; Koutsodendris et al., 2023a). In terrestrial pollen records, determining the exact chronology and duration of these substages based on vegetation change is challenging, because of the intrinsic difficulties in the dating of continental sedimentary successions. Additionally, the direct comparison to marine isotopic records thus is highly uncertain and speculative (Tzedakis et al., 1997; Koutsodendris et al., 2014), due to the different chronological methods used and their intrinsic uncertainties.

The MBE separates the earlier low-amplitude from the later high-amplitude Glacial-Interglacial (G/I) cycles, being MIS 11c the first high-amplitude interglacial. MIS 11c is also considered unusually warm for the last million years (Rodrigues et al., 2011), despite the low values of incoming insolation and eccentricity (Laskar et al., 2004; Rodrigues et al., 2011; Cheng et al., 2016). The discrepancy between the high-amplitude deglacial warming at the beginning of the MIS 11c interglacial and the weak astronomical forcing is known in the literature as the "Stage 11 problem" (Imbrie et al., 1993), questioning the orbital theory of Pleistocene G/I cycles in a fundamental way (Paillard, 2001; Berger and Wefer, 2003; Tzedakis et al., 2017, 2022). The mismatch between modest insolation forcing and the pronounced climatic response during this transition needs further investigation to uncover the mechanisms behind such climatic complexities (Huybers, 2006; Tzedakis et al., 2022).

The complex interplay of tectonics, volcanism, climate variability and lacustrine sedimentations in Mediterranean region offers a unique setting to investigate the dynamics of the G/I cycles (Tzedakis et al.,

1997). Mediterranean pollen records provide important insights into the region's vegetation and climatic history, because they show significant variability over time, representing the change of vegetational ecosystems as a response to climate variations (e.g., Bertini, 2010; Valsecchi et al., 2012; Desprat et al., 2013; Peyron et al., 2013; Donders et al., 2021). The proximity of the previously studied Mediterranean pollen sites (e.g. Balkan Peninsula; Koutsodendris et al., 2019, 2023a; Donders et al., 2021) to refuge areas in which climate sensitive plant taxa persisted during cold stages (Bennett et al., 1991) makes them very interesting to investigate climate and environmental variability, as they are characterised by no significant migrational lags (Magri and Tzedakis, 2000). Previous studies from this area revealed that glacial periods were characterised by reductions in tree populations and environments dominated by open steppe vegetation, whereas warm and humid periods, corresponding to interglacial phases, were marked by more forested landscapes (Cheddadi et al., 2005; Kousis et al., 2018; Hu et al., 2024).

The Fucino Basin, located in central Italy, serves as a crucial nodal point within the Middle Pleistocene paleoclimatic records. The Fucino lacustrine sequence is particularly significant, as it offers a central Mediterranean reference point with an independent radioisotopic chronology and uniquely encompasses the MIS 12–MIS 11 interval (Monaco et al., 2021). Here we extend the high-resolution pollen and geochemical investigations of the Termination V (T-V), i.e. the transition from MIS 12 to MIS 11, in the Fucino sediments (Vera-Polo et al., 2024) to nearly all the MIS 11, in order to get a better understanding of short-term climate change during the best known analogue of the Holocene.

2.2 Study Site: Fucino Basin

2.2.1 Geology

The Fucino Basin (Abruzzo; 42º 00' 00" N; 13º 30' 00" E) is located at 650 m above sea level (m a.s.l.) and is surrounded by the Central Apennine's highest peaks such as Monte Velino (2486 m a.s.l.) and Monte Sirente (2348 m a.s.l.), which hosted mountain glaciers during glacial periods (Giraudi and Giaccio, 2015). It is one of the largest inter-Apennine tectonic depressions (~900 km^2) developed during the Plio-Quaternary extensional phase within the earlier fold-and-thrust belt system (Cavinato et al., 2002). The extensional tectonics primarily acts along a N110º-140º axis high angle faults (Galadini and Galli, 2000; D'Agostino et al., 2001; Galadini and Messina, 2004; Patacca and Scandone, 2007; Giaccio et al., 2019; Mondati et al., 2021). Lake Fucino formed during the Late Pliocene - Early Pleistocene along the depression's lowermost part, covering approximately 140 km^2 with a maximum water depth of 20 m, and was Italy's third largest lake (Mannella et al., 2019; Caielli et al., 2023) (Fig. 1.1). The differential movements along the Fucino Fault System (FFS) (active since the Pliocene), resulted in the formation of a half-graben basin with rising sedimentation rates from West to East and an 900 m-thick succession of Plio-Quaternary fluvial sediments and fine-grained lacustrine carbonated deposits in the depocenter (Galadini and Galli, 2000; Cavinato et al., 2002; Galadini and Messina, 2004; Giaccio et al., 2017, 2019; Mannella et al., 2019). These sedimentary deposits partly originated from the erosion of the

Triassic-Miocene carbonate sequences that form the basin's bedrock and the surrounding high relief (ISPRA, 1934, 1939, 1942, 1967; Mondati et al., 2021; Caielli et al., 2023). More than 130 of tephra layers from peri-Tyrrhenian volcanoes explosive activity occur within the fine-grained fluvio-lacustrine Fucino Basin sedimentary sequence and serve as precise chronological markers for the last 430 ka (Giaccio et al., 2017, 2019; Monaco et al., 2021, 2022; Leicher et al., 2023, 2024). Lake Fucino was definitively artificially drained in 1875 for agricultural purposes (Giaccio et al., 2017).

2.2.2 Climatic setting

The complex orography of the Fucino Basin and is surrounding and a considerable influence of the Mediterranean Sea determine the current climate conditions in the area (Silvestri et al., 2022). The Fucino Basin's climate is typically Mediterranean (warm and dry summers and cold and humid winter; Lionello et al., 2006) with continental characteristics, according to historical regional data from the meteorological network (Peyron et al., 2013) and data acquired from the nearby Borgo Ottomila meteorological station (652 m a.s.l.). According to this meteorological station (https://en.climate-data.org/europe/italy/abruzzo/borgo-ottomila-1068722/, last access: 02 October 2024), monthly average temperatures exceed 10º C from April to October, reaching maximum temperatures of 18 to 21º C in July and. From November to March, monthly average temperatures are below 10º C, with January being the coldest month. The mean annual temperature for Fucino Basin is ~11.1 ºC. Annual precipitation averages 600 to 750 mm in the lowlands and 900 to 1200 mm in the piedmont zone August (average temperature data from 1991 to 2021).

2.2.3 Potential natural vegetation distribution

The climatic and geographical settings of the Fucino Basin and its catchment result in complex vegetation zone distributions, which are today biased by human perturbances (Frate et al., 2018).

Grasslands occur in the basin's lower and flatter areas, extending to the western side of the surrounding reliefs due to pluviometric shading from the main E-W wind pattern (Tomassetti et al., 2003). The potential natural grassland in this area consists mainly of hygrophilous and hydrophytic freshwater plants in the basin's lowest areas (Blasi et al., 2017). In the lower elevation areas (below 1000 m a.s.l.) of the mountainous relief, the vegetation is dominated by *Quercus pubescens* oak forests. In low elevation cooler areas, these woods are composed of mixed taxa such as *Ostrya carpinofolia*, *Quercus cerris*, and *Acer* spp. Evergreen scrub communities, dominated by *Quercus ilex*, flourish in thermally favourable areas over lithoid outcrops. In restricted and humid areas such as valleys and ravines, the lower mountain forests are mainly composed of *Acer pseudoplatanus*, *Ulmus glabra*, *Tilia platyphyllos*, and *Fraxinus excelsior*, indicating particularly humid conditions. *Fagus sylvatica* dominates the mountain bioclimatic belt (between 1000 and 1750 m a.s.l.), frequently appearing alongside *Abies alba*. The beech forest flora varies according to the type of substrate and

temperature, resulting in distinct associations. The occurrence of the relict *Betula pendula* in the mountain belt, highlight the basin's biodiversity conservation relevance. Above 2000 m a.s.l., woodlands give way to sparser formations where herbaceous plants, mostly endemic species and glacial relics, dominate the high mountain vegetation. Alpine meadows, rocky slopes, and scree fields are predominantly composed of Poaceae, Cyperaceae, and alpine herbs adapted to the harsh climatic conditions (Blasi, 2010; Blasi et al., 2017). These vegetation zones are influenced by several factors that differ from those of central Europe, being more similar to the vegetation distribution of south-eastern Europe (Blasi and Del Vico, 2012).

2.3 Materials and methods

2.3.1 F4-F5 core: drilling site and characteristics and investigated interval

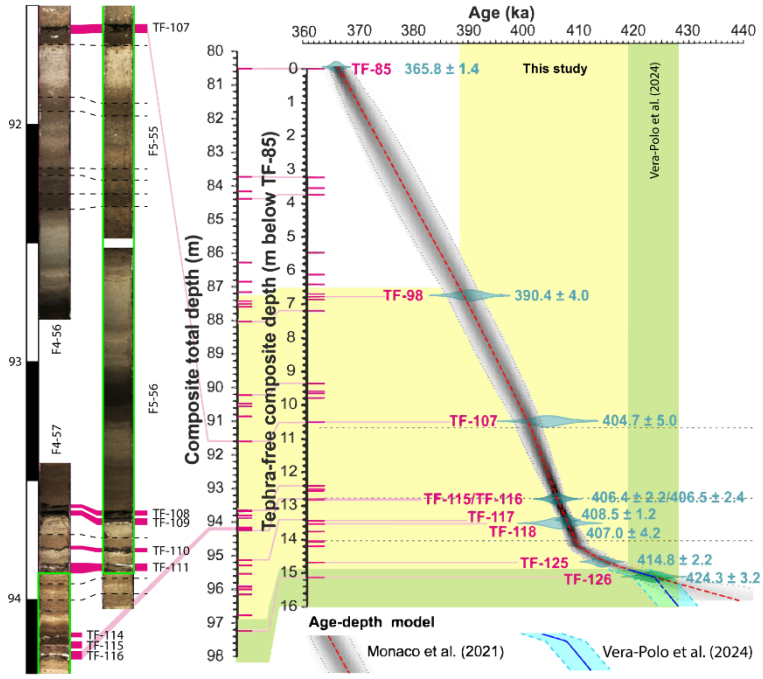

Fig. 2.1.- *Bayesian age-depth model from the 18 m of the composite F4-F5 record modified after Monaco et al. (2021). The yellow rectangle indicates the investigated interval in this study, meanwhile the green one represents the data presented in Vera-Polo et al. (2024). The pink marks are the tephra layers identified in the sedimentary record. The age model corrected (blue lines) from 424.3±3.2 (TF-126) to the bottommost part of the record (already presented in Vera-Polo et al., 2024), is represented in comparison to the previous age extrapolation (dashed red line) from Monaco et al. (2021). An example of the correlations between the individual cores F4 and F5 (from TF-116 to TF-107 tephra layers) are shown with dashed lines at the left side of the figure. Green boxes over the core-scanner image indicates the section where the pollen samples were obtained.*

Two parallel holes (F4 and F5 boreholes) were drilled with a 1.5 m-long core barrel in June 2017 (Giaccio et al., 2019), about 3 m apart from each other. In order to recover the entire sedimentary succession and to minimise potential gaps coring start of each run was set to 0.75 m overlap between succeeding sections in both holes. The composite F4-F5 record is located in the central area of the basin (42º 00' 07" N; 13º 32' 19" E) (Fig. 1.1), reaching depths of 87.00 m and 87.75 m, respectively. The composite F4-F5 record was built using the optical and geochemical information after core opening and core scanning for the correlation of the different cores (Fig. 2.1) (Giaccio et al., 2019). Sediment expansion after core recovery and splicing of individual core segments resulted in a 98.00 m long composite core of which the interval from ~87.30 m to 97.00 m is used for the present study (Fig. 2.1)

2.3.2 Geochemical analyses on discrete samples

The core was sampled each 4 cm from the top of each individual core. A total of 268 discrete samples were analysed for total carbon (TC), total inorganic carbon (TIC), and stable carbon and oxygen isotopes (see Mannella et al., 2018 for details). TOC was determined as the difference between TC and TIC and represents the proportion of organic matter in the sediments. The geochemical data from discrete samples presented in this study was formerly presented in Mannella et al., (2018) for MIS 11.

2.3.3 XRF scanning

The F4-F5 sediment cores were scanned using X-Ray Fluorescence (XRF) on one of the split core halves of the F4-F5 sediment cores using an ITRAX XRF scanner (Cox Analytical Systems, Sweden) with a line-scan camera mounted and a chromium tube set at 55 kV and 30 mA, a dwell time of 10 seconds and a step-size of 2.5 mm. The acquired data was processed using the QSpec 6.5 software (Cox Analytical, Sweden), with the results expressed in counts per second (cps), averaged at 25 cm intervals. They complement the dataset from the interval between ~418-429 ka, which was previously presented in Vera-Polo et al. (2024). According to this study, Ca, Si, Ti, K, and Zr are the predominant geochemical components.

In order to minimize any core scanner detector drifts, dilution effects and sources of irritation, element log-ratios were used for interpretation of relative chemical changes in the sedimentary record (Croudace and Rothwell, 2015; Bertrand et al., 2024). We selected Zr/K, Ca/Ti and Si/Ti ratios to estimate changes in grain size composition, calcite precipitation and biogenic silica accumulation, as they have proven to be reliable for estimating hydrological, sedimentary and environmental variations over time in the Fucino Basin (Vera-Polo et al., 2024).

In order to reduce the noise in the different ratios, to observe the general trend and evolution and to improve the reading and interpretation of the results obtained from calculating the Log-ratios, a smoothed curve has been generated using the locally estimated scatterplot smoothing (LOESS) method with a span value of 0.02 by means of the Past4 software (Hammer et al., 2001).

In addition, a Principal Component Analysis (PCA) was performed on the XRF data using the Past4 software (Hammer et al., 2001). The PCA allows the identification of the variables (components) that capture the majority of variance within multivariable data (Hammer et al., 2001).

2.3.4 Age-depth modelling and geochronology

More than 130 tephra layers deposited during the last ~430 ka from the backbone of the age-depth model of the composite F4-F5 record (Giaccio et al., 2019). Many of the tephra layers have been correlated with proximal records or with the direct $^{40}Ar/^{39}Ar$ dating (Monaco et al., 2021, 2022; Leicher et al., 2023, 2024).

The analytical details of the interval studied here were previously published by Monaco et al. (2021) yielding an age model with a 95%-confidence for the 365-430 ka interval generated using the open-source statistical environment R (R Core Team, 2017) and the Bacon program (Blaauw and Christen, 2011).

The age model of a short interval from the lowermost and oldest (>424.3 ± 3.2 ka) F4-F5 sedimentary record was subsequently modified by Vera-Polo et al. (2024). This was done taking into account a marked lithological change, clearly identified by the Ca results from the XRF data at 97.30 m composite depth (~5.6 cm below TF-126), which marked the limit between the interglacial MIS 11c and glacial MIS 12 (Vera-Polo et al., 2024).

The resulting age of the investigated interval (~87.30-97.00 m) spans from 418.5 ± 3.6 ka to 388.3 ± 3.2 ka, so adding further ~20 kyr of history of the previously investigated interval between 429.0 ± 5.0 ka to 418.5 ± 3.6 ka (Vera-Polo et al., 2024). The overall uncertainty of the modelled ages is ± 2.3 kyr, arranging between ± 1.2 and ± 4.0.

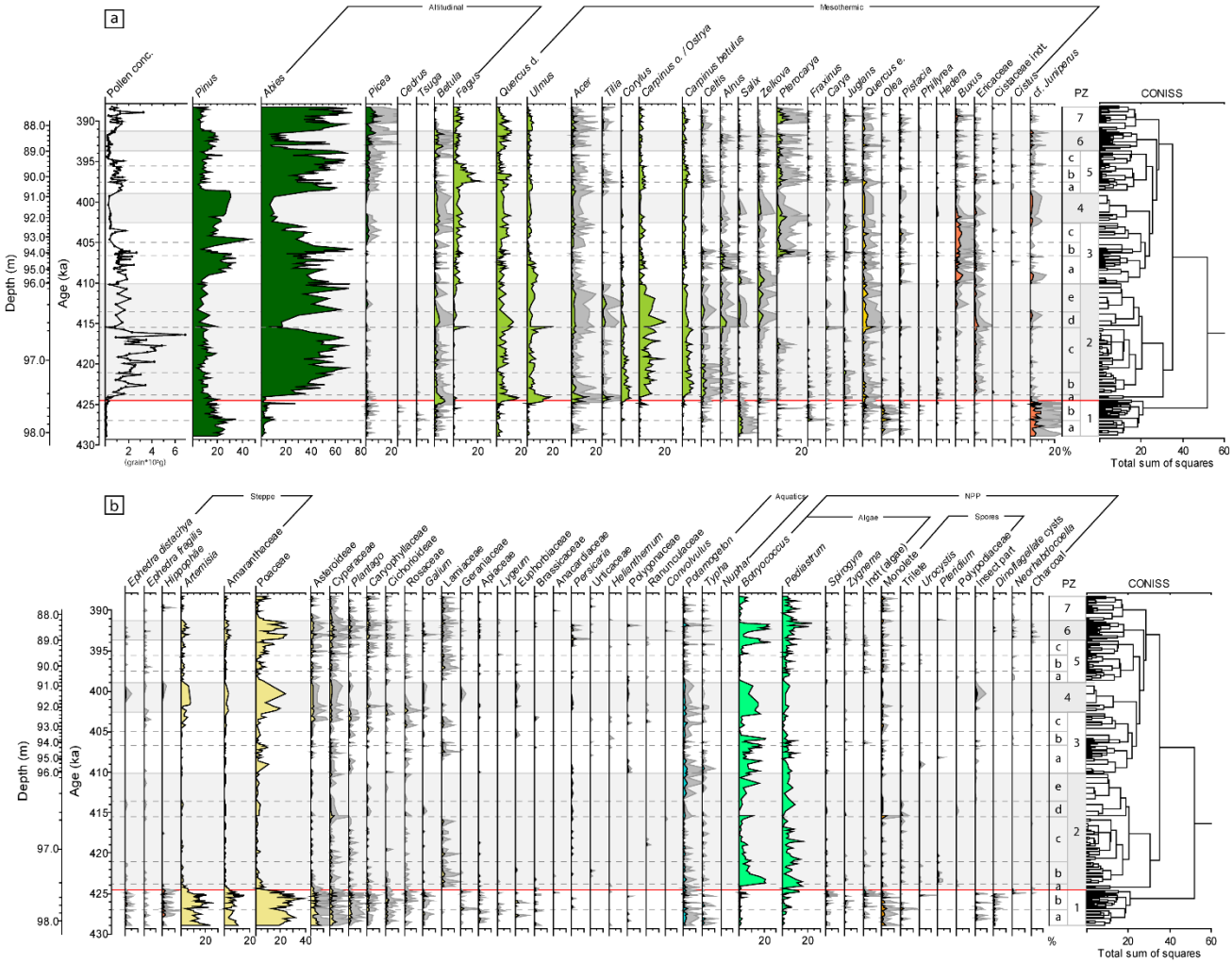

Fig. 2.2.- *a) Detailed percentage pollen diagram from F4-F5 composite record against age and depth. Total pollen concentration, trees and shrubs (indicating their ecological group. b) Herbaceous, aquatics and NPP. In both diagrams are shown in the right side the Pollen Zones and sub-Zones and the CONISS analysis. The dark grey shading in the pollen diagrams represent a x5 abundance exaggeration. The light grey shading and dashed lines across the diagrams are visual helps that indicates the main Pollen Zones and sub-Zones respectively. The red line across the diagrams separates the glacial and interglacial period, defined in Vera-Polo et al., (2024). (Dark-green: coniferous trees; Yellow-green: deciduous trees; Yellow: sclerophyllous trees; Orange-red: shrubs; Pale-yellow: herbaceous; Turquoise: aquatic; Light-green: algae; Orange: spores; Black: other NPP).*

2.3.5 Pollen analysis

A total of 216 samples were studied for palynological analysis in 9.7 m of the composite F4-F5 record. The age model published by Monaco et al. (2021) was used to set the spacing between samples to compensate the estimated variations in sedimentation rates, with the aim of obtaining the highest possible resolution for the studied period between ~429 and ~388 ka. Therefore, the maximum resolution achieved was from the bottommost part of F4-F5, sampling every 2-cm for the section concentrated between 97.7-97.4 m composite depth and 1-cm for the consecutive 50 cm, reaching an age resolution between 200 and 100 years. The rest of the core was sampled at intervals of ~4-cm achieving an average resolution of ~120 years.

A classical treatment for pollen analysis was used to concentrate the pollen grains for each sediment sample (Faegri and Iversen, 1975). It was extracted ~2 g of sediment from the core for each sample and added 1 *Lycopodium* spore tablet to each one to calculate the concentrations. The samples, after being dehydrated by freeze-drying for 24h, were treated with hydrochloric acid (HCl, 37%) to remove carbonates, hydrofluoric acid (HF, 48%) to remove silicates, and sodium hydroxide (NaOH, 10%) to eliminate the cellulose fraction with the aim of concentrating the organic matter. After the chemical treatment, the samples were sieved using a 10 μm nylon sieve to remove clays and particles smaller than pollen grains. The remaining material was mounted on microscope slides by adding glycerine and examined under a transmitted light microscope at 400x magnification. Most of the samples showed a high concentration of pollen grains, counting a total of 300 pollen grains as average for most samples. The classification of this quantity of pollen grains has proved to be sufficient for making a broad paleoenvironmental interpretation (Djamali and Cilleros, 2020). In addition, Non-Pollen Palynomorphs (NPP) were identified to assist the paleoenvironmental interpretations.

The pollen data were integrated into the Tilia Software 2.6.1 to calculate percentages and graphically represent the different pollen taxa, and to establish an objective zonation of the terrestrial pollen data performed by CONISS cluster analysis (Grimm, 1987; Fig. 2.2). The NPP percentage was calculated with respect to the total pollen amount plus the total NPP using this software, however, the NPP data was not used for the CONISS cluster analysis. This software was used to compute the concentration of pollen grains in samples (Fig. 2.2a), considering the mass quantity (~2 g per sample) and the number of *Lycopodium* spores added and counted for each sample.

In addition, a PCA was performed on pollen and NPP percentage data for statistical comparison of the variables with respect to each other, selecting only the first component (PC1) for pollen data and the first two components (PC1 and PC2) for NPPs to summarise the data (Fig. 2.3). This selection of components was done using the percentage of variance that resulted from the PCA analysis.

Based on previous studies (e.g. Joannin et al., 2011; Bertini et al., 2015; Camuera et al., 2019; Vera-Polo et al., 2024) and the PCA results from this study (Fig. 2.3), the different pollen taxa were organised into three ecologically meaningful vegetation groups. These groups have been demonstrated to serve as reliable climate indicators for the Mediterranean region. (Altolaguirre et al., 2020; Camuera et al., 2021). Those groups are xerophytes/steppic taxa (Amaranthaceae, *Artemisia*, *Ephedra*, *Hippophaë*), altitudinal taxa (*Abies*, *Betula*, *Cedrus*, *Fagus*, *Picea*, *Tsuga*), and mesothermic taxa (*Acer*, *Alnus*, *Buxus*, *Carpinus betulus*, *Carpinus orientalis/Ostrya*, *Carya*, *Celtis*, Cistaceae, *Corylus*, *Ericaceae*, *Fraxinus*, *Hedera*, *Juglans*, *Olea*, *Phillyrea*, *Pistacia*, *Pterocarya*, *Quercus* total, *Salix*, *Tilia*, *Ulmus*, *Zelkova*) (Fig. 2.4). Due to their low abundance and the correlation analysis from PCA results, the Mediterranean/sclerophyllous taxa (Cistaceae, *Fraxinus*, *Olea*, *Pistacia*, *Phillyrea* and *Quercus* evergreen) were included into the mesothermic taxa group (Figs. 2.2 and 2.4). The aquatic plants (*Nuphar*, *Potamogeton* and *Typha*) were excluded from the basis pollen sum.

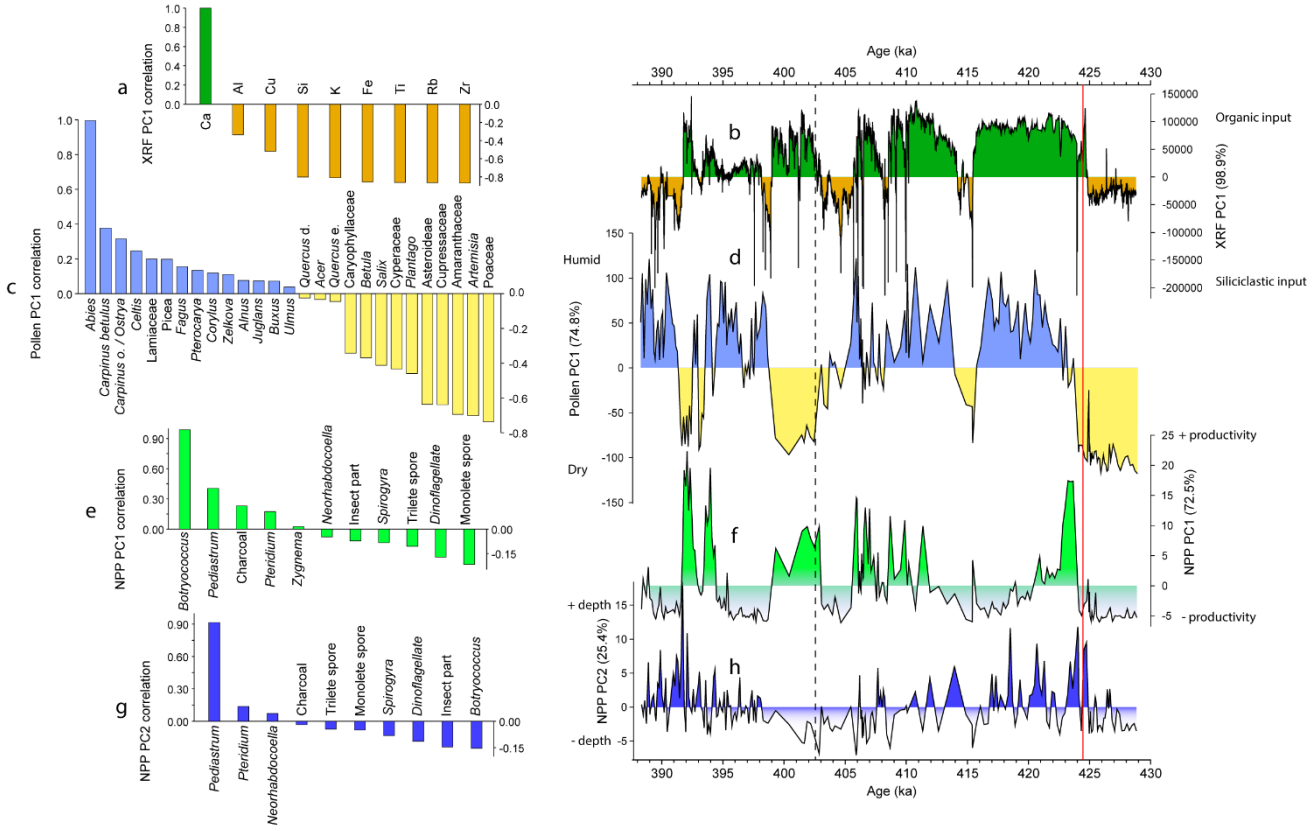

Fig. 2.3.- *PCA results from X-Ray Fluorescence (XRF), Pollen and Non-Pollen Palynomorph (NPP) data. a) XRF PC1 correlation between the geochemical elements. Green bar represents the elements related with organic input; meanwhile light orange bars represent the siliciclastic input. b) XRF PC1 variation plotted in time, with the same colour scheme than panel a. c) Pollen PC1 correlation between the different pollen species identified. Blue bars associated the positive values of the PC1 which are associated with humid conditions. The yellow bars associated the negative values which correspond with taxa related with dry conditions. The pollen taxa plotted in this graph represented more than 0.5 % in the total of the samples and more than ±0.025 loadings of the total variance to enhance readability. d) Pollen PC1 variation plotted in time, with the same colour scheme than panel c. e) NPP PC1 correlation associated with productivity variations in the lake (more productivity is related with the more positive values). f) NPP PC1 variation plotted in time. g) NPP PC2 correlation associated with lake depth variation (more depth is related with the more positive values. h) NPP PC2 variation plotted in time. The dashed line at ~402.35 indicates the moment when the relationship between XRF and pollen PCAs changes (see text for interpretation). The red line indicates the glacial-interglacial boundary in Fucino Basin.*

Relative lake-level changes were estimated by combining algae and pollen data, according to Camuera et al. (2019): Algae total/(Algae total + Aquatic taxa + Poaceae) (Fig. 2.5). This estimation shows the variability of algae with respect to the aquatic taxa and Poaceae, whose percentage would increase in open plains when the lake level is lower and during dry periods (Bush, 2002). However, the proportion of algae also depend on other factors such as the degree of eutrophication of the lake waters and changes in the lake bottom morphology.

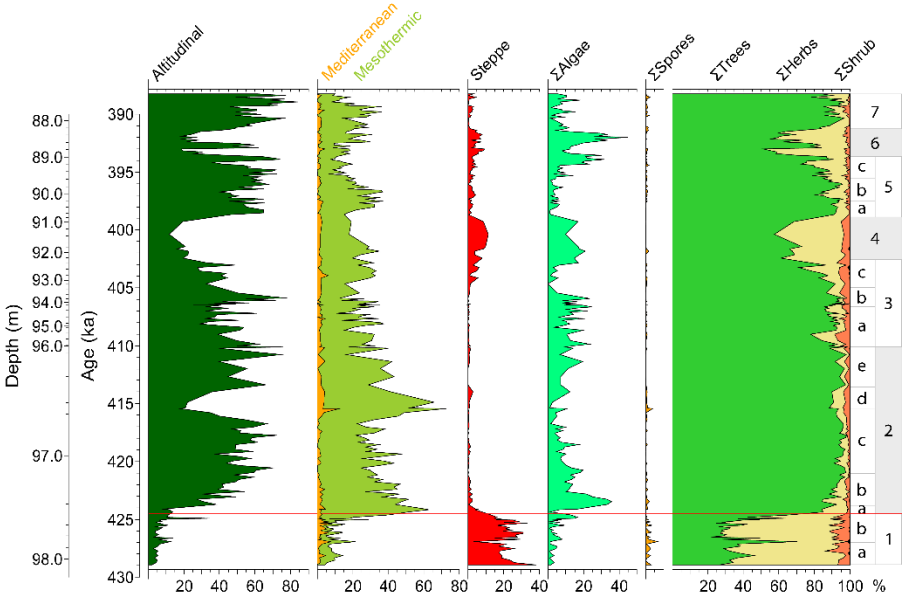

Fig.2.4.- *Terrestrial pollen data grouped into different paleoecological associations and algae and spores Non-Pollen Palynomorphs (NPP). Pollen Zones and sub-Zones are displayed at the right side of the diagrams. The red line marks the glacial-interglacial boundary. The taxa lists are reported in the text and in Fig. 2.2.*

2.4 Results

2.4.1 Geochemistry of discrete samples and XRF data

The age-related fluctuations in the geochemistry of the 268 discrete samples and the XRF scanning dataset allow the identification of 9 distinct phases (Fig. 2.5):

1) Prior to 97.35 m depth (425.2 ± 4.5 ka): the terrigenous elements (Al, K, Ti, Fe, Zr) dominated (Figs. 2.3 and 2.5). The Log(Si/Ti) showed more variability, with a modest increasing trend, than the other geochemical proxies. The TOC values were lower than 1% during most of this period, meanwhile the abundance of TIC was around 4%.

2) Between 97.35 and 97.18 m depth (425.2 ± 4.5 ka to 423.3 ± 3.8 ka), a transitional phase is observed, marked by increasing values in all geochemical proxies. At 424.8 ± 4.4 ka, Ca replaced terrigenous elements (Fig. 2.3b), with Log(Ca/Ti) showing presented the most abrupt increase of the record. TOC exhibits a maximum of 4.5% at 423.6 ± 3.7 ka. After this maximum, TIC presented an abrupt increase similar to Log(Ca/Ti) but at the end of this period.

3) Between 97.18-96.81 m depth (423.3 ± 3.8 ka and 416.0 ± 2.7 ka): Log(Si/Ti) exhibited the largest oscillations with a modest upward trend. Those oscillations were similar to the ones showed in Log (Ca/Ti), but with higher amplitude. TIC and TOC maintained constant values of 8 and 2%, respectively.

4) Between 96.81-96.37 m depth (416.0 ± 2.7 ka and 412.4 ± 2.8 ka): the geochemical composition was largely siliciclastic, with a decrease in every value of the calculated ratios and TOC. The minimum value registered in the geochemical proxies correspond to the TF-125 tephra layer (Monaco et al., 2021).

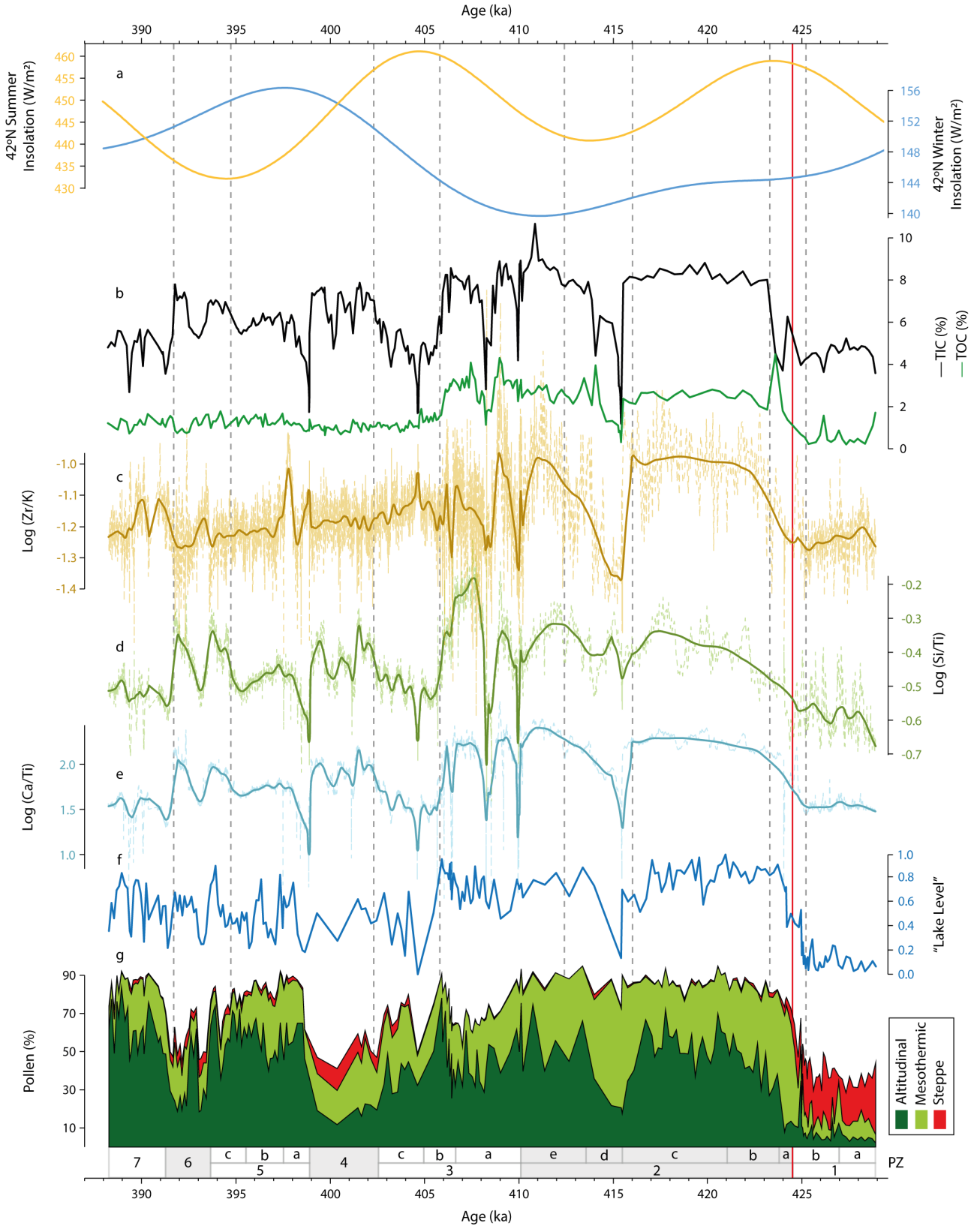

Fig. 2.5.- *Comparison of (a) summer (orange) and winter (blue) insolation at 42ºN (Laskar et al., 2004), (b) Total Inorganic Carbon (TIC; black) and Total Organic Carbon (TOC; green) from discrete samples, (c) Zr/K, (d) Si/Ti, (e) Ca/Ti geochemical log-ratios from XRF scanning (dashed lines depict the actual values, while the continuous smoothed lines represent the mean value calculated by LOESS method with a span value of 0.02), (f) lake level according to Camuera et al. (2019) formula, and (g) pollen associations percentages of F4-F5 sediment record and pollen zones (PZ) as reference. The red line indicates the glacial-interglacial boundary. The dashed lines mark the different XRF log-ratios phases.*

5) Between 96.37-93.73 m depth (412.4 ± 2.8 ka and 405.8 ± 1.5 ka): Log(Ca/Ti), Log(Zr/K) ratios, TOC and TIC reached the same values as the previous period between 423.3 ± 3.8 ka and 416.0 ± 2.7 ka. The minimum values that we observe in log-ratios at 410.0 ± 1.9, 408.3 ± 1.2, and 406.5 ± 1.3 ka correspond to tephra layers. Log(Si/Ti) reached it maximum value at 407.6 ± 1.3 ka.

6) Between 93.73-92.16 m depth (405.8 ± 1.5 ka and 402.3 ± 2.3 ka): Log(Ca/Ti) and Log(Si/Ti) followed an opposite trend from the beginning of this period compared to the Log(Zr/K). Since the beginning of this period all proxies seem to depict a decreasing trend until the end of the record. TOC values reached their minimum at ~1%, maintaining this value until the end of the studied record. Log(Ca/Ti), Log(Si/Ti) and TIC decreased compared to the previous period, reaching a minimum at 404.6 ± 1.9 ka.

7) Between 92.16 and 90.65 m depth (402.3 ± 2.3 ka to 398.7 ± 2.8 ka), two distinct phases are visible, separated by the TF-106 tephra layer at 398.9 ± 2.8 ka. The first phase is characterized by higher variability in the proxies, while the second phase shows a more consistent decreasing trend.

8) Between 90.65-88.37 m depth (398.7 ± 2.8 ka and 391.7 ± 3.2 ka): a bimodal stage is observed with two maximum values in Log(Ca/Ti), Log (Si/Ti) and TIC at 393.9 ± 3.1 and 392.0 ± 3.2 ka.

9) After 88.37 m depth (391.7 ± 3.2 ka) until the end of the studied record: Log(Ca/Ti), Log (Si/Ti) and TIC values decreased and stabilised. The values from Log(Zr/K) depict a first increase, followed by a subsequent decrease at 389.4 ± 3.1 ka.

Generally, Log(Si/Ti) and Log(Ca/Ti) show similar fluctuations through time, with a slightly higher amplitude of Log(Si/Ti). After 405.8 ± 1.5 ka we can observe a change in the relationship between the log-ratios related to productivity and organic matter with Log(Zr/K), becoming opposite since this moment.

2.4.2 Pollen analysis

The microscopic examination of 216 palynological samples from the F4-F5 sedimentary record revealed the overall good preservation of palynomorphs, with the identification of 60 pollen and 14 NPP taxa. The lower 34 samples showed high abundance of steppic and herbaceous taxa (such as *Poaceae*, *Artemisia*, Amaranthaceae and Asteroideae) and lower pollen concentrations (~6300 pollen grains/g as mean value). The rest of the analysed samples presented higher abundance of Arboreal Pollen (AP) taxa (mainly dominated by *Abies* and deciduous trees such as *Quercus*, *Ulmus*, *Carpinus*, *Celtis*, *Corylus*, *Pterocarya* and *Fagus*) and higher pollen concentration values (~120150 pollen grains/g as mean value). During the AP abundance phase, we can observe three main oscillations alternating open vegetation and altitudinal taxa, whereas the mesothermic maintain more stable percentage values throughout time (Table 2.1).

The algae (mainly *Botryococcus* and *Pediastrum*) exhibit two major phases. During the first phase (from 428.0 ± 5.0 to 424.5 ± 4.0), represented by the 36 first samples, algae were very low in abundance. After 424.5 ka, their abundance increased abruptly following a pattern comparable to that altitudinal vegetation. However, the trend changed from ~403.0 ka onwards becoming more similar to changes in herbaceous vegetation.

At shorter timescales and according to the CONISS cluster analysis developed on the terrestrial pollen data, the pollen diagram can be divided into 7 pollen zones (PZ) (Figs. 2.2 and 2.4; see Vera-Polo et al. (2024) for a detailed visualization of PZ-1 until the beginning of PZ-2c):

PZ		Zone description
1a	Depth limits (m): 98.10 – 97.65 Age limits (ka): 428.0 ± 5.0 – 426.9 ± 5.0 Nº samples: 12 Pollen conc. (pollen grains/g): 5850	Herbaceous and steppic taxa are mainly represented by Poaceae (23.9 %), *Artemisia* (13.3 %) and Amaranthaceae (6.4 %). Tree forest is represented by *Pinus* (22.6 %), *Abies* (3.4 %), *Salix* (2.1 %) and *Quercus* d. (1.7 %). *Potamogeton* (1.6 %) prevails among the aquatic taxa.
1b	Depth limits (m): 97.65 – 92.27 Age limits (ka): 426.9 ± 5.0 – 424.5 ± 4.0 Nº samples: 24 Pollen conc. (pollen grains/g): 6540	Poaceae (24.5 %), *Artemisia* (13.8 %), and Amaranthaceae (7.3 %) still dominated the PZ. This zone started with a maximum peak of *Abies* (27.6 %) and mesothermic taxa (39.0 %). *Pinus* (15.7 %) abundance decreased. Deciduous forest was represented by *Quercus* d. (2.1 %) and *Ulmus* (1.4 %). Herbaceous abundance gradual decreased since 425 ± 4.5 ka.
2a	Depth limits (m): 97.27 – 97.22 Age limits (ka): 424.5 ± 4.0 – 423.9 ± 3.8 Nº samples: 4 Pollen conc. (pollen grains/g): 32450	Herbaceous taxa were replaced by deciduous forest dominated by *Ulmus* (15.6 %), *Quercus* d. (15.4 %), *Acer* (8.4 %), *Corylus* (6.0 %) and *Tilia* (4.4 %). *Betula* (5.9 %), *Quercus* e. (2.4 %), and *Fagus* (1.1 %) were rather abundant. *Pediastrum* (8.8 %) was the dominant NPP.
2b	Depth limits (m): 97.22 – 97.08 Age limits (ka): 423.9 ± 3.8 – 421.0 ± 4.2 Nº samples: 13 Pollen conc. (pollen grains/g): 167540	*Abies* (40.9 %) abruptly increased, which followed an upward trend. Deciduous vegetation, composed by *Carpinus o./Ostrya* (7.5 %), *Carpinus b* (5.9 %). *Celtis* (2.3 %), and *Alnus* (1.4 %) suffered a decrease. *Botryococcus* (11.6 %) replaced *Pediastrum* (7.2 %).
2c	Depth limits (m): 97.08 – 96.69 Age limits (ka): 421.0 ± 4.2 – 415.4 ± 2.5 Nº samples: 26 Pollen conc. (pollen grains/g): 266600	Non-Arboreal Pollen (NAP) is nearly inexistent. The forest is mainly composed by *Abies* (50.2 %), *Pinus* (9.8 %), *Carpinus o./Ostrya* (8.3 %), *Quercus* d. (5.8 %), *Carpinus b*. (4.5 %), *Ulmus* (4.4%), and *Corylus* (2.8 %).
2d	Depth limits (m): 96.69 – 96.50 Age limits (ka): 415.4 ± 2.5 – 413.7 ± 2.7 Nº samples: 3 Pollen conc. (pollen grains/g): 106580	Altitudinal taxa (25.9 %) suffered a great decrease. Mesothermic taxa prevails, composed by *Carpinus o./Ostrya* (12.4 %), *Quercus* d. (10.4 %), *Carpinus b*. (4.0 %), *Alnus* (3.8 %), *Corylus* (3.4 %), *Acer* (3.1 %), *Ulmus* (2.9 %), and *Zelkova* (2.1 %). *Pediastrum* (4.3 %) abundance increased.
2e	Depth limits (m): 96.50 – 96.10 Age limits (ka): 413.7 ± 2.7 – 410.2 ± 1.9 Nº samples: 6 Pollen conc. (pollen grains/g): 133530	*Abies* (50.3 %) resume its dominance. Aquatic taxa increased, mostly composed by *Potamogeton* (1.6 %). Algae showed an alternation between *Botryococcus* (6.0 %) and *Pediastrum* (5.0 %).
3a	Depth limits (m): 96.10 – 94.32 Age limits (ka): 410.2 ± 1.9 – 406.7 ± 1.3 Nº samples: 21 Pollen conc. (pollen grains/g): 135120	*Abies* (40.4 %) decreased. *Fagus* (2.9 %) started to be notable since this PZ. Poaceae (4.2 %) abundance increased. Mesothermic taxa was composed by *Ulmus* (4.1 %), *Quercus* d. (3.9 %), and *Carpinus o./Ostrya* (2.8 %). *Buxus* (1.9 %) appeared.
3b	Depth limits (m): 94.32 – 93.36 Age limits (ka): 406.7 ± 1.3 – 405.1 ± 1.7 Nº samples: 14 Pollen conc. (pollen grains/g): 132510	*Abies* reached a maximum (74.3 %) at 406.1 ± 1.4. *Buxus* (2.6 %) maintained constant abundance. Deciduous pollen taxa were formed by *Pterocarya* (6.9 %), *Quercus* d. (5.5 %), *Carpinus o./Ostrya* (1.9 %), *Alnus* (1.6 %), and *Ulmus* (1.5 %). *Botryococcus* (9.8 %) dominated the NPP abundance.
3c	Depth limits (m): 93.36 – 92.30 Age limits (ka): 405.1 ± 1.7 – 402.7 ± 2.3 Nº samples: 8 Pollen conc. (pollen grains/g): 67780	*Abies* (29.4 %) showed a decreasing trend. Altitudinal taxa showed more diversity: *Fagus* (4.8%), *Betula* (1.5 %), and *Picea* (1.2 %). *Artemisia* (2.4 %) started to increase. NPPs are nearly inexistent during this period.
4	Depth limits (m): 92.30 – 90.81 Age limits (ka): 402.7 ± 2.3 – 399.0 ± 2.8 Nº samples: 7 Pollen conc. (pollen grains/g): 38600	Important substitution from forest to steppic taxa and other herbaceous (NAP: 33.4 %). Hygrophilous taxa are mainly represented by *Cyperaceae* (1.4 %) and *Potamogeton* (1.2 %). Algae (16.4 %) increased.

5a	Depth limits (m): 90.81 – 90.21 Age limits (ka): 399.0 ± 2.8 – 397.5 ± 3.0 Nº samples: 7 Pollen conc. (pollen grains/g): 114980	*Abies* (47.7 %) increased abruptly. *Picea* (1.2 %) appeared at the beginning of this PZ. Mesothermic taxa (25.5 %) increased. Herbaceous, mainly represented by Poaceae (2.6 %), decreased.
5b	Depth limits (m): 90.21 – 89.57 Age limits (ka): 397.5 ± 3.0 – 395.5 ± 3.2 Nº samples: 16 Pollen conc. (pollen grains/g): 99940	Altitudinal taxa abundance decreased but its diversity increased, being composed by *Abies* (40.6 %), *Fagus* (12.2 %), and *Picea* (1.8 %).
5c	Depth limits (m): 89.57 – 89.01 Age limits (ka): 395.5 ± 3.2 – 393.7 ± 3.2 Nº samples: 14 Pollen conc. (pollen grains/g): 52910	*Abies* (52.3 %) dominated the PZ. Poaceae (8.4 %) started to gain importance. *Botryococcus* (7.0 %) increased abruptly at the end of the PZ.
6	Depth limits (m): 89.01 – 88.02 Age limits (ka): 393.7 ± 3.2 – 390.6 ± 3.2 Nº samples: 18 Pollen conc. (pollen grains/g): 40840	Open vegetation abundance increased being composed by Poaceae (17.2 %), *Artemisia* (2.6 %), Amaranthaceae (2.4 %), and Asteroideae (1.4 %). *Botryococcus* (12.2 %) and *Pediastrum* (8.9 %) abundances increased.
7	Depth limits (m): 88.02 – 87.23 Age limits (ka): 390.6 ± 3.2 – 388.3 ± 3.2 Nº samples: 23 Pollen conc. (pollen grains/g): 104010	*Abies* (50.0 %), *Picea* (5.0 %), and *Fagus* (4.3 %) dominated this period. *Quercus* d. (5.8 %), *Pterocarya* (3.4 %), *Ulmus* (2.3 %), and *Acer* (2.0 %) abundances increased. Algae (7.4 %) percentage decreased.

Table 2.1.- *Main vegetational characteristics of Fucino F4-F5 composite record pollen zones (PZ). The percentage displayed after the species is the mean value (except if the text specifies a maximum or minimum value) The zones are visually displayed in Figs. 2.2 and 2.4.*

2.4.3 PCA results

Qualitative PCA analysis (Ter Braak and Juggins, 1993), allows the observation of the general trend of the evolution of past environmental conditions of the G/I dynamics. PCAs were carried out on the geochemical elements obtained from XRF, the different pollen taxa, and the NPPs (Fig. 2.3).

We only considered the PC1 component off the XRF PCA, because it represents the 98.9% of total variance of the data. The correlation to PC1 separates the elements into two separate groups. Positive XRF PC1 values corresponds to Ca and the negative ones to siliciclastics elements (Fig 2.3a).

The PCA of the pollen data shows that PC1 represents the 74.8% of total variance of the pollen data, which separates the pollen into two groups: positive values correspond to deciduous and water demanding forest species, and negative values are associated to herbaceous and xerophytic species, associated with dry conditions. The PCA of the NPP gives us information about the lake productivity (NPP PC1) and the relative lake depth (NPP PC2). The NPP PC1 is

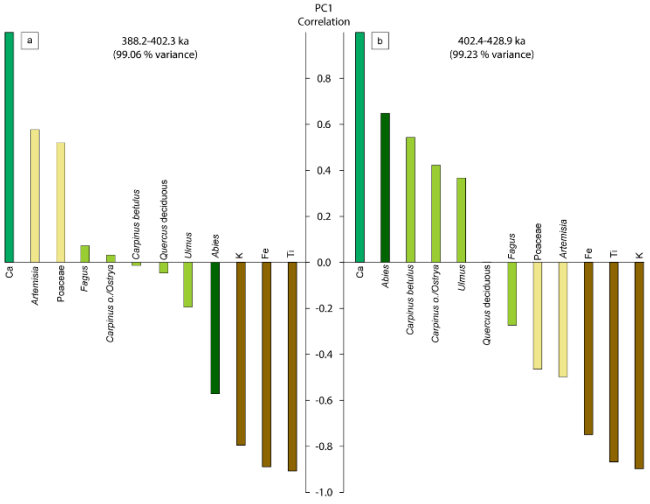

Fig. 2.6.- *PCA correlations for XRF and Pollen data. The pollen taxa shown occur with abundances higher than 2% in the record to enhance readability. a) PC1 for the period after 402.35 ka. It shows positive correlation between herbaceous plants and Ca, and negative correlation between altitudinal plants (mainly represented by Abies) and siliciclastic geochemical elements. b) PC1 for the period before 402.35 shows positive correlation between altitudinal taxa and deciduous trees with Ca, meanwhile negative correlations occur between herbs and siliciclastic material. (Green: organic material; Light-yellow: herbaceous plants; Yellow-green: deciduous trees; Dark-green: altitudinal taxa; Brown: siliciclastic material).*

interpreted to be a proxy for productivity (which represents the 72.5% of the total NPP values variance) considering the abundance of algae in the samples. The NPP PC2 (25.4% of total variance) was interpreted as a proxy for lake depth as *Botryococcus* is associated with shallower lake water (negative values) than *Pediastrum* (positive values) (Guy-Ohlson, 1992; Nielsen and Sørensen, 1992; Jiménez-Moreno et al., 2023).

The comparison of all the PCAs, shows two main periods, before and after 402.4 ± 2.3 ka. Additionally, another PCA was calculated for those two periods including in the analysis all the data available (Fig. 2.6). Before this point, XRF PC1 and pollen PC1 are directly correlated, increasing the carbonate material when the humid periods occurred. After that the tendencies abruptly changed inverting this correlation, being the XRF PC1 more similar to NPP PC1 and pollen PC1 being inverted, correlating the "dry components" with more abundance of carbonate material.

2.5 Discussion

2.5.1 Proxies' interpretation

The high-resolution Fucino pollen record provides significant information about vegetation and climate variations during the interval 429.0 ± 5.0 ka to 388.0 ± 3.3 ka, encompassing several important climate changes including the T-V (430.5 ± 1.5 ka to 425.0 ± 2.0 ka; Cheng et al., 2016; González-Lanchas et al., 2022), the MIS 12-MIS 11 boundary (424.0 ± 4.0 ka; Lisiecki and Raymo, 2005), and great part the MIS 11 interglacial (424.0 ± 4.0 ka to 367 ± 3.0 ka; Prokopenko et al., 2010; Railsback et al., 2015; Regattieri et al., 2016; Kousis et al., 2018; Ardenghi et al., 2019; Tzedakis et al., 2022; Sassoon et al., 2023).

The basin's surrounding vegetation has changed through time as a result of local and regional temperature and humidity variations. Previous studies (e.g. Joannin et al., 2011; Bertini et al., 2015; Camuera et al., 2019) have demonstrated that the abundance of temperate forest taxa serves as a valuable indicator of temperature and precipitation changes over time. In our study, we utilised deciduous and temperate-adapted forest species, such as *Quercus*, *Ulmus*, *Acer*, *Corylus*, and *Pterocarya* (e.g. Joannin et al., 2008). Notably, the *Quercus* abundance has proven to be an excellent proxy for distinguishing warm-humid from cold-arid paleoclimatic phases (e.g. Denk et al., 2001; Joannin et al., 2008). The presence of *Pterocarya* in the record indicates restricted warm temperatures values (mean annual temperatures of 7.6 ºC), which can give us an approximation of the temperatures when this taxon is rather abundant (Svenning, 2003). On the other hand, *Abies* can be used as a direct proxy for precipitation and humidity conditions (Xiang et al., 2007). Previous palynological studies indicate that increases in *Abies* abundance typically occur after the interglacial thermal maximum and during a post-temperate phase, commonly associated with decreased summer insolation, indicating cooler but overall humid conditions (Tzedakis, 2007). Due to their big size, *Abies* pollen grains cannot be transported for long distances by the wind, and hence their occurrence indicates proximity to the pollen source (Erdtman, 1969; Pidek et al., 2013; Moreno-Amat et al., 2017). This means that the variation through time of this pollen curve indicates local variation of the climatic conditions. The abundance of herbaceous and steppic xerophytic plants

(such as Amaranthaceae, *Artemisia*, *Ephedra* and *Hippophäe*) is associated with arid and likely cold conditions (e.g. Fauquette et al., 1998; Tzedakis, 2007).

The presence of algae species like *Botryococcus*, *Pediastrum*, *Spirogyra*, and *Zygnema* indicates lake depth and productivity (Jiménez-Moreno et al., 2023). *Pediastrum*, a colonial green alga, can signal eutrophication or changes in lake depth depending on the species (Fig. 2.3g and h; Nielsen and Sørensen, 1992; Anderson et al., 2020; Xiang et al., 2021; Jiménez-Moreno et al., 2023). Similarly, *Botryococcus* grows in shallow waters but is also influenced by nutrient availability (Fig. 2.3e and f; Guy-Ohlson, 1992; Jiménez-Moreno et al., 2023). Small lake-level fluctuations likely affected algae populations and nutrient levels, leading to significant changes in *Pediastrum* and *Botryococcus*.

Geochemical log-ratios can be interpreted as follows:

- Zr/K: reflects grain size. Zr resists weathering and is common in coarse sediments, while K is linked to finer clays and feldspars (Cuven et al., 2011; Wang et al., 2011; Wu et al., 2020). Higher Zr/K values indicate coarser sediment composition.
- Ca/Ti: the source of Ca in the Fucino Basin is unclear and can be either endogenic (carbonate precipitation, biogenic shell calcification in ostracods…) or product of detrital influx (from the abundant Miocene-Mesozoic marine limestones outcropping nearby; Fig. 1.1) or a mixture of both (Mannella et al., 2019). Endogenic carbonates form as a result of lower dissolved CO_2 levels caused by warmer water temperatures or photosynthesis (Kylander et al., 2011). Ti is tied to terrigenous material via runoff, can also be concentrated in tephra layers. High Ca/Ti values likely point to authigenic carbonate precipitation without detrital influx (Bertrand et al., 2024).
- Si/Ti: this ratio determines siliceous productivity (biogenic silica) (e.g Stansell et al., 2010; Brown, 2011; Melles et al., 2012; Bertrand et al., 2024), as it separates the biogenic Si from the detritic Ti.

The Log(Si/Ti) and Log(Ca/Ti) help to corroborate the productivity data provided by the algae community, showing similar variations through time (Fig. 2.5).

2.5.2 Glacial period: MIS 12

Full glacial cold and dry climate conditions occurred in Fucino Basin between 428.9 ± 5.0 ka and 426.7 ± 5.0 ka (PZ-1a; Table 2.1), conditioning a vegetation dominated by xerophytic and herbaceous plants and *Pinus*, also corroborated by the occurrence of *Hippophaë* at this time, a typical glacial taxon (e.g. Krupiński, 1992). During the dry and cold MIS 12 glacial, the algae abundance was very low (Fig. 2.4) as well as TOC, TIC, Log(Si/Ti), and Log(Ca/Ti), indicating the low productivity and the lowest lake level registered for this record. During this time, the main sedimentary input was siliciclastic fine-grained material, corroborated by Log(Zr/K), which indicates restricted erosion due to low precipitation and dry conditions. The abundance of steppic taxa also implies moderate to low precipitation. The $\delta^{13}C$ (which is sensitive to temperature and precipitation

variations; McDermott, 2004) and $\delta^{18}O$ (sensitive to precipitation) from Bàsura cave (northern Italy) also registered cold-arid paleoclimatic conditions during MIS 12 (Hu et al., 2024). At the end of this period, a small brief humid event occurred in Fucino (Vera-Polo et al., 2024), characterised by a tree forest increase and steppic taxa decrease at 426.7 ± 5.0 ka.

After this event, the steppe taxa resume their dominance in the area, indicating the continuation of cold-arid conditions during the rest of the glaciation. A variation on steppic abundances can be observed (PZ-1b; Table 2.1), with a slightly warmer and wetter period between two colder periods with higher abundances of steppic plants, following a "W" pattern characteristic of the Heinrich type events (Ht) (Singh et al., 2023). This Ht could correspond with the defined Ht4 identified at the Iberian Margin at the end of the MIS 12 glacial period by Rodrigues et al. (2011), associated with a Sea Surface Temperature (SST) cooling and reduction in the Atlantic Meridional Overturning Circulation (AMOC), favouring the southward displacement of the Polar Front to the mod-latitudes of the North Atlantic, producing colder conditions (López-Martínez et al., 2006; Rodrigues et al., 2011, 2017; Singh et al., 2023). The Ht are associated with the beginning of the termination stages (Cheng et al., 2009), so we can assume that the T-V stage started at that time. However, it is uncertain if the Ht are necessarily "required" to initiate a termination, or if they are the outcome of deglacial collapse of ice-sheets, and hence consequences rather than causes of these important climatic changes (Hodell et al., 2008; Vázquez Riveiros et al., 2013). The Ht4 is described as one of the most extreme Ht between MIS 15 and MIS 9 (Rodrigues

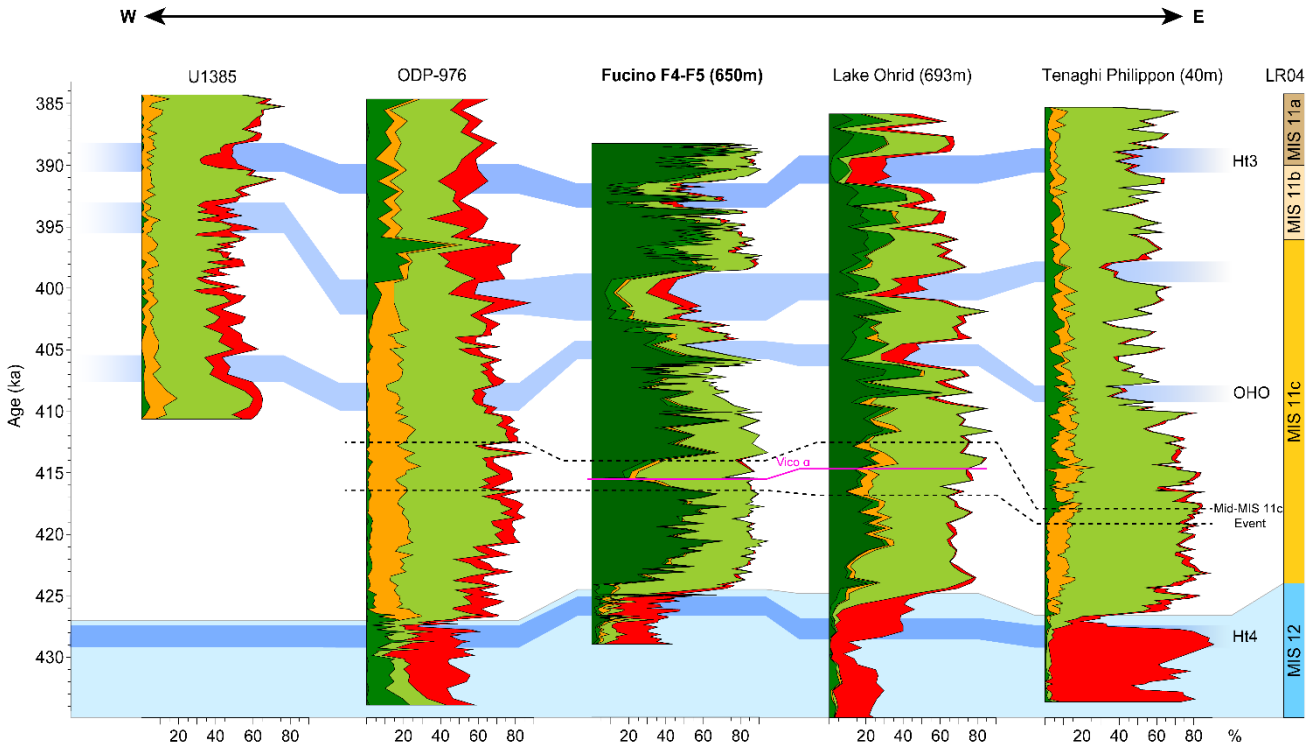

Fig. 2.7.- *Comparison of pollen records from Iberian Margin (U-1385 site; Oliveira et al., 2016), Alboran Sea (ODP-976 site; Sassoon et al., 2023), Fucino Basin (F4-F5 composite record; this study), Lake Ohrid (Kousis et al., 2018; Koutsodendris, 2020), and Tenaghi Philippon (Koutsodendris et al., 2023a, 2023b). The blue and orangish boxes at the right of the panel depict the limits between the different MIS according to Railsback et al. (2015) from the record LR04 (Lisiecki and Raymo, 2005). Blue boxes correlated cold-dry periods. Dashed lines correlate the Mid-MIS11c event. Pink line between Fucino and Lake Ohrid indicates the same tephra layer from Vico a. Red: Steppic taxa; Yellow-green: Mesothermic taxa; Orange: Mediterranean taxa; Green: Altitudinal Taxa (Abies excluded); Dark-green: Abies.*

et al., 2011), because its occurrence implies the change of climatic conditions from one of the most extreme glacial interval (MIS 12) to the first high-amplitude interglacial (MIS 11c) (Rodrigues et al., 2011; Hu et al., 2024).

After the Ht4 (at 425.3 ± 4.7 ka), in Fucino Basin there was an increase in mesothermic taxa abundance followed by a peak in altitudinal taxa (mainly *Abies*; Fig. 2.2), indicating that the temperature slightly increased, generating an increase in deciduous forest in the Fucino area, just before the G/I boundary. Also, the Log(Si/Ti) and Log(Ca/Ti) values increased, indicating higher productivity in the lake waters. This increase would correspond to more algae and calcite precipitation triggered by warmer temperatures, more nutrients and more Ca ions supply from the catchment area (Wagner et al., 2019).

2.5.3 Interglacial period: MIS 11

2.5.3.1 The early MIS 11c (424.5 ± 4.0 ka - 415.4 ± 3.5 ka)

The pollen boundary between the glacial MIS 12 and the interglacial MIS 11c can be placed at 424.5 ± 4.0 ka in Fucino Basin (Fig. 2.7), using a value higher than 75% of arboreal pollen (AP) according to Allen et al. (2000) and to the Fucino terrestrial pollen CONISS results. A considerably increase in mesothermic taxa, dominated by deciduous and water demanding forest species such as *Quercus* deciduous type, *Ulmus*, *Acer*, *Corylus* and *Tilia* (from this point on this association will be referenced as *Quercus* association; PZ-2a; Table 2.1), occurred after the G/I boundary. This could be interpreted as a great increase in humidity. Additionally, a great increase in nutrient input to the lake occurred, evidenced by the high percentage of TOC that occurred at that time. The precipitation increased abruptly in central Italy then, reaching estimated annual values of ~1200 mm (Regattieri et al., 2016; Vera-Polo et al., 2024). This generated an increase in the lake level during the interglacial, which likely added up to the water influx from the melting of the local mountain glaciers. Furthermore, an increase in pollen concentration occurred during this interglacial at global scales (Brandon et al., 2020). At Fucino, the increase in mesothermic taxa was followed by the dominance of altitudinal taxa, with *Abies* as the main representative species, until the end of the MIS 11 record (Fig. 2.2), coupled with an elevated sedimentation rate and diminished terrigenous input in the lake.

The occurrence of *Betula* and the appearance of mesothermic taxa like *Quercus*, *Ulmus*, *Acer* and *Tilia,* which are deciduous taxa need greater quantities of water, during the G/I boundary confirms the increase in both temperature and precipitation (controlling the relative humidity: balance between evapotranspiration and precipitation) shaping the vegetation in the Mediterranean area (Ilvonen et al., 2022; Vera-Polo et al., 2024). The G/I transition in the Lake Ohrid pollen record is represented by the expansion of *Pinus* and *Betula* and the presence of *Salix* and *Hippophaë*, which are light demanding taxa and can grow on nutrient-poor soils (consequence of the arid conditions during MIS 12; Kousis et al., 2018). The transition to more humid conditions was also registered in northern Italy, identifying the G/I boundary at 427.0 ± 2.0 in the isotopic Bàsura cave speleothem record (Hu et al., 2024; Fig. 2.8). The difference between the G/I boundary between Fucino and

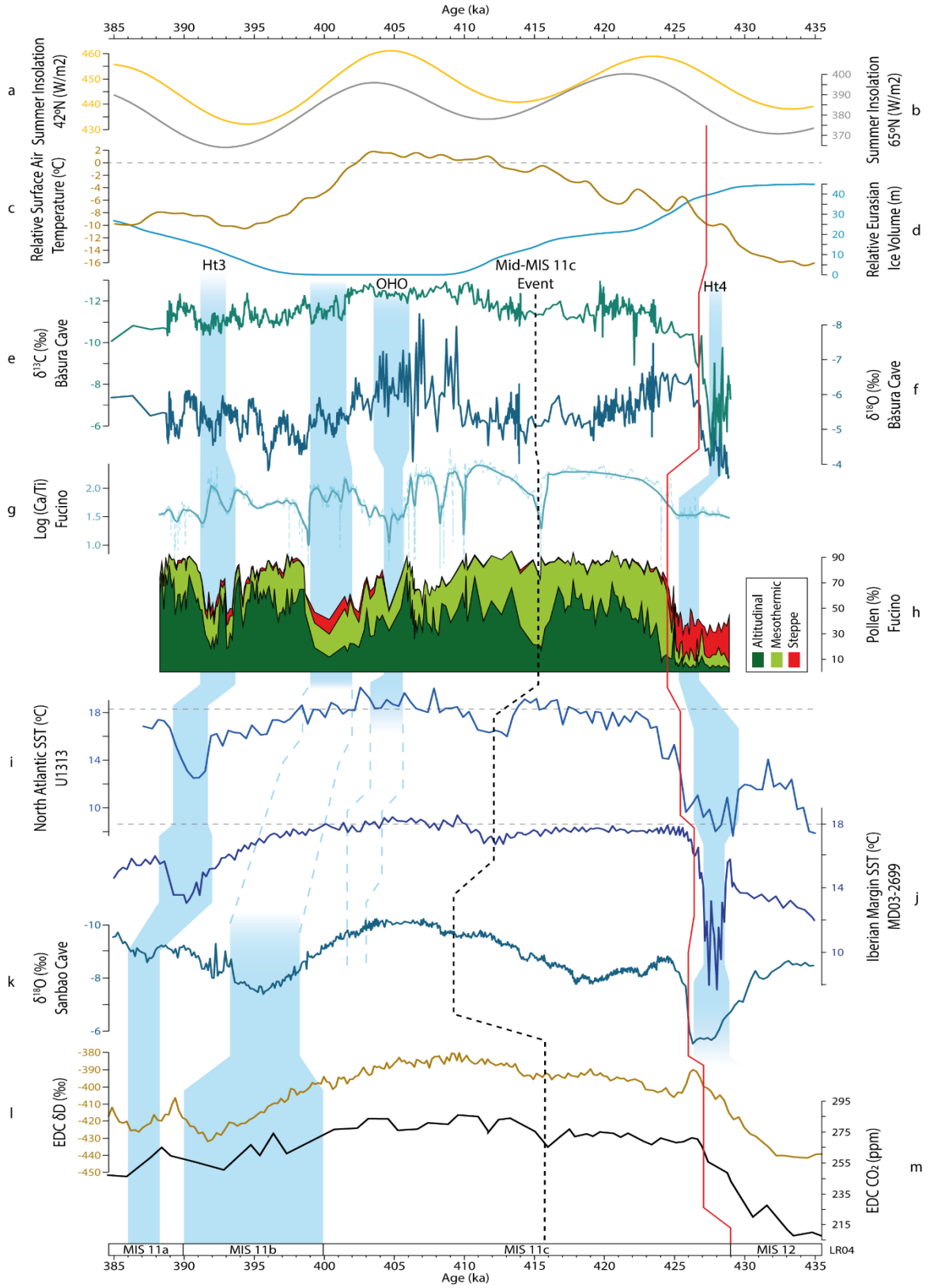

Fig. 2.8.- *a) Summer insolation at 42ºN and b) 65ºN (Laskar et al., 2004). c) Eurasian atmospheric surface air temperature relative to present values (Bintanja and van de Wal, 2008). d) Eurasian ice volume relative to present (Bintanja and van de Wal, 2008). e) $\delta^{13}C$ and f) $\delta^{18}O$ from Bàsura Cave speleothem (N Italy; Hu et al., 2024). g) Log(Ca/Ti) and h) pollen record from Fucino Basin (this study.) i) North Atlantic Sea Surface Temperature (SST) (Naafs et al., 2013a, 2014). j) Iberian Margin SST (Rodrigues et al., 2011). k) $\delta^{18}O$ from Sanbao Cave (China; Cheng et al., 2016). l) Antarctic EDC δD and m) CO_2 (Bouchet et al., 2023). The different records are represented from North (top) to South (bottom). The blue boxes correlate cold-dry periods. The Heinrich type events (Ht) were identified in j and correlated with the rest of the records. The red line indicates the limit between MIS 12 glacial and MIS 11 interglacial defined by each author from each record. The dashed line correlates the Mid-MIS 11c event that separates the MIS 11c interglacial into two other sub-periods. Dashed lines in c, i and j mark the present value. At the bottom are represented the MIS stages limits defined by Railsback et al. (2015) over the LR04 record (Lisiecki and Raymo, 2005).*

Bàsura cave could be due to the chronology uncertainties, being each record dated from different methods. The comparison of Fucino Basin record with other Mediterranean pollen records also shows the substitution of xerophytic vegetation for mesothermic taxa at the G/I boundary (Fig. 2.7). The altitudinal taxa played a more important role in this transition in the central region of the Mediterranean area (e.g. Lake Ohrid, Ioannina, this study), than in the eastern and western Mediterranean, where the Mediterranean forest is more abundant (Tzedakis, 1993; Tzedakis et al., 2001; Kousis et al., 2018; Hes et al., 2022; Koutsodendris et al., 2023a; Sassoon et al., 2023; Fig. 2.7). This could be consequence of the altitude and latitude of the compared sites, registering Lake Ohrid and Fucino Basin slight colder and more humid conditions during the interglacial period (Kousis et al., 2018).

At global scale, the climate changed to warmer and more humid conditions at 423.1 ± 1.3 ka in the subtropical and mid-latitude North Atlantic (Hu et al., 2024). This coincided with the beginning of an interglacial phase of the AMOC, enabling North Atlantic Deep Water to ventilate the deep Atlantic Ocean resulting in unusually high northward heat transmission from subtropical latitudes. This scenario is consistent with the warming observed in the eastern North Atlantic, Eirik Drift, and southern Greenland during MIS 11c (Rodrigues et al., 2011; Hu et al., 2024).

At the beginning of MIS 11c in Fucino Basin, mesothermic deciduous tree taxa display a vegetation succession starting by *Quercus* association at 424.5 ± 4.0 ka, followed by *Carpinus betulus*, *Carpinus orientalis/Ostrya*, and *Celtis* from 423.9 ± 3.8 ka to 415.4 ± 2.5 ka (indicating a slightly cooler phase; Desprat et al., 2005) (from this point on this association will be referenced as *Carpinus* association), then *Alnus*, *Salix* and *Zelkova* (from this point on this association will be referenced as *Alnus* association) appeared between 415.4 ± 2.5 ka and 405.1 ± 1.7 ka and finally *Pterocarya* in a late phase of the interglacial. The appearance of each association through time doesn't imply that the previous associations disappeared. This sequence of appearance was also observed in other records from the same age (e.g. Okuda et al., 2001; Desprat et al., 2005; Kousis et al., 2018). The *Quercus* association appeared in the first insolation maxima that occurred at the beginning of the interglacial. After that moment, the summer insolation values started to decrease, generating a decrease in temperatures, producing the increase in the *Carpinus* association at 423.9 ± 3.8. Since this moment, *Abies* increased abruptly its abundance, indicating an increase in the precipitation values.

The pollen records from South to Central Europe, including Fucino, exhibited a unique tree composition for MIS 11, presenting a strong expansion of *Abies* associated with the presence of *Pterocarya* and *Buxus* during the warmer periods (e.g. Tzedakis et al., 2001; Desprat et al., 2005; Koutsodendris et al., 2010; Kousis et al., 2018).

If we compare the beginning of the interglacial period in the Mediterranean pollen records (Fig. 2.7), we can observe that the increase in temperatures triggered an increase in *Abies* at Fucino Basin, Lake Ohrid and Ioannina and the increase in mesothermic taxa at western and eastern Mediterranean (Tenaghi Philippon, Alboran Sea and Iberian Margin). The abundance of altitudinal taxa at Fucino, Lake Ohrid and Ioannina pollen

records could be related to more humid conditions due to the relative higher altitudes and/or latitudes at which they are located (650, 693 and 469 m a.s.l. respectively; Fig. 2.7).

2.5.3.1.1 Mid-MIS 11c Event (415.4 ± 3.5 ka and 413.7 ± 3.2)

An important decrease in the abundance of altitudinal taxa occurred in the Fucino Basin during MIS 11c between 415.4 ± 3.5 ka and 413.7 ± 3.2 ka that corresponds to the Mid-MIS 11c event. This event is associated with a decrease in the summer insolation, which separates the two precessional-cycles insolation maxima that characterised MIS 11c. This event has previously been described with a reduction of the SST due to the insolation variability with a duration of ~3 kyrs (Rodrigues et al., 2011; Naafs et al., 2014), but has never been described in pollen records. This event is not so obvious in other Mediterranean pollen records but could correspond to a shorter duration change in vegetation dynamics between the first insolation maxima and the second insolation cycle (Fig. 2.7). The insolation second cycle reached it maxima at ~405.0 ka, presenting higher temperatures and precipitation values across the globe, producing the vanishing of glacial sheets in Eurasia (Bintanja and van de Wal, 2008). Those climatic characteristics can also be observed in Fucino pollen record, since the Mid-MIS 11c event until the beginning of MIS 11b (Figs 2.7 and 2.8).

In Fucino, a significant and abrupt decrease in altitudinal taxa, TOC, TIC, Log(Zr/K), and Log(Ca/Ti) can be observed during the Mid-MIS 11c event (Fig. 2.5). This can be interpreted as a decrease in precipitation, producing a decrease in the sedimentary input into the basin (low Log(Zr/K) values), probably related to a minimum of summer insolation (Fig. 2.5). A comparison of Fucino with Lake Ohrid pollen records shows the decrease in altitudinal taxa and an increase in mesothermic taxa, especially in Mediterranean taxa, at this moment (Fig. 2.7). Also, the Fucino tephra layer TF-125, corresponding to a pyroclastic deposit from Vico α eruption (415.5 ± 2.5 ka, Fucino modelled age Monaco et al., 2021; 414.8 ± 2.2 ka $^{40}Ar/^{39}Ar$ age, Pereira et al., 2020), which allows a direct correlation with Lake Ohrid record, which contains the same tephra layer, OH-DP-1700.6, dated according to Ohrid Modelled age, to 414.75 ± 3.2 (Leicher et al., 2021; Fig. 2.7).

The Mid-MIS 11c event produced an increase in altitudinal taxa at Tenaghi Philippon, indicating higher precipitation levels during the second precession maxima (Koutsodendris et al., 2023a). This event was longer in duration at Lake Ohrid and Fucino, generating an increase in the Mediterranean vegetation abundance and a reduction in the altitudinal taxa (Fig. 2.7). A decrease in precipitation is also recorded in the Bàsura and Sanbao speleothem record during the Mid-MIS 11c event (Cheng et al., 2016; Hu et al., 2024; Fig. 2.8).

This event seems to be highly correlated with the summer insolation, either weak during this time compared with other interglacial periods as MIS 5 (Laskar et al., 2004). Although, in other records is defined as a decrease in temperatures, the Fucino pollen record shows that it was more related to drier conditions, as only hygrophilous species such as *Abies* reduced their abundance, being replaced by mesothermic taxa and lacking steppic and herbaceous cold indicators.

2.5.3.1.2 The end of the MIS 11c (413.7 ± 3.2 ka – 402.7 ± 2.3 ka)

After the event at 413.7 ± 3.2 ka, altitudinal taxa resume its dominance in Fucino Basin. There was a maximum peak of *Abies* abundance at 405.9 ± 1.4 ka, coinciding in time with the interglacial thermal maximum registered in the North Atlantic SST (Fig. 2.8; Voelker et al., 2010; Rodrigues et al., 2011). This maximum could also correspond with the full interglacial conditions in northern Italy at ~408.5 ka (Hu et al., 2024).

Just after the insolation maxima, a cold-dry event that produced a decrease in altitudinal taxa (PZ-3b, c; Fig. 2.2; Table 2.1) occurred, probably related to the previously described "Older Holsteinian Oscillation" (OHO) (Oliveira et al., 2016; Kousis et al., 2018). The forest contraction related to the OHO can also be observed in the Iberian Margin, Alboran Sea, Lake Ohrid and Tenaghi Philippon with a decrease in mesothermic taxa abundance (Fig. 2.7). *Fagus* occurrence started to be important during the OHO cold phase, however the summer temperatures were still high, evidenced by the presence of *Buxus* (Desprat et al., 2005) (also evidenced by the pollen PC2 results; Fig. 2.3). The U1385-11-fe1 event identified by Oliveira et al. (2016) in the Iberian Margin show that the OHO may have been associated with drier rather than cooler conditions and related to positive North Atlantic Oscillation (NAO), affecting the distribution of the Westerlies and, as consequence, the precipitation across Europe (Fig. 2.7; Kousis et al., 2018). After the OHO occurred, the pollen records across the Mediterranean area showed a diminution of the mesothermic taxa abundances, indicating colder temperatures.

Since the end of the OHO event, at 403.7 ± 2.0 ka, the Fucino lake level and its productivity decreased. *Abies* decreased in a late phase of the interglacial the reaching a minimum at 400.4 ± 2.5. However, *Fagus* and *Pterocarya* forest species increased (depicting a similar pattern through time like the vegetation succession described at the Iberian Margin; Desprat et al., 2005).

2.5.3.2 The MIS 11b-a stages (402.7 ± 2.3 ka – 388.3 ± 3.2 ka)

A colder and drier period is observed between 402.7 ± 2.3 ka and 399.0 ± 2.8 ka, when the herbs and steppic taxa dominated at lower elevation. This period could be related to a decrease in seasonality and summer insolation (Fig. 2.5) during MIS 11b, when the global temperatures decreased until reaching a minimum during the interglacial (Bintanja and van de Wal, 2008; Bouchet et al., 2023; Fig. 2.8). A diminution in precipitation values deduced by an increase in $\delta^{18}O$ is also registered at Sanbao Cave (China), confirming that this decrease in summer insolation had global implications (Cheng et al., 2016; Fig. 2.8). Since this moment, the Fucino paleolake suffered an abrupt change documented by the PCA correlation, when Ca was more correlated to herbaceous and steppic taxa, indicating colder and drier periods (Fig. 2.6). The Ca input at that time seems to be exclusively associated with algae productivity related to drier conditions rather than input from Ca ion caption in warmer conditions in the lake (Fig. 2.3 and 2.6).

After 399.0 ± 2.8 ka, in a context of decreasing summer insolation, the Fucino mesothermic pollen taxa displayed the same association succession previously described at the beginning of the MIS 11c interglacial, but

completed in a shorter period of time, with the sequence of *Quercus*, *Carpinus* and *Alnus* associations in less than 2 kyrs duration (PZ-5a; Table 2.1). Since this moment it could be described as the beginning of the MIS 11a stage. The coldest conditions during this period were reached between 397.5 ± 3.0 ka and 395.5 ± 3.2 ka (PZ-5b; Table 2.1), when *Fagus* reached peak values. The Alboran Sea record indicates colder conditions during this time, in which the mesothermic and Mediterranean taxa suffered an important decrease, being substituted by steppe and altitudinal taxa (Sassoon et al., 2023).

Another cold event occurred at 393.7 ± 3.2 ka, just after the insolation minimum when the values started to increase again. This cold event could be correlated to Ht3 described by González-Lanchas et al. (2022) in the Alboran Sea and by Rodrigues et al. (2011) in the Iberian Margin as a SST reduction, also observed in North Atlantic SST (Naafs et al., 2014; Fig. 2.8). Although, steppic and altitudinal taxa followed the typical "W" pattern distribution described in Singh et al. (2023). This Ht also affected the algae concentration in the lake, shown by the increase in eutrophic water conditions due to the decrease in the lake levels during drier conditions. The Ht3 is also observed in Lake Ohrid, with a similar vegetation composition as Fucino pollen record.

The youngest part of the studied Fucino pollen record between 391.0 ± 3.2 and ~388.3 ± 3.2 ka show a similar evolution as the registered after MIS 11b at 399.0 ± 2.8 ka. However, a difference between these two periods is that mesothermic taxa abundance is slightly lower than the period comprehended between 399.0 ± 2.8 and 394.5 ± 3.2 ka colder conditions. Additionally, the precipitation increased during that time, deduced by the enhanced fluvial siliciclastic input evidenced by Log(Zr/K), and the dominance of altitudinal taxa. This increase in precipitation at similar age can be also observed in northern Italy, evidenced by a decrease in $\delta^{18}O$ values at Bàsura cave (Hu et al., 2024).

2.6 Conclusions

The palynological record from the Fucino F4-F5 composite record, independently dated between 429.0 ± 5.0 ka and 388.3 ± 3.2 ka, permitted us to reconstruct vegetation and environmental dynamics over the late MIS 12 to the beginning of MIS 11a.

MIS 12 in Fucino Basin was characterised by a very dry and cold climate, evidenced by the dominance of steppic taxa and low lake levels.

The change from the MIS 12 glacial to the MIS 11 interglacial is detected in Fucino at 424.5 ± 4.0 ka, with a significant increase in forest taxa and sedimentological properties indicating warming and more humid conditions. High lake levels and lake productivity occurred during the MIS 11 interglacial but there were significant lake level fluctuations depending on climate conditions.

Millennial-scale variability is noticed in the studied pollen sequence and allowed the characterisation of several climatic events through time, such as Ht4 and Ht3 at 426.0 ± 5.0 ka and at 393.7 ± 3.2 ka, respectively. In addition, the Mid-MIS 11c event was identified in the Fucino pollen record between 415.4 ± 3.5 ka and 413.7 ± 3.2 ka. This event seems to also occur in other Mediterranean pollen records and was characterised by drier climatic conditions separating the two MIS 11c warm-humid precessional cycles.

The Fucino pollen record also shows a dry period, deduced by the decrease in forest abundance, during MIS 11 and centred at 405.5 ± 1.6 ka, which could be related to the OHO that occurred before MIS 11b colder conditions.

The vegetation changes in Fucino seem to be related to the variations in summer insolation, controlling the humidity and temperature in the study area during the interglacial period.

This study shows regional differences in the vegetation dynamics associated to climate change during MIS 12 and MIS 11 due to dissimilar altitudinal and latitudinal setting, being the central Mediterranean site different, with high *Abies* representation and less abundance of Mediterranean taxa, compared to the records located at the eastern and western Mediterranean area.

Chapter 3: Quantitative paleoclimatic reconstruction of MIS 11 in Fucino Basin

- Vera-Polo, P., Sadori, L., Jiménez-Moreno, Camuera, J., G., Masi, A., Giaccio, B., Zanchetta, G., Tzedakis, P.C., Wagner, B.. Pollen-based temperature and precipitation quantitative reconstructions of MIS 11 interglacial from the Fucino Basin (central Italy).

Pollen-based temperature and precipitation quantitative reconstructions of MIS 11 interglacial from the Fucino Basin (central Italy).

Vera-Polo, P.[a b], Sadori, L.[a], Jiménez-Moreno, G.[b], Camuera, J.[c], Masi, A[a], Giaccio, B.[d e], Zanchetta, G.[f], Tzedakis, C[g], Wagner, B[h]

a Dipartimento di Biologia Ambientale, University of Rome "La Sapienza", Rome, Italy

b Departamento de Estratigrafía y Paleontología, Universidad de Granada, Granada, Spain

c Departamento de Farmacología, Farmacognosia y Botánica, Universidad Complutense de Madrid, Madrid, Spain

d Istituto di Geologia Ambientale e Geoingegneria, CNR-IGAG, Monterotondo, Rome, Italy

e Istituto Nazionale di Geofisica e Vulcanologia, INGV, Rome, Italy

f Dipartimento di Scienze della Terra, University of Pisa, Pisa, Italy

g Environmental Change Research Centre, Department of Geography, University College London, London, UK

h Institute of Geology and Mineralogy, University of Cologne, Cologne, Germany

Abstract

Pollen-based paleoclimatic reconstructions offer insights into historical climate variability and provide quantitative data that can be directly compared with present-day climatic conditions. The Quaternary period, known for its significant climatic variability, is marked by alternating glacial and interglacial cycles. Among these, Marine Isotope Stage (MIS) 11c stands out as a notable interglacial period, considered an orbital analogue to the Holocene (MIS 1) due to similar conditions without the influence of human activities. In this study, we present a detailed quantitative paleoclimatic reconstruction for the MIS 11c period based on pollen data from the Fucino Basin. Using the weighted averaging partial least squares (WA-PLS) method, we reconstruct past climate conditions to examine regional and global climatic changes as reflected in vegetation dynamics during MIS 11c. Our analysis reveals that vegetation in the Fucino region was highly sensitive to variations in insolation, reflecting climate shifts on millennial scales. Notably, we identified the Mid-MIS 11c event, a significant climatic shift that split MIS 11c into two distinct phases, each corresponding to a precessional cycle characterized by a peak in insolation. Overall, our findings indicate that during the MIS 11c interglacial, the Fucino Basin experienced warmer temperatures and slightly drier conditions compared to the present climate.

Key words: Quantitative reconstruction, Pollen-based reconstruction, Climatic change, MIS 11, Mediterranean region, Glacial-Interglacial cycle

3.1 Introduction

Fossil pollen records have been used around the world (and particularly in the Mediterranean region) during the Pleistocene as a source to develop quantitative paleoclimatic reconstructions for (e.g. Seppä et al., 2004; Fawcett et al., 2011; Kousis et al., 2018; Ardenghi et al., 2019; Sinopoli et al., 2019). Several transfer functions have been employed to obtain quantitative values of temperature and precipitation from pollen data, comparing the fossil pollen assemblages with the modern pollen distributions (e.g. Seppä et al., 2009; Xu et al., 2010; Liang et al., 2020; Wei et al., 2021; Zhao et al., 2021). The two most widely employed techniques are the modern analogue technique (MAT; Guiot, 1990) and the weighted averaging partial least squares (WA-PLS; Ter Braak and Juggins, 1993). The paleoclimatic quantitative reconstruction derived from these techniques facilitate the assessment of interglacial climatic changes and their implications for understanding natural dynamics in the context of the Quaternary climate cycles without the influence of human impact (Ruddiman, 2003; Kleinen et al., 2014).

The Quaternary climate is defined by a cyclical alternation between glacials and interglacials (G/I), mainly controlled by Earth's orbital parameters fluctuations (Hays et al., 1976). One of the most interesting interglacials occurred during the Quaternary was the Marine Isotope Stage (MIS) 11. This interglacial (ca. 424-367 ka; Ardenghi et al., 2019) serves as a crucial interglacial period that is often regarded as a Holocene (MIS 1) analogue due to its similarities in orbital configuration to present-day conditions (McManus et al., 2003; Tzedakis, 2010; Candy et al., 2014), weak precessional variations (Berger and Loutre, 2003) and occurred after a large magnitude glacial termination (EPICA Community Members, 2004; Tzedakis, 2010), but without human impact that could affect the climatic signal (Loutre and Berger, 2000; Cheddadi et al., 2005; Tzedakis et al., 2022; Sassoon et al., 2023).

The MIS 11 interglacial is traditionally subdivided into three substages (Hrynowiecka et al., 2019), with MIS 11c (424-396 ka; Ardenghi et al., 2019; Tzedakis et al., 2022) representing the first interstadial phase characterized by significant warming and ecological transitions (Tzedakis et al., 2022). This period follows the Mid-Brunhes Event (MBE), which marks a shift from low-amplitude G/I cycles to high-amplitude G/I cycles, significantly influencing climatic conditions (Rodrigues et al., 2011; Tzedakis et al., 2022). The transition from MIS 12, one of the coldest glacial periods in the Quaternary (Ehlers and Gibbard, 2008; Hu et al., 2024), to the warm-humid interglacial conditions of MIS 11c is defined as one of the most notable climatic changes in the past 800,000 years (Berger and Wefer, 2003; Laskar et al., 2004; Rodrigues et al., 2011). The occurrence of MIS 11c deglacial warming is considered unusual, because it occurs when the incoming isolation and eccentricity values were very low (Laskar et al., 2004; Rodrigues et al., 2011; Cheng et al., 2016), questioning the orbital theory of Pleistocene G/I cycles (Paillard, 2001; Berger and Wefer, 2003; Tzedakis et al., 2017). This discrepancy between the beginning of MIS 11c interglacial and the weak astronomical forcing triggering it is known as the "Stage 11 problem" (Imbrie et al., 1993). The MIS 11c interstadial (424-396 ka; Tzedakis et al., 2022) was exceptionally long (~30 kyr), spanning two precessional cycles (Kukla, 2003), and was characterised by high sea levels (6-13 m above the present level; Spratt and Lisiecki, 2016; Christ et al., 2023) and higher

atmospheric greenhouse gases concentrations compared to the Holocene (Ruddiman et al., 2016; Vavrus et al., 2018).

The Mediterranean region serves as an interesting setting to investigate the G/I dynamics (Tzedakis et al., 1997) due to its strong seasonal contrast (warm-dry summers vs cold-humid winters; Lionello et al., 2006) and the influence of many regional factors that control the climate as the North Atlantic Oscillation (NAO; Harding et al., 2009), the seasonal expansion northward of the Hadley Cell circulation (Roberts et al., 2011) and the indirect effects of the African and Asian monsoons in the southern regions (Lionello et al., 2006). All these factors interact with the altitudinal contrast of the region, having a wide range of regional climatic conditions (Fletcher et al., 2010; Jiménez-Moreno et al., 2013).

The Fucino Basin, located in central Italy, offers a distinctive environment to study the interplay between vegetation and diverse climatic conditions (Blasi et al., 2017), particularly those associated with both mountainous and Mediterranean climates (Blasi, 2010). This region's ecological variability provides a valuable lens through which we can explore historical climatic changes and their impacts on vegetation dynamics. In this study, we present a detailed paleoclimatic reconstruction of MIS 11 based on high-resolution fossil pollen data from the Fucino Basin.

3.2 Regional setting: current climate and vegetational distribution

The Fucino Basin (Abruzzo; 42º 00' 00" N; 13º 30' 00" E; Fig. 3.1) is located at 650 m in elevation and is surrounded by the Central Apennines's highest peaks, which hosted mountain glaciers during glacial periods (Giraudi and Giaccio, 2015). It is one of the largest inter-Apennine tectonic depressions (~900 km^2), originated during the Plio-Quaternary extensional phase (Cavinato et al., 2002). Lake Fucino was formed in this basin during the Early Pleistocene, covering ~140 km^2 and registering a maximum depth of 20 m, being the Italy's third largest lake during the time was formed (Mannella et al., 2019; Caielli et al., 2023) until the moment that was drained in 1875 for agricultural purposes (Giaccio et al., 2017). The interplay between the lake and the tectonic activity resulted in continuous sedimentation, hosting ~900 m thick Plio-Quaternary fluvio-glacial carbonated deposits in the depocenter (Galadini and Galli, 2000; Cavinato et al., 2002; Galadini and Messina, 2004; Giaccio et al., 2017, 2019; Mannella et al., 2019). The carbonated deposits were often interrupted by tephra layers deposited from peri-Tyrrhenian magmatic region, serving as age markers from the Plio-Quaternary deposits (Giaccio et al., 2017, 2019; Monaco et al., 2021, 2022; Leicher et al., 2023, 2024).

Various microclimates occur in the area due to the complex orography and the influence of the Mediterranean Sea (Silvestri et al., 2022). The current Fucino Basin climate can be described as Mediterranean with continental characteristics (Lionello et al., 2006; Peyron et al., 2013). Borgo Ottomila Fucino Meteorological Station (FMS) (Fig. 3.1) registered mean annual temperature (TAnn) of 11.1 ºC and mean annual precipitation (PAnn) value of 1116 mm as an average value recollected from 1991 to 2021 (https://en.climate-data.org/europe/italy/abruzzo/borgo-ottomila-1068722/, last access: 02 October 2024). In the last year the

temperatures increased 1.9 ºC and the precipitations decreased 38.5 mm (https://www.meteoaquilano.it/index.php?option=com_content&view=article&id=344&Itemid=525, last access: 02 October 2024). The coldest temperatures (below 10 ºC) are registered from November to March, reaching daily minima of -5 to -2 ºC in January. From June to August, the mean monthly temperature is ~20 ºC. July and August are the driest moths in Fucino (43 mm and 41 mm respectively), evidencing the Mediterranean climatic influence (warm-dry summers and cold-humid winters; e.g. Lionello et al., 2006). The more humid months in the area are from October to December, peaking in November with 151 mm (Fig. 3.1). The PAnn in the region varies depending on the orographic factor, ranging from 650 to 750 mm in the plains to 900 to 1200 mm in the piedmont zone. According to the WorldClim v2.1 database (Fick and Hijmans, 2017) (employed in this study to develop the quantitative reconstructions) the present-day TAnn and PAnn are around 10 ºC and 750 mm respectively.

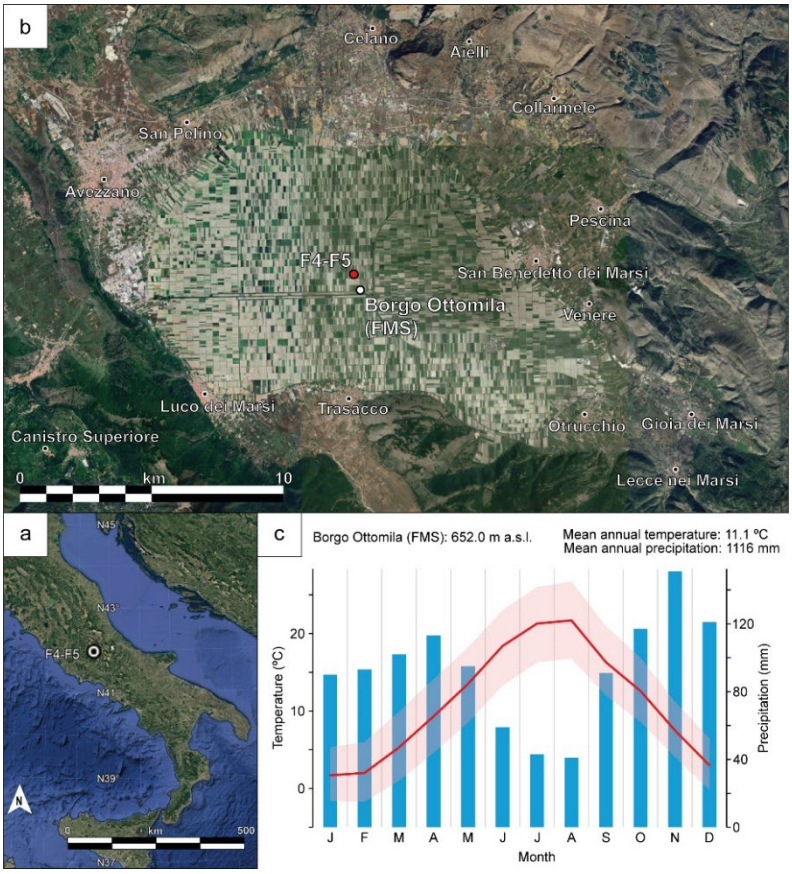

Fig. 3.1.- *a) Geographical location of the F4-F5 composite record in Italy. b) Geographical location of the F4-F5 composite record and Borgo Ottomila Fucino Meteorological Station (FMS) in the Fucino Basin. c) Ombrothermic diagram of Borgo Ottomila (FMS) (https://en.climate-data.org/europe/italy/abruzzo/borgo-ottomila-1068722/, last access: 02 October 2024). Blue column diagram represents the monthly precipitation and the red line the mean monthly average temperature. The transparent border that involves the temperature line represent the maximum and minimum values for each month. a and b images were obtained from Google Earth.*

In the Fucino Basin there is a complex vegetation zone distribution due to the geomorphological setting of the Apennines and the Mediterranean influence (Blasi and Del Vico, 2012). It is challenging to describe precisely these natural vegetation zones because the area has a significant present-day human impact and agricultural use (Frate et al., 2018; Giaccio et al., 2017). The grassland composed by hygrophilous and hydrophytic freshwater plants dominates the basin's lower flatter areas (Blasi et al., 2017). This vegetation zone also extends towards western side of the surrounding reliefs due to pluviometric shading generated from the main E-W wind pattern (Tomassetti et al., 2003). Oak forest, dominated by *Quercus pubescens*, is found in the surrounding relief at low elevation areas (below 1000 m a.s.l.). In cooler areas of the same elevation zone, the forest is composed by mixed taxa as *Ostrya carpinofolia*, *Quercus cerris*, and *Acer* spp. Evergreen scrub communities, dominated by *Quercus ilex*, can be found over lithoid outcrops. Other taxa as *Acer pseudoplatanus*, *Ulmus glabra*, *Tilia platyphyllos*, and *Fraxinus excelsior* can be found in restricted and humid areas (e.g. valleys and ravines). *Fagus*

sylvatica forest association, frequently appearing alongside *Abies alba*, can be found at higher elevations (1000-1750 m). Endemic herbaceous plants and glacial herbaceous relicts dominate the high mountain vegetation above 2000 m a.s.l. elevation. Poaceae, Cyperaceae, and alpine herbs adapted to harsh climatic conditions characterise the alpine meadows, rocky slopes, and scree fields (Blasi, 2010; Blasi et al., 2017).

3.3 Material and methods

3.3.1 F4-F5 Pollen record

The sedimentary succession was reconstructed according to the composite record (42º 00' 07'' N; 13º 32' 19'' E; Fig. 3.1) from F4-F5 boreholes, drilled in June 2017 (Giaccio et al., 2019). F4 and F5, separated 3 m from each other, exhibit a 0.75 m overlap between 1.5 m-long core barrel from each borehole using physical and lithological parameters for the correlation (Giaccio et al., 2019).

The age model reconstructed by Monaco et al. (2021) (Fig. 2.1) for the F4-F5 composite record was essential to set the spacing between the pollen samples to obtain the highest resolution possible. The maximum resolution was obtained from the bottommost part of F4-F5 (97.7-97.4 m), with a spacing between samples every 2-cm. For the consecutive 50 cm, the sample spacing is 1-cm, reaching an age resolution between 200 and 100 years. The rest of the core was sampled at intervals of ~4-cm achieving an average resolution of ~120 years.

A total of 216 samples were collected for palynological analysis from the composite F4-F5 record. Each sediment sample was treated following the conventional method to concentrate the pollen grains (Faegri and Iversen, 1975). Samples consisted of 2 g of sediment to which we added 1 *Lycopodium* tablet to calculate pollen concentration. The samples were treated with acids (HCl, 37% to remove carbonates and HF, 48% to remove silicates), and bases (NaOH, 10% used to remove the cellulose fraction and deflocculate the organic matter). After the chemical treatment, the samples were sieved using a 10 μm nylon sieve to remove particles smaller than pollen grains. The remaining material was mounted on microscope slides and examined using a transmitted light microscope at 400x magnification. An average of 300 total pollen grains were counted per sample. This quantity has proved to be enough for making a broad paleoenvironmental interpretation (Djamali and Cilleros, 2020). The pollen percentage and graphic representation of the data were obtained using the Tilia Software v2.6.1 (Fig. 2.2 and 2.4).

Previous literature was employed as a base to group the identified pollen taxa into three main ecologically significant specific vegetation: Altitudinal, Mesothermic and Steppic taxa (e.g. Joannin et al., 2011; Bertini et al., 2015; Camuera et al., 2019; Vera-Polo et al., 2024) (Fig. 2.4) These categories have previously been shown to be successful as trustworthy as climatic proxy indicators for the Mediterranean region (Altolaguirre et al., 2020; Camuera et al., 2021). Due to their low abundance the Mediterranean/sclerophyllous taxa were included into the mesothermic taxa group (Fig. 2.4). The aquatic and plants (*Nuphar*, *Potamogeton* and *Typha*) were excluded from the total pollen sum.

3.3.2 Quantitative paleoclimatic reconstruction: MAT and WA-PLS

The reconstruction of the past TAnn and PAnn from Fucino pollen data was carried out by using the C2 software (Juggins, 2007), integrating 8174 modern pollen data from the Eurasian Modern Pollen Database (EMPDv2; Davis et al., 2020) and the climate parameters obtained from WordClim v2.1 database (Fick and Hijmans, 2017) (Fig. S1.5). During the harmonization process of both Fucino record and the EMPDv2 minor taxa/species with low relative abundances were integrated within major taxa/genera/families with the help of the Plants of the World online database (http://www.plantsoftheworldonline.org) and the Integrated Taxonomic Information System (http://www.itis.gov), which resulted in a total of 389 pollen taxa. Aquatic and cultivated species were removed since the distribution of these plant could be influenced by other factors rather than climate.

Two transfer functions were employed in this study to develop the quantitative paleoclimate reconstruction: MAT (Guiot, 1990) and WA-PLS (Ter Braak and Juggins, 1993). The MAT employs the paleoecological dataset in a statistical analysis called "k-nearest-neighbours" (k-NN; Cover and Hart, 1967). The results from this method are not explicit related with the response of the taxa to climate variations, but are based on the measurement of the degree of similarity ("degree of analogy") between fossil pollen assemblages and the elements from the modern database (Chevalier et al., 2020). The MAT developed for this analysis was calculated for the nearest 5, 10, 15, 20 and 30 analogues (Fig. S3.1). The similarity between pollen samples was measured by the squared chord distance, which reduces the influence of the most common species, while keeping their relative order to each other, meaning that the low pollen production species are not overshadowed (Overpeck et al., 1985).

WA-PLS regression is a non-linear unimodal technique which assumes that plant species have their maximum abundances in different climate niches and that niche breadth drives the species environmental tolerance (Chevalier et al., 2020). A total of five components were run to generate WA-PLS regressions. We choose the second component (2C) of the WA-PLS technique under leave-one-out cross-validation method. Increasing the number of components reduces the root mean squared error, but it can also result in overfitting the data, leading to a drop in the model predictive value (Ter Braak and Juggins, 1993). The graphic results obtained from this method were smoothed using the locally estimated scatterplot smoothing (LOESS) with a span value of 0.05 employing the Past4 software (Hammer et al., 2001).

The MAT is more affected by spatial autocorrelation, whereas the WA-PLS has a better correlation between the observed and reconstructed values (Da et al., 2023). In Fucino, although both reconstruction methods show similar evolution through time, the WA-PLS results are less noisy, so we chose the WA-PLS as the main reconstruction method and the one used in the comparisons with other regional and global paleoclimate records (Figs. 3.2 and S3.1).

We conducted a goodness-of-fit analysis over the WA-PLS reconstruction to evaluate the similarity between fossil and modern pollen samples (Fig. S3.2), specifically identifying those samples that exhibit strong affinities

with the modern samples from the training set (Simpson, 2012). The analysis was run under the R Studio v.2024.09.0 (R Core Team, 2021) and using *Rioja* (Juggins, 2024) *tidyverse* (Wickham et al., 2019), *analogue* (Simpson and Oksanen, 2024) and *ggplot2* (Wickham, 2016) packages. This analysis employed pairwise distributions of squared-chord distances between Fucino pollen samples and their best analogues in the modern training-set. A sample is classified as a "good analogue" when its minimum dissimilarity coefficient (squared-chord distance) is lower than the 5th percentile of all distances, whereas samples with distances larger than the 10th percentile are considered to be “no analogues”.

The Past4 software (Hammer et al., 2001) was employed to determine the correlation between the reconstructed paleoclimatic variables and the pollen taxa. The univariate correlation analysis resulted in two statistical values for each correlation: the correlation value (R; a value between 1 and -1 representing a positive or an inverse correlation between the variables) and the statistical significance (p; a value near 0 means that the correlation between the variables is statistically significative, being negligible values higher than 0.05).

3.4 Results

3.4.1 Pollen analysis

The microscopic examination of the 216 palynological samples revealed a good preservation of palynomorphs, identifying 60 different pollen taxa. Herbaceous and steppic taxa dominated the bottommost part of the record until 424.5±4.0 ka representing more than 60% of the total pollen abundance, mainly composed by Poaceae (24.3%), *Artemisia* (13.6%) and Amaranthaceae (7.0%) (Figs. 2.2 and 2.4). Since that moment, the herbaceous pollen was replaced by tree pollen taxa, which maintained an average abundance of 90% throughout the record. Two abundance drops of tree pollen can be observed between 403.5 ± 2.1 ka and 398.7 ± 2.8 ka, and 393.7 ± 3.2 ka and 391.3 ± 3.2 ka, reaching values near 60%. Other pollen variations can be identified when the taxa are grouped by altitudinal, mesothermic and steppic at millennial-scales. Since the 424.5 ± 4.0 ka limit, there is a first increase in mesothermic taxa (mainly formed by *Quercus* deciduous: 15.4%; *Ulmus*: 15.6%; *Acer*: 8.4%; and *Tilia*: 4.4%) that was gradually substituted by altitudinal taxa (mainly composed by *Abies*: 43.0%), reaching its maximum at 417.8 ± 3.6 ka. A change in vegetation occurred between 415.4 ± 2.5 ka and 413.7 ± 2.7 ka with an increase in Mediterranean (12.3%) and mesothermic (65.1%) taxa mainly composed by *Quercus* deciduous (10.4%); *Carpinus orientalis/Ostrya* (12.4%); *Alnus* (3.8%); and *Quercus* evergreen (3.3%), meanwhile the altitudinal taxa reached a minimum (17.5%). Since that point, mesothermic taxa followed an average decreasing trend until the end of the record. Steppic pollen taxa became dominant since 403.5 ± 2.1 ka, maintaining an average value of 4% until 391.2 ± 3.2 ka.

3.4.2 Quantitative reconstructions

The results obtained from the goodness-of-fit analysis indicate a good match between Fucino and the modern pollen training-set, with 40.3% classified as "good analogues", 49.1% as "fair analogues", and 10.6% as "poor analogues".

The TAnn and PAnn WA-PLS reconstructions showed coefficients of determination (R^2) of 0.82 and 0.52 respectively (Fig. S3.3). PAnn reconstruction is highly correlated with *Abies* abundance (R=0.87) and anticorrelated with steppic and herbaceous taxa as *Artemisia* (R=-0.84), Amaranthaceae (R=-0.84), Asteroideae (R=-0.78) and Poaceae (R=-0.86) (Fig. S3.4). The TAnn reconstruction exhibits a positive correlation with deciduous trees taxa like *Pterocarya* (R=0.58), *Fagus* (R=0.48), *Quercus* deciduous (R=0.30), and *Celtis* (R=0.38) and a negative correlation with herbaceous taxa as Poaceae (R=-0.49), *Artemisia* (R=-0.40), Amaranthaceae (R=-0.39), and *Galium* (R=-0.46) (Fig. S3.4).

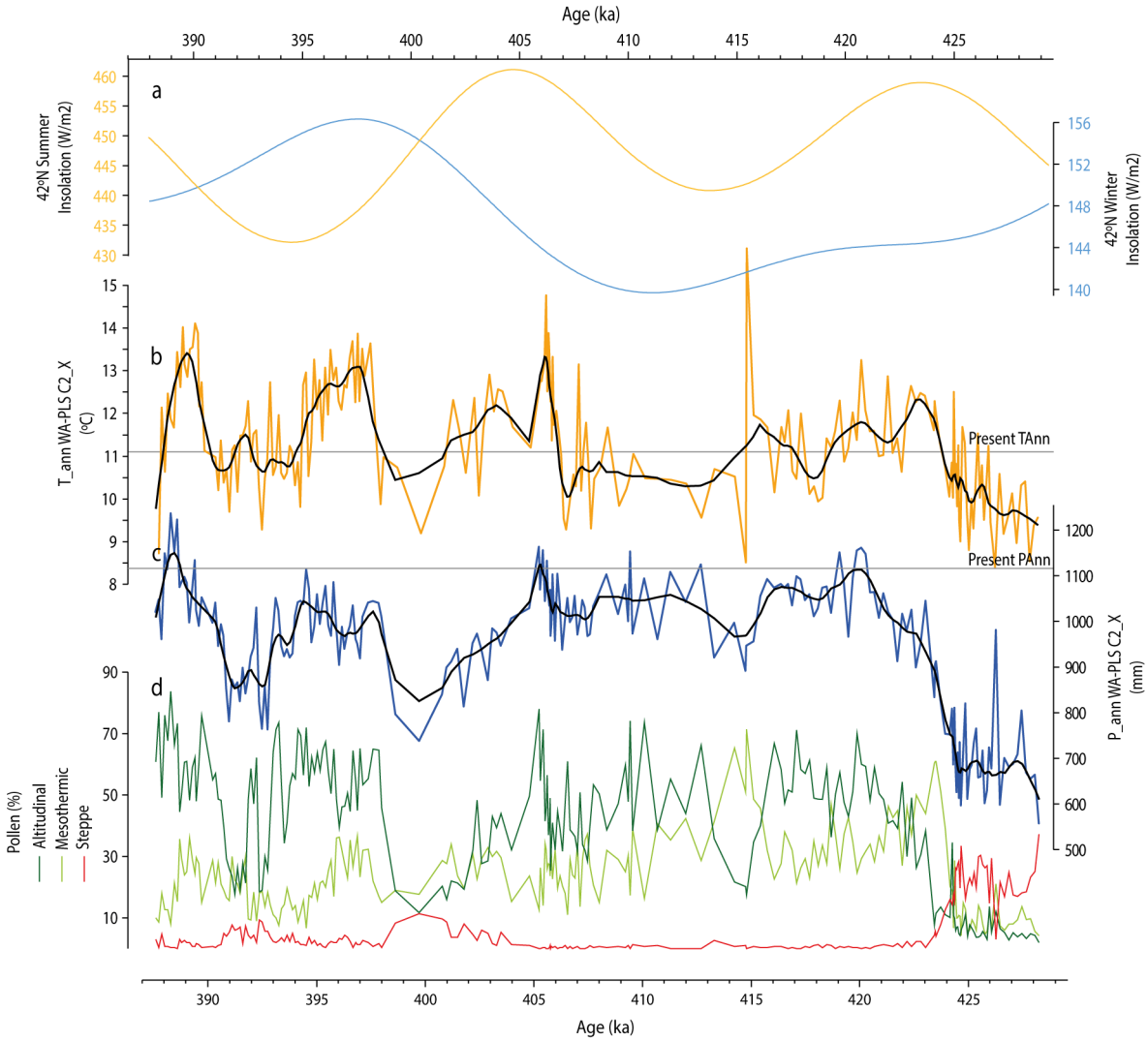

Fig. 3.2.- *Comparison between (a) summer (orange) and winter (blue) insolation at 42°N (Laskar et al., 2004), (b) mean annual temperature (T_ann) reconstruction using Weighted-Averaging Partial-Least Squares (WA-PLS) method (second cross validated component), (c) mean annual precipitation (P_ann) reconstruction using WA-PLS method (second cross validated component), and (d) pollen group percentages of the F4-F5 Fucino record. Black lines from b and c plots indicate the locally estimated scatterplot smoothing (LOESS, span 0.05).*

Three main periods can be distinguished according to the variations of the quantitative reconstructions (Fig. 3.2). The first one occurred before 424.5 ± 4.0 ka and was characterised by an increasing trend in TAnn from 9.5 ºC to 11.0 ºC. PAnn maintained constant values ~680 mm until 425.2 ± 4.6 ka, when the values abruptly increased up to ~850 mm at the end of this first period. The second period could be defined between 424.5 ± 4.0 ka to 406.5 ± 1.3 ka. During this time the TAnn oscillated between 12.5 ºC and 10.5 ºC. The first half of this period exhibits more oscillations and higher values peaking at 423.3 ± 3.8 ka, 420.7 ± 3.6 ka, and 415.4 ± 2.5 ka estimating values of 12.3 ºC, 13.3 ºC, and 15.9 ºC respectively. However, this last value is classified by the goodness-of-fit analysis as a poor analogue. From 415.4 ± 2.5 ka to 406.5 ± 1.3 ka the TAnn decreased maintaining constant values of ~10.5 ºC with a slight increasing trend. The high increase in the estimated PAnn from the previous period, ended at 420.5 ± 3.8 ka reaching a maximum value of 1120 mm. After this maximum, the PAnn maintained constant values between 970 mm and 1150 mm, except for the period between 415.4 ± 2.5 ka and 413.7 ± 2.7 ka, reaching a minimum peak of 890 mm. The third period registered in this record occurred from 406.5 ± 1.3 ka to 388.3 ± 3.2 ka was characterised by more variability in the estimated values with an overall higher TAnn and lower PAnn values. The main oscillations in the TAnn were characterised by three maximum peaks of 14.8 ºC, 13.7 ºC, and 13.9 ºC at 406.2 ± 1.3 ka, 397.2 ± 3.1 ka, and 390.1 ± 3.2 ka respectively. PAnn shows similar peaks but with a slight delay compared to TAnn, being the maximum values of 1160 mm, 1080 mm and 1220 mm at 405.9 ± 1.4 ka, 396.1 ± 3.1 ka and 389.3 ± 3.2 ka respectively. These three maximum peaks are separated by two minimum values in TAnn and PAnn at 400.4 ± 2.5 ka (9.2 ºC, 740 mm) and 393.4 ± 3.2 ka (9.3 ºC, 760 mm).

3.5 Discussion: quantitative reconstruction and regional comparison

The high-resolution Fucino pollen record offers significant regional information about vegetation and climate oscillations during the interval between 429.0 ± 5.0 ka and 388.0 ± 3.3 ka, encompassing several important global climate changes including the Termination V (T-V; 430.5 ± 1.5 ka to 425.0 ± 2.0 ka; Cheng et al., 2016; González-Lanchas et al., 2022), the MIS 12-MIS 11 boundary (424.0 ± 4.0 ka; Lisiecki and Raymo, 2005), and great part the MIS 11 interglacial (424.0 ± 4.0 ka to 367 ± 3.0 ka; Prokopenko et al., 2010; Railsback et al., 2015; Regattieri et al., 2016; Kousis et al., 2018; Ardenghi et al., 2019; Tzedakis et al., 2022; Sassoon et al., 2023).

At present, the Fucino Basin is located in a region dominated by grasslands and deciduous forest including beech forest at the treeline and isolated conifer patches at higher elevations (Blasi, 2010; Blasi et al., 2017). This vegetation distribution changed through time due to regional climatic variations that affected the temperature and humidity conditions in the area. Variations in temperate forest taxa can be used as a reliable indicator of temperature and precipitation changes over time (e.g. Joannin et al., 2011; Bertini et al., 2015; Camuera et al., 2019). *Abies* could also be used as a proxy for precipitation and humidity conditions (Xiang et al., 2007). The increase in this taxon typically occurs after the interglacial thermal maximum and during a post-

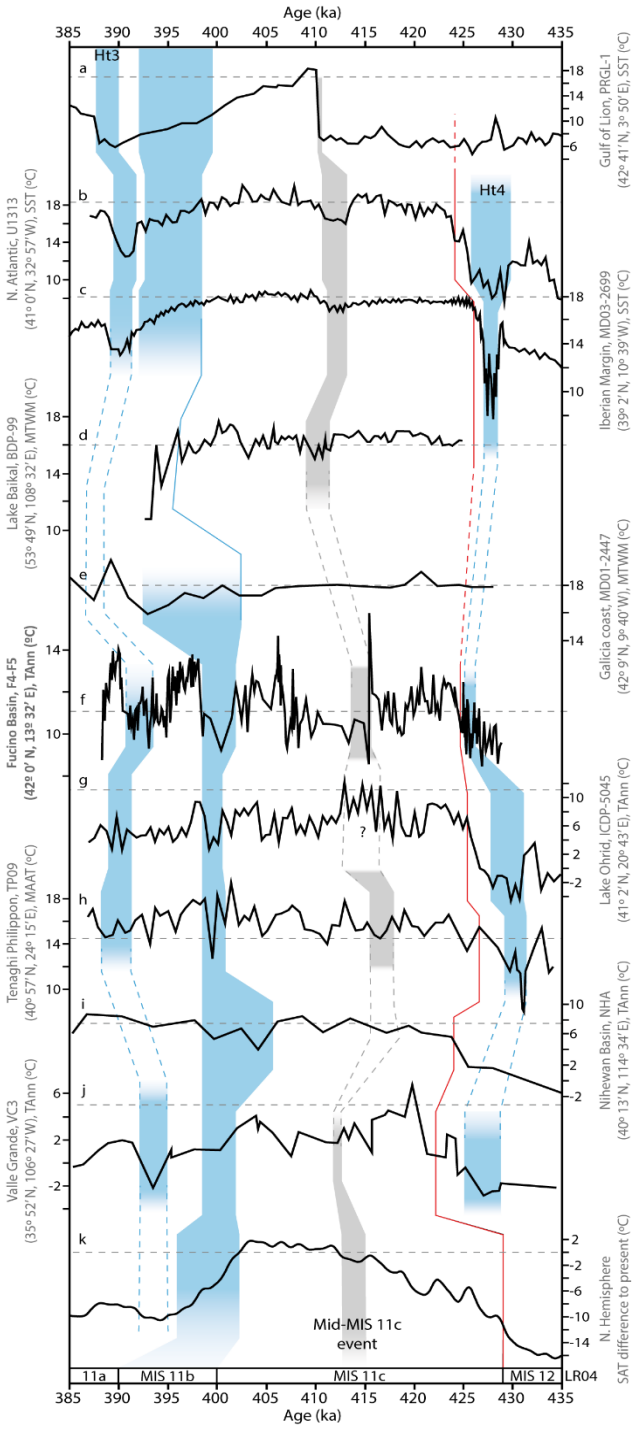

Fig. 3.3.- *Comparison of temperature reconstructions. a) Gulf of Lion Sea Surface Temperature (SST; Cortina et al., 2015). b) North Atlantic SST (Naafs et al., 2013a, 2013b). c) Iberian Margin SST (Rodrigues et al., 2011). d) Lake Baikal mean temperature of the warmest month (MTWM; Prokopenko et al., 2010). e) Galicia coast MTWM (Desprat et al., 2005). f) Fucino Basin mean annual temperature (TAnn; this study). g) Lake Ohrid TAnn (Kousis et al., 2018). h) Tenaghi Philippon mean annual air temperature (MAAT; Ardenghi et al., 2019). i) Nihewan Basin TAnn (Da et al., 2023). j) Valle Grande TAnn (Fawcett et al., 2011) k) North hemisphere surface air temperature (SAT) difference to present values (Bintanja and van de Wal, 2008). Horizontal dashed lines in each curve represent the present-day TAnn value. The blue boxes represent the Ht4, MIS 11b and Ht3. The grey box represents the Mid-MIS 11c. The red line indicates the MIS 12-MIS 11c boundary.*

temperate phase, commonly associated with decreased summer insolation, indicating cooler but overall humid conditions (Tzedakis, 2007). The variation of *Abies* pollen through time indicates regional to local scale humidity changes, because those pollen grains cannot be transported for long distances by the wind due to their big pollen grain size, and hence their immediate occurrence by the pollen source (Erdtman, 1969; Pidek et al., 2013; Moreno-Amat et al., 2017). The abundance of herbaceous and steppic xerophytic plants (such as Amaranthaceae, *Artemisia*, *Ephedra* and *Hippophäe*) is associated with arid and likely cold conditions (e.g. Fauquette et al., 1998; Tzedakis, 2007). In this study, we could corroborate all those climatic correlations with each pollen taxa by knowing the current climatic parameter range in which each one can be present, allowing the quantitative reconstructions (Figs. S1.4 and S3.4).

The reconstructed climatic parameters from Fucino reveal cold and dry conditions during MIS 12 (previous the MIS 12-MIS 11c boundary established by Vera-Polo et al., 2024 at 424.5 ± 4.0 ka) with TAnn ~2ºC cooler and PAnn ~455 mm drier than present time. Those cold-dry conditions also happened in the North of Italy and were registered by the Bàsura cave speleothems (Hu et al., 2024). A small increase in Tann at 426.1 ± 2.0 ka can be observed during the glacial period in Fucino (Fig. 3.2). This slight TAnn peak could be related with the peak registered in paleoclimatic reconstructions of the North Atlantic Sea Surface Temperature (SST; Naafs et al., 2013a, 2013b), Iberian Margin SST (Rodrigues et al., 2011), Lake Ohrid TAnn (Kousis et al., 2018) and Tenaghi Philippon mean annual air temperature (MAAT) (Ardenghi et al., 2019) (Fig. 3.3). This small peak occurred previously to the Heinrich-type event (Ht)

described in the Iberian Margin, the Ht4 (Rodrigues et al., 2011), indicating the beginning of the T-V. The Hts are considered a cold period related with SST cooling and reduction in Atlantic Meridional Overturning Circulation (AMOC), favouring the southward displacement of the Polar Front to the mid-latitudes of the North Atlantic at the beginning of the glacial terminations (López-Martínez et al., 2006; Cheng et al., 2009; Rodrigues et al., 2011, 2017; Singh et al., 2023). The Ht4 is not that obvious in the estimated Fucino PAnn. PAnn maintained constant values through the glacial period, presenting values of ~650 mm, being slightly more humid than at Lake Ohrid (Kousis et al., 2018) (Fig. 3.4).

The paleoclimatic reconstructions indicate that the glacial-interglacial boundary was less transitional in marine records than in terrestrial records (Figs. 3.3 and 3.4). The global paleoclimatic reconstructions indicate an increase of ~5-6 ºC, being Fucino Basin the location where experimented less change in TAnn, with an increase of ~2 ºC. This could be explained by the site location and presence of mountain glaciers in the region, which started melting at the beginning of MIS 11c (Giaccio et al., 2019).

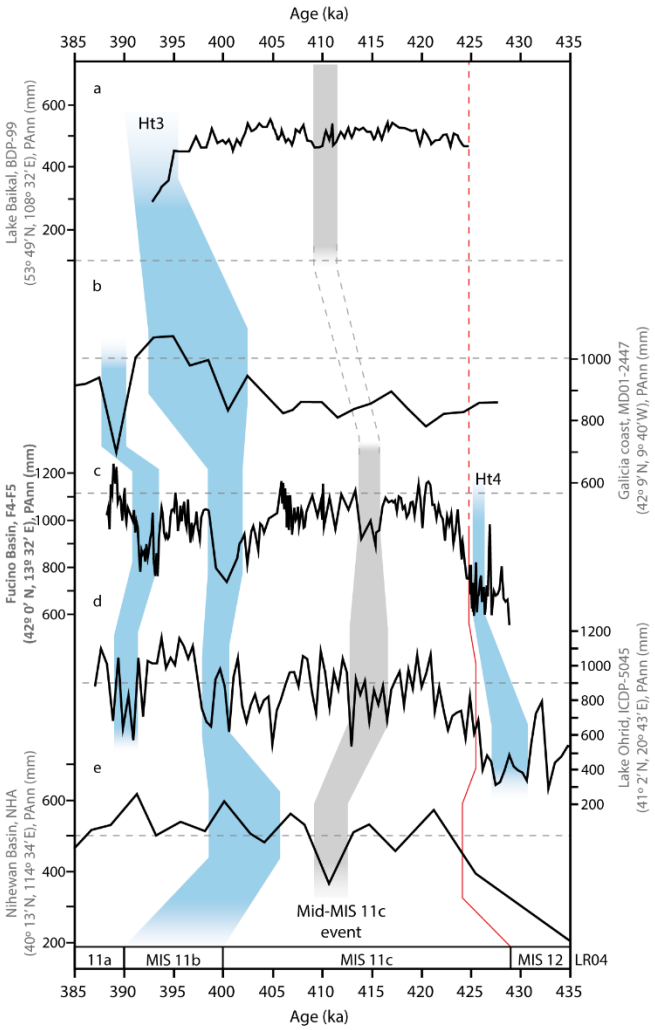

Fig. 3.4.- *Comparison of precipitation reconstructions. a) Lake Baikal mean annual precipitation (PAnn; Prokopenko et al., 2010). b) Galicia coast PAnn (Desprat et al., 2005). c) Fucino Basin PAnn (this study). d) Lake Ohrid Pann (Kousis et al., 2018) e) Nihewan Basin PAnn (Da et al., 2023). Horizontal dashed lines in each curve represent the present-day PAnn value. The blue boxes represent the Ht4, MIS 11b and Ht3. The grey box represents the Mid-MIS 11c. The red line indicates the Mis 12-MIS 11c boundary.*

MIS 11c was characterised for being an unusually long interglacial period, spanning two precessional cycles, as shown in summer insolation patterns (Brandon et al., 2020; Nehrbass-Ahles et al., 2020; Tzedakis et al., 2022) (Fig. 3.2). These cycles influenced vegetation in the Fucino region, reflected in fluctuations in TAnn and PAnn. The first insolation cycle at Fucino started at the beginning of MIS 11c, peaking at 423.5 ± 3.8 ka with a TAnn of 12.4 °C, which is 1.3 °C warmer than today, aligning with maximum insolation values (Laskar et al., 2004). After this peak, TAnn gradually decreased together with insolation levels. However, PAnn increased, reaching slightly higher levels to those registered on present day around 420.5 ± 3.8 ka (1140 mm). This increase could be product due to the effect of evapotranspiration, which decreases as evaporation decreases with decreasing summer insolation trend. This maxima in PAnn can be observed in Lake Ohrid (Kousis et al., 2018) and Nihewan Basin (Da et al., 2023) at similar ages (Fig. 3.4)

Between 415.4 ± 2.5 ka and 413.7 ± 2.7 ka, the Mid-MIS 11c event took place in Fucino, characterised by the lowest insolation values during MIS 11c. TAnn and PAnn registered in Fucino were 0.6 °C and 224 mm below current averages. This event was previously defined as a SST slight decrease (Fig. 3.3; Rodrigues et al., 2011; Naafs et al., 2014). This event never being described in pollen records; however, it can be seen in the global paleoclimatic pollen-based reconstructions show a slight decrease in TAnn and a drop in PAnn, confirming that it was an event that affected the vegetation globally (Figs. 3.3 and 3.4). At Lake Ohrid the Tann showed an increase of their values during this time. This could be product of the MAT reconstruction, which associated the increase of Mediterranean taxa occurred at this location with an increase of temperature (Fig. 3.3; Kousis et al., 2018), however this increase could be related with drier conditions (Fig. 3.4) and a decrease of seasonality during the Mid-MIS 11c event, which it seems to be highly correlated with summer insolation minima (Laskar et al., 2004). Although it was originally defined as a slight drop in SST, the Fucino climatic reconstructions reveal that it was rather caused by drier conditions. Also, this event is more clearly indicated by the longer decline in PAnn than by the changes in TAnn, which exhibited a rapid shift (Figs. 3.2, 3.3 and 3.4). This significant event divided the two cycles within MIS 11c, with the second cycle being the warmest. In Lake Ohrid, however, temperatures during this later cycle were lower than those recorded in the previous one.

In the Fucino Basin, the cooler conditions reached during the Mid-MIS 11c event persisted until the insolation peak at 406.2 ± 1.3 ka, when TAnn rose to 14.8 °C. During this second cycle, sea surface temperatures (SST) in the Gulf of Lion (Cortina et al., 2015), the North Atlantic (Naafs et al., 2013a), and the Iberian margin (Rodrigues et al., 2011) were also significantly warmer. The highest recorded temperatures were observed at Tenaghi Philippon (Ardenghi et al., 2019), which reached a maximum of 19.4 °C, almost 5 °C warmer than today. The results from Bintanja and van de Wal (2008) showed that all the Northern Hemisphere reached 2 ºC above the current TAnn values during this second precessional cycle (Fig. 3.3)

After 399.0 ± 2.8 ka, in a global context of decreasing summer insolation, a colder and drier period was documented in the Fucino record, which can be associated with the MIS 11b stage. This period showed limited seasonal variability with reduced differences between winter and summer temperatures (Fig. 3.2). SST records, however, did not capture the MIS 11b stage as distinctly as the terrestrial records (such as in Fucino, between ~402.7 ± 2.3 ka and 399.0 ± 2.8 ka); it is instead indicated by a steady temperature decline leading into the next Ht at 393.7 ± 3.2 ka (the Ht3; Rodrigues et al., 2011; González-Lanchas et al., 2022). The Ht3 was also recorded by the Tann and Pann reconstructions from Fucino, presenting the typical “W” pattern (Singh et al., 2023) (Figs. 3.3 and 3.4). It occurred in a context of minima in summer insolation and the beginning of increasing values (Fig. 3.2).

3.6 Conclusion

The pollen-based WA-PLS TAnn and PAnn reconstructions from the Fucino F4-F5 composite record chronologically dated between 429-388 ka, give us important insight about climatic dynamics during MIS 11, and allows a direct comparison to present-day TAnn and PAnn values.

The climatic transition from the MIS 12 glacial to the MIS 11c interglacial in terrestrial pollen-based reconstructions was slightly gradual compared to the SST records from the Iberian Margin and North Atlantic.

The Fucino paleoclimatic reconstructions reveal that vegetation in central Italy was highly influenced by the insolation variations forcing the subdivision of the MIS 11c interglacial into two cycles, being the first one colder than the second. The two cycles were separated by the Mid-MIS 11c event, which in Fucino was rather drier than colder.

The overall Tann reconstruction for the studied MIS 11 period reveals that the temperatures were 1-2 ºC higher than present-day, however it was a slightly drier period.

The Fucino climatic reconstruction also shows evidence of millennial-scale global climatic events such as the Ht4 and Ht3. Those events also occurred in other pollen paleoclimatic sites but were never previously described.

Finally, the coldest and driest conditions registered in Fucino pollen record during the MIS 11 interglacial could correspond to the MIS 11b stadial, with estimations of 2 ºC colder and 380 mm drier than today.

Chapter 4: Conclusions

The high-resolution palynological record from the Fucino F4-F5 sediment core studied in this PhD thesis revealed important insights about vegetation changes occurred between 429.0 ± 5.0 ka and 388.3 ± 3.2 ka. This interval recorded important climatic changes from the glacial period (corresponding to MIS 12) to most of the MIS 11 interglacial. The palynological data obtained from this PhD was compared with geochemical data available from the same sediment core, which corroborated several climatic changes occurred in the past interglacial and added more information, giving us a better understanding of the climatic fluctuation in the studied area. The major climatic oscillations recorded in the Fucino Basin also correspond to regional to global fluctuations that affected the climate variability around the world.

The MIS 12 in Fucino Basin was characterised by a very dry and cold climate evidenced by the abundant steppic taxa and low lake level. Those conditions were also recorded in other Mediterranean palynological records which presented a similar vegetation distribution.

The centennial-scale resolution from Fucino pollen record allowed to reconstruct events such as Heinrich-type events (Ht), which occurred within the T-V, characterised by low temperatures and precipitation values. The Ht seems to be related with glacial terminations. This Ht was described in marine SST record as an abrupt drop in temperatures. The fact that it could be correlated with millennial-scale climate variability in Mediterranean terrestrial records implies that was a global climatic change that affected the vegetation distribution around the world.

One of the major climatic changes of Quaternary was the MBE, which divides the climatic history into two periods, one characterised by low-amplitude interglacials (previous MBE) and other with high-amplitude interglacials. The first High amplitude interglacial that occurred was the MIS 11c, which occurs after one of the coldest glacial periods. Fucino pollen record registered this change.

The onset of warmest, interglacial conditions at Fucino, demarcated by the increase in mesothermic taxa, is independently dated to 424.5 ± 4.0 ka, which corresponds with the MIS 12/11 boundary. High lake levels and lake productivity occurred during the MIS 11 interglacial but there were significant lake level fluctuations depending on climate conditions. This boundary is also recorded in geochemical ratios, which represented a rapid shift in the climatic conditions. The fact that the geochemical ratios varied quicker than pollen record could be explained with the adaptability of the vegetation to new climatic conditions

One of the main features of MIS 11c is that it was a very long interglacial period spanning 2 precessional cycles. Those cycles were separated by an insolation minimum, that is reflected in the Fucino pollen record. Is the first time that the Mid-MIS 11c event was identified in a pollen sequence. In Fucino, this event occurred between 415.4 ± 3.5 ka and 413.7 ± 3.2 ka and can be noticed that also occur in other Mediterranean pollen records. The characteristic of the Mid-MIS 11c is that is a drier event in terrestrial records but is also associated

by a slight decrease in SST and a diminution of the seasonality. This event divided the first warm-humid period of the MIS 11c interglacial from the second warmer period.

The Fucino pollen record also shows a dry period, deduced by the decrease in forest abundance, during MIS 11 and centred at 405.5 ± 1.6 ka, which could be related to the OHO that occurred before MIS 11b stadial, characterised by colder conditions. This event seems to affect other Mediterranean areas, showing a decrease of mesothermic taxa abundances and a contraction in vegetation.

The vegetation changes in Fucino seem to be mainly related to the variations in summer insolation, controlling the humidity and temperature in the study area during the interglacial period.

One of the main differences between the vegetation from MIS 11c and from the current interglacial is the striking abundance of *Abies*. The pollen grain from this tree cannot reach long distances by wind transport from the pollen source due to its big size, so it can be deduced that the *Abies* forest dominated most of the vegetation ecosystem, being resistant to humid conditions. This could be related with the altitudinal situation of the studied area, being Lake Ohrid (with a similar altitudinal and latitudinal situation) other area were high abundance of *Abies* occurred.

The pollen-based WA-PLS TAnn and PAnn reconstructions from the Fucino F4-F5 composite record, give us important insight about climatic dynamics during MIS 11, and allows a direct comparison to present-day TAnn and PAnn values.

The overall Tann reconstruction for the studied MIS 11 period suggests that the temperatures were 1-2 ºC higher than present-day, however a slightly drier period occurred. These conditions are also recorded globally, reconstructing even higher temperatures in Tenaghi Philippon.

The Fucino paleoclimatic reconstructions support that vegetation in central Italy was highly influenced by the insolation variations forcing the subdivision of the MIS 11c interglacial into two cycles, being the first one colder than the second.

Finally, the coldest and driest conditions registered in Fucino pollen record during the MIS 11 interglacial could correspond to the MIS 11b stadial, with estimations of 2 ºC colder and 380 mm drier than today.

This PhD work allowed to have a better understanding on vegetation dynamics, giving an idea of possible future scenarios in the context of the current global warming. The human impact in the ecosystems is very marked, alternating significatively vegetation distribution and giving us an altered picture of the vegetation adaptations to climate changes. Because of this, it is important the study of past interglacials without human influence, not only to know how the vegetation responded to climate changes, but also to know the millennial scale climatic cycles that can be extrapolated to predict future conditions and know how big the natural background of the climatic change is and how much the human activity influenced in it. The Fucino paleoclimatic reconstructions stablished a natural regional climatic background without anthropogenic influence, informing about past climatic scenarios warmer than today and its evolution through time.

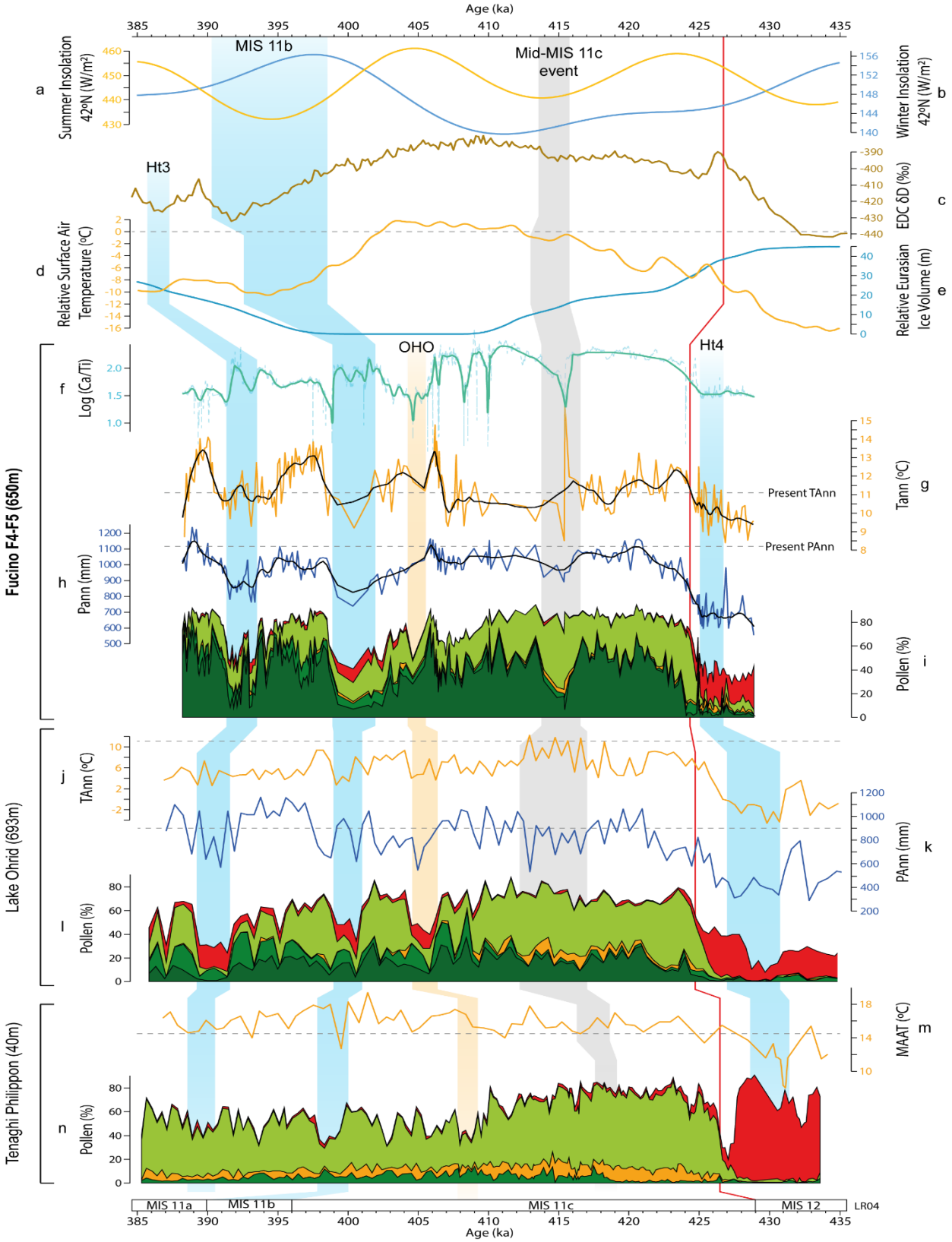

Fig. 4.1.- *Synthesis figure comparing the main proxies presented in this study. (a) Summer and (b) winter insolation at 42ºN (Laskar et al., 2004). (c) Antarctic EDC δD (Bouchet et al., 2023). (d) Eurasian atmospheric surface air temperature relative to present values (Bintanja and van de Wal, 2008). (e) Eurasian ice volume relative to present (Bintanja and van de Wal, 2008). Fucino Basin (650m altitude) (f) Log(Ca/Ti), (g) Tann and (h) Pann reconstructions, and (i) Pollen record (this study). Lake Ohrid (693m altitude) (j) TAnn and (k) Pann reconstructions, and (l) pollen record (Kousis et al., 2018; Koutsodendris, 2020). Tenaghi Philippon (40m altitude) (m) MAAT reconstruction and (n) pollen record (Ardenghi et al., 2019; Koutsodendris et al., 2023a, 2023b). Horizontal dashed lines in d, g, h, j, k and m represent the present-day values. The orange box represents the dry OHO event. The blue boxes represent the cold periods Ht4, MIS 11b and Ht3. The grey box represents the Mid-MIS 11c. The red line indicates the Mis 12-MIS 11c boundary. At the bottom are represented the MIS stages limits defined by Railsback et al. (2015) over the LR04 record (Lisiecki and Raymo, 2005). Pollen records legend: Red: Steppic taxa; Yellow-green: Mesothermic taxa; Orange: Mediterranean taxa; Green: Altitudinal Taxa (Abies excluded); Dark-green: Abies.*

Acknowledgments

Firstly, I would like to express my gratitude to the PhD programs “Dottorato in Scienze della Terra” from University of Rome “La Sapienza” and “Doctorado en Ciencias de la Tierra” from University of Granada for making this PhD thesis possible, for offer me a space, material and all the facilities to develop this research.

I would also be grateful to thank the “Ministerio dell’Università e della Ricerca” to providing me a financial support for the duration of this PhD, being beneficiary of the “dotazione PON Ricerca e Innovazione 2014-2020 con riferimento alle azioni IV.5, Dottorati su tematiche green (DOT 11094; CUP B89J21024760001)”. Additionally, I would like to thank other projects related to my PhD such as “Fucino Tephrochronology Unite Quaternary Records (FUTURE)” for collecting the geochemical and tephrocronological data used in this research. Others include the PID2021-125619OB-C21 project, funded by the “Ministerio de Ciencia e Innovación” of Spain, the “Agencia Estatal de Investigación” and the “Fondo Europeo de Desarrollo Regional FEDER MCIN/AEI/10.13039/ 501100011033/FEDER, UE”; the RNM-190 research group (“Junta de Andalucía”) of the University of Granada, and the Paleos Research group.

My sincere thanks go to Gran Guizza S.p.A. for allowing me to complete a scientific collaboration with them.

I would also like to express my deepest gratitude for both of my PhD tutors, Laura and Gonzalo. For your time, support, kindness, and for always being there for me through thick and thin. Both of you have become an example for me to follow, in both professional and personally.

I also want to thank all my co-authors in this thesis: Biagio, Alessia, Giovanni, Chronis, Bernd, and Jon. Your contributions have significantly enhanced the quality of this research, and I appreciate your openness to discussions.

A special thanks to Katerina Kouli and the incredible researchers that made my six-month period abroad at the National and Kapodistrian University of Athens so enjoyable. I would also like to thank my colleagues Katerina, Katerini, Katia, and Mirka; I hope we can spend more time together in Athens in the future.

To my beloved wife, Emma: you are my inspiration and my rock, supporting me at every step, not only during my PhD but in all aspects of my life. You are my best friend and life partner.

Thank you to all the Paleobecarios and the Department of Stratigraphy and Paleontology for sharing many wonderful moments with me over these three years: Javi, Santi, Natalia, Angie, Bob, Jon, Nono, Marta, Charo, Mapi, Claudia, and Willy. Special thanks to Christian and Raef, without you, these years would not have been the same. What began as a partnership grew into a strong friendship.

I would also like to thank my fellow Minebecarios, Aurélie, Teodora and Sarah, for making our coffee breaks more enjoyable, and a special mention to Francesco for sharing our passion for 3D printing.

Thank you to all the people from Italy that make my PhD more easy-going and for helping me out without any queries every time: Chiara, Lucrezia, Lorenzo, Cristiano and Alessia.

Thanks to Jairo, Vázquez, Dani and Paniagua. We grew up together and we are still the best group in Zafra. You have always supported me in every step of my life, and I deeply appreciate our great friendship.

Thank you, Carlos, who left us all too early, you were always there for me during the first year of this PhD. I miss you so much and I hope that, wherever you are, you are proud of me.

To Diego, Sami and Rubén for sharing and teaching me one of my lifelong passions.

Special thanks to my friends Fabián, Montoro, Luis, and Ronda for supporting me during tough times, cheering me up, and always making me laugh.

Thank you, Carmen, for being there since we started studying our undergraduate degree in geology together.

To my family, my mother, my father, Bea, Aure, Samantha, Luisa and Jim. All of you represented an important role in my life. You supported me in my most difficult times and there are no words to express my gratitude and love.

Thank you to my cousin Francis. Without you I would be richer, but I would never have experienced the happiness of playing Warhammer.

A heartfelt thank you to Uncle David. You taught me that anything is possible and showed me the value of university and academic life. Thank you for being always there, supportive and bringing joy to my life.

I want to thank my grandparents, Maruja, Pepe and Leli. I wish you could see the person I have become. I owe much of who I am to the lessons you taught me.

Lastly, thank you to all the wonderful people I have met throughout these years.

Reference list

Alba-Sánchez, F., López-Sáez, J.A., Pando, B.B., Linares, J.C., Nieto-Lugilde, D., López-Merino, L., 2010. Past and present potential distribution of the Iberian Abies species: a phytogeographic approach using fossil pollen data and species distribution models. Divers. Distrib. 16, 214–228. https://doi.org/10.1111/j.1472-4642.2010.00636.x

Allen, J.R.M., Watts, W.A., Huntley, B., 2000. Weichselian palynostratigraphy, palaeovegetation and palaeoenvironment; the record from Lago Grande di Monticchio, southern Italy. Quat. Int. 73–74, 91–110. https://doi.org/10.1016/S1040-6182(00)00067-7

Altolaguirre, Y., Bruch, A.A., Gibert, L., 2020. A long Early Pleistocene pollen record from Baza Basin (SE Spain): Major contributions to the palaeoclimate and palaeovegetation of Southern Europe. Quat. Sci. Rev. 231, 106199. https://doi.org/10.1016/j.quascirev.2020.106199

Anderson, R.S., Jiménez-Moreno, G., Belanger, M., Briles, C., 2020. Fire history of the unique high-elevation Snowmastodon (Ziegler Reservoir) site during MIS 6–4, with comparisons of TII to TI in the southern Colorado Rockies. Quat. Sci. Rev. 232, 106213. https://doi.org/10.1016/j.quascirev.2020.106213

Ardenghi, N., Mulch, A., Koutsodendris, A., Pross, J., Kahmen, A., Niedermeyer, E.M., 2019. Temperature and moisture variability in the eastern Mediterranean region during Marine Isotope Stages 11–10 based on biomarker analysis of the Tenaghi Philippon peat deposit. Quat. Sci. Rev. 225, 105977. https://doi.org/10.1016/j.quascirev.2019.105977

Barker, S., Chen, J., Gong, X., Jonkers, L., Knorr, G., Thornalley, D., 2015. Icebergs not the trigger for North Atlantic cold events. Nature 520, 333–336. https://doi.org/10.1038/nature14330

Bakker, P., Clark, P.U., Golledge, N.R., Schmittner, A., Weber, M.E., 2017. Centennial-scale Holocene climate variations amplified by Antarctic Ice Sheet discharge. Nature 541, 72–76. https://doi.org/10.1038/nature20582

Bennett, K.D., Tzedakis, P.C., Willis, K.J., 1991. Quaternary Refugia of North European Trees. J. Biogeogr. 18, 103–115. https://doi.org/10.2307/2845248

Berger, A., Loutre, M.-F., 2003. Climate 400,000 Years Ago, a Key to the Future? Wash. DC Am. Geophys. Union Geophys. Monogr. Ser. 17–26. https://doi.org/10.1029/137GM02

Berger, W., Wefer, G., 2003. On the Dynamics of The Ice Ages: Stage-11 Paradox, Mid-Brunhes Climate Shift, and 100-Ky Cycle. Wash. DC Am. Geophys. Union Geophys. Monogr. Ser. 137, 41–59. https://doi.org/10.1029/137GM04

Berger, A., Yin, Q.Z., Herold, N., 2012. MIS-11 and MIS-19, analogs of our Holocene interglacial, in: Quaternary Science Reviews. pp. 1–11.

Bertini, A., 2010. Pliocene to Pleistocene palynoflora and vegetation in Italy: State of the art. Quat. Int. 225, 5–24. https://doi.org/10.1016/j.quaint.2010.04.025

Bertini, A., Toti, F., Marino, M., Ciaranfi, N., 2015. Vegetation and climate across the Early–Middle Pleistocene transition at Montalbano Jonico, southern Italy. Quat. Int., The Quaternary System and its formal subdivision 383, 74–88. https://doi.org/10.1016/j.quaint.2015.01.003

Bertrand, S., Tjallingii, R., Kylander, M.E., Wilhelm, B., Roberts, S.J., Arnaud, F., Brown, E., Bindler, R., 2024. Inorganic geochemistry of lake sediments: A review of analytical techniques and guidelines for data interpretation. Earth-Sci. Rev. 249, 104639. https://doi.org/10.1016/j.earscirev.2023.104639

Bintanja, R., van de Wal, R.S.W., 2008. North American ice-sheet dynamics and the onset of 100,000-year glacial cycles. Nature 454, 869–872. https://doi.org/10.1038/nature07158

Blaauw, M., Christen, J.A., 2011. Flexible paleoclimate age-depth models using an autoregressive gamma process. Bayesian Anal. 6, 457–474. https://doi.org/10.1214/11-BA618

Blasi, C. (Ed.), 2010. Carta delle Serie di Vegetazione d'Italia (Scala 1:500.000). Palombi & Partner Roma.

Blasi, C., Del Vico, E., 2012. High mountain vegetation of the Apennines. Rintelner Symp. X 24, 179–194.

Blasi, C., Capotorti, G., Alós Ortí, M.M., Anzellotti, I., Attorre, F., Azzella, M.M., Carli, E., Copiz, R., Garfì, V., Manes, F., Marando, F., Marchetti, M., Mollo, B., Zavattero, L., 2017. Ecosystem mapping for the implementation of the European Biodiversity Strategy at the national level: The case of Italy. Environ. Sci. Policy 78, 173–184. https://doi.org/10.1016/j.envsci.2017.09.002

Bouchet, M., Landais, A., Grisart, A., Parrenin, F., Prié, F., Jacob, R., Fourré, E., Capron, E., Raynaud, D., Lipenkov, V.Y., Loutre, M.-F., Extier, T., Svensson, A., Legrain, E., Martinerie, P., Leuenberger, M., Jiang, W., Ritterbusch, F., Lu, Z.-T., Yang, G.-M., 2023. The AICC2023 chronological framework and associated timescale for the EPICA Dome C ice core (preprint). Ice Dynamics/Ice Cores/Milankovitch. https://doi.org/10.5194/egusphere-2023-1081

Bouchet, M., Donner, A., Grimmer, M., Jasper, C., Krauss, F., Legrain, E., Vera-Polo, P., 2024. The atypical interglacial of MIS 11c and the long-term change in interglacial intensity over the past 800 kyr. Past Glob. Chang. Mag. 32, 55–55. https://doi.org/10.22498/pages.32.1.55

Brandon, M., Landais, A., Duchamp-Alphonse, S., Favre, V., Schmitz, L., Abrial, H., Prié, F., Extier, T., Blunier, T., 2020. Exceptionally high biosphere productivity at the beginning of Marine Isotopic Stage 11. Nat. Commun. 11, 2112. https://doi.org/10.1038/s41467-020-15739-2

Brown, E.T., 2011. Lake Malawi's response to "megadrought" terminations: Sedimentary records of flooding, weathering and erosion. Palaeogeogr. Palaeoclimatol. Palaeoecol., Southern hemisphere tropical climate over the past 145ka: Results of the Lake Malawi Scientific Drilling Project, East Africa 303, 120–125. https://doi.org/10.1016/j.palaeo.2010.01.038

Burga, C.A., Hussendörfer, E., 2001. Vegetation history of Abies alba Mill. (silver fir) in Switzerland – pollen analytical and genetic surveys related to aspects of vegetation history of Picea abies (L.) H. Karsten (Norway spruce). Veg. Hist. Archaeobotany 10, 151–159. https://doi.org/10.1007/PL00006927

Bush, M.B., 2002. On the interpretation of fossil Poaceae pollen in the lowland humid neotropics. Palaeogeogr. Palaeoclimatol. Palaeoecol., Reconstruction and Modeling of grass-dominated ecosystems 177, 5–17. https://doi.org/10.1016/S0031-0182(01)00348-0

Caielli, G., Maffucci, R., de Franco, R., Bigi, S., Parotto, M., Mollica, R., Gaudiosi, I., Simionato, M., Romanelli, M., De Marchi, N., Cavinato, G.P., 2023. Fucino Basin structure revealed by the tomography and the reusing of the CROP11 seismic data. Tectonophysics 865, 230043. https://doi.org/10.1016/j.tecto.2023.230043

Camuera, J., Jiménez-Moreno, G., Ramos-Román, M.J., García-Alix, A., Toney, J.L., Anderson, R.S., Jiménez-Espejo, F., Bright, J., Webster, C., Yanes, Y., Carrión, J.S., 2019. Vegetation and climate changes during the last two glacial-interglacial cycles in the western Mediterranean: A new long pollen record from Padul (southern Iberian Peninsula). Quat. Sci. Rev. 205, 86–105. https://doi.org/10.1016/j.quascirev.2018.12.013

Camuera, J., Jiménez-Moreno, G., Ramos-Román, M.J., García-Alix, A., Jiménez-Espejo, F.J., Toney, J.L., Anderson, R.S., 2021. Chronological control and centennial-scale climatic subdivisions of the Last Glacial Termination in the western Mediterranean region. Quat. Sci. Rev. 255, 106814. https://doi.org/10.1016/j.quascirev.2021.106814

Camuera, J., Ramos-Román, M.J., Jiménez-Moreno, G., García-Alix, A., Ilvonen, L., Ruha, L., Gil-Romera, G., González-Sampériz, P., Seppä, H., 2022. Past 200 kyr hydroclimate variability in the western Mediterranean and its connection to the African Humid Periods. Sci. Rep. 12, 9050. https://doi.org/10.1038/s41598-022-12047-1

Candy, I., Schreve, D.C., Sherriff, J., Tye, G.J., 2014. Marine Isotope Stage 11: Palaeoclimates, palaeoenvironments and its role as an analogue for the current interglacial. Earth-Sci. Rev. 128, 18–51. https://doi.org/10.1016/j.earscirev.2013.09.006

Cavinato, G.P., Carusi, C., Dall'Asta, M., Miccadei, E., Piacentini, T., 2002. Sedimentary and tectonic evolution of Plio–Pleistocene alluvial and lacustrine deposits of Fucino Basin (central Italy). Sediment. Geol. 148, 29–59. https://doi.org/10.1016/S0037-0738(01)00209-3

Cheddadi, R., de Beaulieu, J.-L., Jouzel, J., Andrieu-Ponel, V., Laurent, J.-M., Reille, M., Raynaud, D., Bar-Hen, A., 2005. Similarity of vegetation dynamics during interglacial periods. Proc. Natl. Acad. Sci. 102, 13939–13943. https://doi.org/10.1073/pnas.0501752102

Cheng, H., Edwards, R.L., Broecker, W.S., Denton, G.H., Kong, X., Wang, Y., Zhang, R., Wang, X., 2009. Ice Age Terminations. Science 326, 248–252. https://doi.org/10.1126/science.1177840

Cheng, H., Edwards, R.L., Sinha, A., Spötl, C., Yi, L., Chen, S., Kelly, M., Kathayat, G., Wang, X., Li, X., Kong, X., Wang, Y., Ning, Y., Zhang, H., 2016. The Asian monsoon over the past 640,000 years and ice age terminations. Nature 534, 640–646. https://doi.org/10.1038/nature18591

Chevalier, M., Davis, B.A.S., Heiri, O., Seppä, H., Chase, B.M., Gajewski, K., Lacourse, T., Telford, R.J., Finsinger, W., Guiot, J., Kühl, N., Maezumi, S.Y., Tipton, J.R., Carter, V.A., Brussel, T., Phelps, L.N., Dawson, A., Zanon, M., Vallé, F., Nolan, C., Mauri, A., de Vernal, A., Izumi, K., Holmström, L., Marsicek, J., Goring, S., Sommer, P.S., Chaput, M., Kupriyanov, D., 2020. Pollen-based climate reconstruction techniques for late Quaternary studies. Earth-Sci. Rev. 210, 103384. https://doi.org/10.1016/j.earscirev.2020.103384

Christ, A.J., Rittenour, T.M., Bierman, P.R., Keisling, B.A., Knutz, P.C., Thomsen, T.B., Keulen, N., Fosdick, J.C., Hemming, S.R., Tison, J.-L., Blard, P.-H., Steffensen, J.P., Caffee, M.W., Corbett, L.B., Dahl-Jensen, D., Dethier, D.P., Hidy, A.J., Perdrial, N., Peteet, D.M., Steig, E.J., Thomas, E.K., 2023. Deglaciation of northwestern Greenland during Marine Isotope Stage 11. Science 381, 330–335. https://doi.org/10.1126/science.ade4248

Cortina, A., Sierro, F.J., Flores, J.A., Martrat, B., Grimalt, J.O., 2015. The response of SST to insolation and ice sheet variability from MIS 3 to MIS 11 in the northwestern Mediterranean Sea (Gulf of Lions). Geophys. Res. Lett. 42, 10,366-10,374. https://doi.org/10.1002/2015GL065539

Cover, T., Hart, P., 1967. Nearest neighbor pattern classification. IEEE Trans. Inf. Theory 13, 21–27. https://doi.org/10.1109/TIT.1967.1053964

Croudace, I.W., Rothwell, R.G. (Eds.), 2015. Micro-XRF Studies of Sediment Cores: Applications of a non-destructive tool for the environmental sciences, Developments in Paleoenvironmental Research. Springer Netherlands, Dordrecht. https://doi.org/10.1007/978-94-017-9849-5

Cuven, S., Francus, P., Lamoureux, S., 2011. Mid to Late Holocene hydroclimatic and geochemical records from the varved sediments of East Lake, Cape Bounty, Canadian High Arctic. Quat. Sci. Rev. 30, 2651–2665. https://doi.org/10.1016/j.quascirev.2011.05.019

Da, S., Zhang, Z., Li, Y., Xu, Q., Fan, B., Wang, S., Dong, J., Wang, Y., Chi, Z., 2023. Pollen-based quantitative paleoclimatic record spanning the Mid-Brunhes Event in the Nihewan Basin, north China. Palaeogeogr. Palaeoclimatol. Palaeoecol. 612, 111377. https://doi.org/10.1016/j.palaeo.2022.111377

D'Agostino, N., Jackson, J.A., Dramis, F., Funiciello, R., 2001. Interactions between mantle upwelling, drainage evolution and active normal faulting: an example from the central Apennines (Italy). Geophys. J. Int. 147, 475–497. https://doi.org/10.1046/j.1365-246X.2001.00539.x

Davis, B.A.S., Chevalier, M., Sommer, P., Carter, V.A., Finsinger, W., Mauri, A., Phelps, L.N., Zanon, M., Abegglen, R., Åkesson, C.M., Alba-Sánchez, F., Anderson, R.S., Antipina, T.G., Atanassova, J.R., Beer, R., Belyanina, N.I., Blyakharchuk, T.A., Borisova, O.K., Bozilova, E., Bukreeva, G., Bunting, M.J.,

Clò, E., Colombaroli, D., Combourieu-Nebout, N., Desprat, S., Di Rita, F., Djamali, M., Edwards, K.J., Fall, P.L., Feurdean, A., Fletcher, W., Florenzano, A., Furlanetto, G., Gaceur, E., Galimov, A.T., Gałka, M., García-Moreiras, I., Giesecke, T., Grindean, R., Guido, M.A., Gvozdeva, I.G., Herzschuh, U., Hjelle, K.L., Ivanov, S., Jahns, S., Jankovska, V., Jiménez-Moreno, G., Karpińska-Kołaczek, M., Kitaba, I., Kołaczek, P., Lapteva, E.G., Latałowa, M., Lebreton, V., Leroy, S., Leydet, M., Lopatina, D.A., López-Sáez, J.A., Lotter, A.F., Magri, D., Marinova, E., Matthias, I., Mavridou, A., Mercuri, A.M., Mesa-Fernández, J.M., Mikishin, Y.A., Milecka, K., Montanari, C., Morales-Molino, C., Mrotzek, A., Muñoz Sobrino, C., Naidina, O.D., Nakagawa, T., Nielsen, A.B., Novenko, E.Y., Panajiotidis, S., Panova, N.K., Papadopoulou, M., Pardoe, H.S., Pędziszewska, A., Petrenko, T.I., Ramos-Román, M.J., Ravazzi, C., Rösch, M., Ryabogina, N., Sabariego Ruiz, S., Salonen, J.S., Sapelko, T.V., Schofield, J.E., Seppä, H., Shumilovskikh, L., Stivrins, N., Stojakowits, P., Svobodova Svitavska, H., Święta-Musznicka, J., Tantau, I., Tinner, W., Tobolski, K., Tonkov, S., Tsakiridou, M., Valsecchi, V., Zanina, O.G., Zimny, M., 2020. The Eurasian Modern Pollen Database (EMPD), version 2. Earth Syst. Sci. Data 12, 2423–2445. https://doi.org/10.5194/essd-12-2423-2020

Denk, T., Frotzler, N., Davitashvili, N., 2001. Vegetational patterns and distribution of relict taxa in humid temperate forests and wetlands of Georgia (Transcaucasia). Biol. J. Linn. Soc. 72, 287–332. https://doi.org/10.1111/j.1095-8312.2001.tb01318.x

Desprat, S., Sánchez Goñi, M.F., Turon, J.-L., McManus, J.F., Loutre, M.F., Duprat, J., Malaizé, B., Peyron, O., Peypouquet, J.-P., 2005. Is vegetation responsible for glacial inception during periods of muted insolation changes? Quat. Sci. Rev. 24, 1361–1374. https://doi.org/10.1016/j.quascirev.2005.01.005

Desprat, S., Combourieu-Nebout, N., Essallami, L., Sicre, M.A., Dormoy, I., Peyron, O., Siani, G., Bout Roumazeilles, V., Turon, J.L., 2013. Deglacial and Holocene vegetation and climatic changes in the southern Central Mediterranean from a direct land–sea correlation. Clim. Past 9, 767–787. https://doi.org/10.5194/cp-9-767-2013

Djamali, M., Cilleros, K., 2020. Statistically significant minimum pollen count in Quaternary pollen analysis; the case of pollen-rich lake sediments. Rev. Palaeobot. Palynol. 275, 104156. https://doi.org/10.1016/j.revpalbo.2019.104156

Dobrowolska, D., 1998. Structure of silver fir (*Abies alba* Mill.) natural regeneration in the `Jata' reserve in Poland. For. Ecol. Manag. 110, 237–247. https://doi.org/10.1016/S0378-1127(98)00286-2

Donders, T., Panagiotopoulos, K., Koutsodendris, A., Bertini, A., Mercuri, A.M., Masi, A., Combourieu-Nebout, N., Joannin, S., Kouli, K., Kousis, I., Peyron, O., Torri, P., Florenzano, A., Francke, A., Wagner, B., Sadori, L., 2021. 1.36 million years of Mediterranean forest refugium dynamics in response to glacial–interglacial cycle strength. Proc. Natl. Acad. Sci. 118, e2026111118. https://doi.org/10.1073/pnas.2026111118

Ehlers, J., Gibbard, P., 2008. Extent and chronology of Quaternary glaciation. Episodes J. Int. Geosci. 31, 211–218. https://doi.org/10.18814/epiiugs/2008/v31i2/004

EPICA Community Members, 2004. Eight glacial cycles from an Antarctic ice core. Nature 429, 623–628. https://doi.org/10.1038/nature02599

Erdtman, G., 1969. Handbook of palynology: morphology-taxonomy-ecology: an introduction to the study of pollen grains and spores.

Faegri, K., Iversen, J., 1975. Textbook of pollen analysis. Blackwell Scientific Publications.

Fauquette, S., Guiot, J., Suc, J.-P., 1998. A method for climatic reconstruction of the Mediterranean Pliocene using pollen data. Palaeogeogr. Palaeoclimatol. Palaeoecol. 144, 183–201. https://doi.org/10.1016/S0031-0182(98)00083-2

Fawcett, P.J., Werne, J.P., Anderson, R.S., Heikoop, J.M., Brown, E.T., Berke, M.A., Smith, S.J., Goff, F., Donohoo-Hurley, L., Cisneros-Dozal, L.M., Schouten, S., Sinninghe Damsté, J.S., Huang, Y., Toney, J., Fessenden, J., WoldeGabriel, G., Atudorei, V., Geissman, J.W., Allen, C.D., 2011. Extended megadroughts in the southwestern United States during Pleistocene interglacials. Nature 470, 518–521. https://doi.org/10.1038/nature09839

Fick, S.E., Hijmans, R.J., 2017. WorldClim 2: new 1-km spatial resolution climate surfaces for global land areas. Int. J. Climatol. 37, 4302–4315. https://doi.org/10.1002/joc.5086

Fletcher, W.J., Sanchez Goñi, M.F., Peyron, O., Dormoy, I., 2010. Abrupt climate changes of the last deglaciation detected in a Western Mediterranean forest record. Clim. Past 6, 245–264. https://doi.org/10.5194/cp-6-245-2010

Frate, L., Carranza, M.L., Evangelista, A., Stinca, A., Schaminée, J.H.J., Stanisci, A., 2018. Climate and land use change impacts on Mediterranean high-mountain vegetation in the Apennines since the 1950s. Plant Ecol. Divers. 11, 85–96. https://doi.org/10.1080/17550874.2018.1473521

Freytet, P., Verrecchia, E.P., 2002. Lacustrine and palustrine carbonate petrography: An overview. J. Paleolimnol. 27, 221–237. https://doi.org/10.1023/A:1014263722766

Galadini, F., Galli, P., 2000. Active Tectonics in the Central Apennines (Italy) – Input Data for Seismic Hazard Assessment. Nat. Hazards 22, 225–268. https://doi.org/10.1023/A:1008149531980

Galadini, F., Messina, P., 2004. Early–Middle Pleistocene eastward migration of the Abruzzi Apennine (central Italy) extensional domain. J. Geodyn. 37, 57–81. https://doi.org/10.1016/j.jog.2003.10.002

Giaccio, B., Regattieri, E., Zanchetta, G., Wagner, B., Galli, P., Mannella, G., Niespolo, E., Peronace, E., Renne, P.R., Nomade, S., Cavinato, G.P., Messina, P., Sposato, A., Boschi, C., Florindo, F., Marra, F., Sadori, L., 2015. A key continental archive for the last 2 Ma of climatic history of the central Mediterranean

region: A pilot drilling in the Fucino Basin, central Italy. Sci. Drill. 20, 13–19. https://doi.org/10.5194/sd-20-13-2015

Giaccio, B., Niespolo, E.M., Pereira, A., Nomade, S., Renne, P.R., Albert, P.G., Arienzo, I., Regattieri, E., Wagner, B., Zanchetta, G., Gaeta, M., Galli, P., Mannella, G., Peronace, E., Sottili, G., Florindo, F., Leicher, N., Marra, F., Tomlinson, E.L., 2017. First integrated tephrochronological record for the last ~190 kyr from the Fucino Quaternary lacustrine succession, central Italy. Quat. Sci. Rev. 158, 211–234. https://doi.org/10.1016/j.quascirev.2017.01.004

Giaccio, B., Leicher, N., Mannella, G., Monaco, L., Regattieri, E., Wagner, B., Zanchetta, G., Gaeta, M., Marra, F., Nomade, S., Palladino, D.M., Pereira, A., Scheidt, S., Sottili, G., Wonik, T., Wulf, S., Zeeden, C., Ariztegui, D., Cavinato, G.P., Dean, J.R., Florindo, F., Leng, M.J., Macrì, P., Niespolo, E., Renne, P.R., Rolf, C., Sadori, L., Thomas, C., Tzedakis, P.C., 2019. Extending the tephra and palaeoenvironmental record of the Central Mediterranean back to 430 ka: A new core from Fucino Basin, central Italy. Quat. Sci. Rev. 225, 106003. https://doi.org/10.1016/j.quascirev.2019.106003

Giaccio, B., Marino, G., Marra, F., Monaco, L., Pereira, A., Zanchetta, G., Gaeta, M., Leicher, N., Nomade, S., Palladino, D.M., Sottili, G., Guillou, H., Scao, V., 2021. Tephrochronological constraints on the timing and nature of sea-level change prior to and during glacial termination V. Quat. Sci. Rev. 263, 106976. https://doi.org/10.1016/j.quascirev.2021.106976

Giraudi, C., Giaccio, B., 2015. Middle Pleistocene glaciations in the Apennines, Italy: new chronological data and preservation of the glacial record. Geol. Soc. Lond. Spec. Publ. 433, 161–178. https://doi.org/10.1144/SP433.1

González-Lanchas, A., Dorador, J., Rodríguez-Tovar, F.J., Sierro, F.J., Flores, J.-A., 2022. Trace fossil characterization during Termination V and MIS 11 at the western Mediterranean: Connection between surface conditions and deep environment. Mar. Geol. 446, 106774. https://doi.org/10.1016/j.margeo.2022.106774

Grimm, E.C., 1987. CONISS: a FORTRAN 77 program for stratigraphically constrained cluster analysis by the method of incremental sum of squares. Comput. Geosci. 13, 13–35. https://doi.org/10.1016/0098-3004(87)90022-7

Guiot, J., 1990. Methodology of the last climatic cycle reconstruction in France from pollen data. Palaeogeogr. Palaeoclimatol. Palaeoecol., Methods for the Study of Stratigraphical Records 80, 49–69. https://doi.org/10.1016/0031-0182(90)90033-4

Guy-Ohlson, D., 1992. *Botryococcus* as an aid in the interpretation of palaeoenvironment and depositional processes. Rev. Palaeobot. Palynol. 71, 1–15. https://doi.org/10.1016/0034-6667(92)90155-A

Hammer, O., Harper, D.A.T., Ryan, P.D., 2001. PAST: Paleontological Statistics Software Package for Education and Data Analysis.

Harding, A., Palutikof, J., Holt, T., 2009. The climate system, in: Woodward, J.C. (Ed.), The Physical Geography of the Mediterranean. Oxford University Press, Oxford, pp. 69–88.

Hays, J.D., Imbrie, J., Shackleton, N.J., 1976. Variations in the Earth's Orbit: Pacemaker of the Ice Ages: For 500,000 years, major climatic changes have followed variations in obliquity and precession. Science 194, 1121–1132. https://doi.org/10.1126/science.194.4270.1121

Hes, G., Sánchez Goñi, M.F., Bouttes, N., 2022. Impact of terrestrial biosphere on the atmospheric CO_2 concentration across Termination V. Clim. Past 18, 1429–1451. https://doi.org/10.5194/cp-18-1429-2022

Hodell, D.A., Channell, J.E.T., Curtis, J.H., Romero, O.E., Röhl, U., 2008. Onset of "Hudson Strait" Heinrich events in the eastern North Atlantic at the end of the middle Pleistocene transition (~640 ka)? Paleoceanography 23. https://doi.org/10.1029/2008PA001591

Hrynowiecka, A., Żarski, M., Drzewicki, W., 2019. The rank of climatic oscillations during MIS 11c (OHO and YHO) and post-interglacial cooling during MIS 11b and MIS 11a in eastern Poland. Geol. Q. 63, 375-doi: 10.7306/gq.1470. https://doi.org/10.7306/gq.1470

Hu, H.-M., Marino, G., Pérez-Mejías, C., Spötl, C., Yokoyama, Y., Yu, J., Rohling, E., Kano, A., Ludwig, P., Pinto, J.G., Michel, V., Valensi, P., Zhang, X., Jiang, X., Mii, H.-S., Chien, W.-Y., Tsai, H.-C., Sung, W.-H., Hsu, C.-H., Starnini, E., Zunino, M., Shen, C.-C., 2024. Sustained North Atlantic warming drove anomalously intense MIS 11c interglacial. Nat. Commun. 15, 5933. https://doi.org/10.1038/s41467-024-50207-1

Huybers, P., 2006. Early Pleistocene Glacial Cycles and the Integrated Summer Insolation Forcing. Science 313, 508–511. https://doi.org/10.1126/science.1125249

Ilvonen, L., López-Sáez, J.A., Holmström, L., Alba-Sánchez, F., Pérez-Díaz, S., Carrión, J.S., Ramos-Román, M.J., Camuera, J., Jiménez-Moreno, G., Ruha, L., Seppä, H., 2022. Spatial and temporal patterns of Holocene precipitation change in the Iberian Peninsula. Boreas 51, 776–792. https://doi.org/10.1111/bor.12586

Imbrie, J., Mix, A.C., Martinson, D.G., 1993. Milankovitch theory viewed from Devils Hole. Nature 363, 531–533. https://doi.org/10.1038/363531a0

IPCC. Climate Change, 2013. The Physical Science Basis. Contribution of Working Group I to the 5th Assessment Report of the Intergovernmental Panel on Climate Change. Cambridge University Press.

ISPRA, 1934. Note illustrative della Carta Geologica d'Italia alla scala 1:100 000, foglio 145, Avezzano. https://sgi.isprambiente.it/geologia100k/mostra_foglio.aspx?numero_foglio=145

ISPRA, 1939. Note illustrative della Carta Geologica d'Italia alla scala 1:100 000, foglio 151, Alatri. https://sgi.isprambiente.it/geologia100k/mostra_foglio.aspx?numero_foglio=151

ISPRA, 1942. Note illustrative della Carta Geologica d'Italia alla scala 1:100 000, foglio 146, Sulmona. https://sgi.isprambiente.it/geologia100k/mostra_foglio.aspx?numero_foglio=146

ISPRA, 1967. Note illustrative della Carta Geologica d'Italia alla scala 1:100 000, foglio 152, Sora. https://sgi.isprambiente.it/geologia100k/mostra_foglio.aspx?numero_foglio=152

Jiménez-Moreno, G., García-Alix, A., Hernández-Corbalán, M.D., Anderson, R.S., Delgado-Huertas, A., 2013. Vegetation, fire, climate and human disturbance history in the southwestern Mediterranean area during the late Holocene. Quat. Res. 79, 110–122. https://doi.org/10.1016/j.yqres.2012.11.008

Jiménez-Moreno, G., Anderson, R.S., Markgraf, V., Staley, S.E., Fawcett, P.J., 2023. Environmental and climate evolution in the Southwest USA since the last interglacial deduced from the pollen record from Stoneman lake, Arizona. Quat. Sci. Rev. 300, 107883. https://doi.org/10.1016/j.quascirev.2022.107883

Joannin, S., Ciaranfi, N., Stefanelli, S., 2008. Vegetation changes during the late Early Pleistocene at Montalbano Jonico (Province of Matera, southern Italy) based on pollen analysis. Palaeogeogr. Palaeoclimatol. Palaeoecol. 270, 92–101. https://doi.org/10.1016/j.palaeo.2008.08.017

Joannin, S., Bassinot, F., Nebout, N.C., Peyron, O., Beaudouin, C., 2011. Vegetation response to obliquity and precession forcing during the Mid-Pleistocene Transition in Western Mediterranean region (ODP site 976). Quat. Sci. Rev. 30, 280–297. https://doi.org/10.1016/j.quascirev.2010.11.009

Juggins, S., 2007. C2 Version 1.5: Software for ecological and palaeoecological data analysis and visualisation. https://eprints.ncl.ac.uk.

Juggins, S., 2024. Rioja: Analysis of Quaternary Science Data. R package version 1.0-7, https://cran.r-project.org/package=rioja. https://eprints.ncl.ac.uk.

Kleinen, T., Hildebrandt, S., Prange, M., Rachmayani, R., Müller, S., Bezrukova, E., Brovkin, V., Tarasov, P.E., 2014. The climate and vegetation of Marine Isotope Stage 11 – Model results and proxy-based reconstructions at global and regional scale. Quat. Int., The Bridging Eurasia Research Initiative: Modes of mobility and sustainability in the palaeoenvironmental and archaeological archives from Eurasia 348, 247–265. https://doi.org/10.1016/j.quaint.2013.12.028

Kousis, I., Koutsodendris, A., Peyron, O., Leicher, N., Francke, A., Wagner, B., Giaccio, B., Knipping, M., Pross, J., 2018. Centennial-scale vegetation dynamics and climate variability in SE Europe during Marine Isotope Stage 11 based on a pollen record from Lake Ohrid. Quat. Sci. Rev. 190, 20–38. https://doi.org/10.1016/j.quascirev.2018.04.014

Koutsodendris, A., Müller, U.C., Pross, J., Brauer, A., Kotthoff, U., Lotter, A.F., 2010. Vegetation dynamics and climate variability during the Holsteinian interglacial based on a pollen record from Dethlingen (northern Germany). Quat. Sci. Rev. 29, 3298–3307. https://doi.org/10.1016/j.quascirev.2010.07.024

Koutsodendris, A., Pross, J., Zahn, R., 2014. Exceptional Agulhas leakage prolonged interglacial warmth during MIS 11c in Europe. Paleoceanography 29, 1062–1071. https://doi.org/10.1002/2014PA002665

Koutsodendris, A., Kousis, I., Peyron, O., Wagner, B., Pross, J., 2019. The Marine Isotope Stage 12 pollen record from Lake Ohrid (SE Europe): Investigating short-term climate change under extreme glacial conditions. Quat. Sci. Rev. 221, 105873. https://doi.org/10.1016/j.quascirev.2019.105873

Koutsodendris, A., 2020. Palynological data and pollen-based climate reconstructions from Lake Ohrid during MIS 12-11. https://doi.org/10.1594/PANGAEA.915920

Koutsodendris, A., Dakos, V., Fletcher, W.J., Knipping, M., Kotthoff, U., Milner, A.M., Müller, U.C., Kaboth-Bahr, S., Kern, O.A., Kolb, L., Vakhrameeva, P., Wulf, S., Christanis, K., Schmiedl, G., Pross, J., 2023a. Atmospheric CO2 forcing on Mediterranean biomes during the past 500 kyrs. Nat. Commun. 14, 1664. https://doi.org/10.1038/s41467-023-37388-x

Koutsodendris, A., Dakos, V., Fletcher, W.J., Knipping, M., Kotthoff, U., Milner, A.M., Müller, U.C., Kaboth-Bahr, S., Kern, O.A., Kolb, L., Vakhrameeva, P., Wulf, S., Christanis, K., Schmiedl, G., Pross, J., 2023b. Pollen data from Tenaghi Philippon (Greece) spanning the past 500 kyrs. https://doi.org/10.1594/PANGAEA.943593

Kozáková, R., Šamonil, P., Kuneš, P., Novák, J., Kočár, P., Kočárová, R., 2011. Contrasting local and regional Holocene histories of Abies alba in the Czech Republic in relation to human impact: Evidence from forestry, pollen and anthracological data. The Holocene 21, 431–444. https://doi.org/10.1177/0959683610385721

Krupiński, K.M., 1992. Significance of Hippophae rhamnoides L. in evolution of the Eemian Interglacial' flora in Warsaw area. Acta Soc. Bot. Pol. 61, 131–144. https://doi.org/10.5586/asbp.1992.011

Kuhlmann, H., Meggers, H., Freudenthal, T., Wefer, G., 2004. The transition of the monsoonal and the N Atlantic climate system off NW Africa during the Holocene. Geophys. Res. Lett. 31. https://doi.org/10.1029/2004GL021267

Kukla, G., 2003. Continental Records of MIS 11. Geophys. Monogr. Ser. 137, 207–211. https://doi.org/10.1029/137GM14

Kylander, M.E., Ampel, L., Wohlfarth, B., Veres, D., 2011. High-resolution X-ray fluorescence core scanning analysis of Les Echets (France) sedimentary sequence: new insights from chemical proxies. J. Quat. Sci. 26, 109–117. https://doi.org/10.1002/jqs.1438

Laskar, J., Robutel, P., Joutel, F., Gastineau, M., Correia, A.C.M., Levrard, B., 2004. A long-term numerical solution for the insolation quantities of the Earth. Astron. Astrophys. 428, 261–285. https://doi.org/10.1051/0004-6361:20041335

Leicher, N., Giaccio, B., Zanchetta, G., Sulpizio, R., Albert, P.G., Tomlinson, E.L., Lagos, M., Francke, A., Wagner, B., 2021. Lake Ohrid's tephrochronological dataset reveals 1.36 Ma of Mediterranean explosive volcanic activity. Sci. Data 8, 231. https://doi.org/10.1038/s41597-021-01013-7

Leicher, N., Giaccio, B., Pereira, A., Nomade, S., Monaco, L., Mannella, G., Galli, P., Peronance, E., Palladino, D.M., Sottili, G., Zanchetta, G., Wagner, B., 2023. Central Mediterranean tephrochronology between 313 and 366 ka: New insights from the Fucino palaeolake sediment succession. Boreas 52, 240–271. https://doi.org/10.1111/bor.12610

Leicher, N., Monaco, L., Giaccio, B., Nomade, S., Pereira, A., Mannella, G., Wulf, S., Sottili, G., Palladino, D.M., Zanchetta, G., Wagner, B., 2024. Central Mediterranean tephrochronology for the time interval 250–315 ka derived from the Fucino sediment succession. Boreas 53, 164–185. https://doi.org/10.1111/bor.12637

Li, Y., Fleitmann, D., Wang, X., Pérez-Mejías, C., Sha, L., Dong, X., Wang, D., Zhang, R., Qu, X., Cheng, H., 2023. 550-Year Climate Periodicity in the Yunnan-Guizhou Plateau During the Late Mid-Holocene: Insights and Implications. Geophys. Res. Lett. 50, e2023GL103523. https://doi.org/10.1029/2023GL103523

Liang, C., Zhao, Y., Qin, F., Zheng, Z., Xiao, X., Ma, C., Li, H., Zhao, W., 2020. Pollen-based Holocene quantitative temperature reconstruction on the eastern Tibetan Plateau using a comprehensive method framework. Sci. China Earth Sci. 63, 1144–1160. https://doi.org/10.1007/s11430-019-9599-y

Lionello, P., Malanotte-Rizzoli, P., Boscolo, R., Alpert, P., Artale, V., Li, L., Luterbacher, J., May, W., Trigo, R., Tsimplis, M., Ulbrich, U., Xoplaki, E., 2006. The Mediterranean climate: An overview of the main characteristics and issues, in: Lionello, P., Malanotte-Rizzoli, P., Boscolo, R. (Eds.), Developments in Earth and Environmental Sciences, Mediterranean. Elsevier, pp. 1–26. https://doi.org/10.1016/S1571-9197(06)80003-0

Lisiecki, L.E., Raymo, M.E., 2005. A Pliocene-Pleistocene stack of 57 globally distributed benthic δ18O records. Paleoceanography 20. https://doi.org/10.1029/2004PA001071

López-Martínez, C., Grimalt, J.O., Hoogakker, B., Gruetzner, J., Vautravers, M.J., McCave, I.N., 2006. Abrupt wind regime changes in the North Atlantic Ocean during the past 30,000–60,000 years. Paleoceanography 21. https://doi.org/10.1029/2006PA001275

Loutre, M.F., Berger, A., 2000. Future Climatic Changes: Are We Entering an Exceptionally Long Interglacial? Clim. Change 46, 61–90. https://doi.org/10.1023/A:1005559827189

Loutre, M.F., 2003. Clues from MIS 11 to predict the future climate – a modelling point of view. Earth Planet. Sci. Lett. 212, 213–224. https://doi.org/10.1016/S0012-821X(03)00235-8

Magri, D., Tzedakis, P.C., 2000. Orbital signatures and long-term vegetation patterns in the Mediterranean. Quat. Int., EDLP - Med Special 73–74, 69–78. https://doi.org/10.1016/S1040-6182(00)00065-3

Mannella, G., Giaccio, B., Zanchetta, G., Regattieri, E., Leicher, N., Scheidt, S., Grelle, T., Lehne, C., Rolf, C., Wonik, T., Nomade, S., Pereira, A., Niespolo, E., Renne, P., Leng, M., Dean, J., Thomas, C., Ariztegu, D., Gaeta, M., Florindo, F., Cavinato, G.P., Provenzale, A., Wagner, B., 2018. Fucino Palaeo-Lake: towards the Palaeoenvironmental History of the last 430 ka. Alp. Mediterr. Quat. 31, 141–145.

Mannella, G., Giaccio, B., Zanchetta, G., Regattieri, E., Niespolo, E.M., Pereira, A., Renne, P.R., Nomade, S., Leicher, N., Perchiazzi, N., Wagner, B., 2019. Palaeoenvironmental and palaeohydrological variability of mountain areas in the central Mediterranean region: A 190 ka-long chronicle from the independently dated Fucino palaeolake record (central Italy). Quat. Sci. Rev. 210, 190–210. https://doi.org/10.1016/j.quascirev.2019.02.032

McDermott, F., 2004. Palaeo-climate reconstruction from stable isotope variations in speleothems: a review. Quat. Sci. Rev., Isotopes in Quaternary Paleoenvironmental reconstruction 23, 901–918. https://doi.org/10.1016/j.quascirev.2003.06.021

McManus, J., Oppo, D., Cullen, J., Healey, S., 2003. Marine Isotope Stage 11 (MIS 11): Analog for Holocene and future climate? Wash. DC Am. Geophys. Union Geophys. Monogr. Ser. 137, 69–85. https://doi.org/10.1029/137GM06

Melles, M., Brigham-Grette, J., Minyuk, P.S., Nowaczyk, N.R., Wennrich, V., DeConto, R.M., Anderson, P.M., Andreev, A.A., Coletti, A., Cook, T.L., Haltia-Hovi, E., Kukkonen, M., Lozhkin, A.V., Rosén, P., Tarasov, P., Vogel, H., Wagner, B., 2012. 2.8 Million Years of Arctic Climate Change from Lake El'gygytgyn, NE Russia. Science 337, 315–320. https://doi.org/10.1126/science.1222135

Monaco, L., Palladino, D.M., Gaeta, M., Marra, F., Sottili, G., Leicher, N., Mannella, G., Nomade, S., Pereira, A., Regattieri, E., Wagner, B., Zanchetta, G., Albert, P.G., Arienzo, I., D'Antonio, M., Petrosino, P., Manning, C.J., Giaccio, B., 2021. Mediterranean tephrostratigraphy and peri-Tyrrhenian explosive activity revaluated in light of the 430-365 ka record from Fucino Basin (central Italy). Earth-Sci. Rev. 220, 103706. https://doi.org/10.1016/j.earscirev.2021.103706

Monaco, L., Leicher, N., Palladino, D.M., Arienzo, I., Marra, F., Petrelli, M., Nomade, S., Pereira, A., Sottili, G., Conticelli, S., D'Antonio, M., Fabbrizio, A., Jicha, B.R., Mannella, G., Petrosino, P., Regattieri, E., Tzedakis, P.C., Wagner, B., Zanchetta, G., Giaccio, B., 2022. The Fucino 250–170 ka tephra record: New insights on peri-Tyrrhenian explosive volcanism, central mediterranean tephrochronology, and timing of the MIS 8-6 climate variability. Quat. Sci. Rev. 296, 107797. https://doi.org/10.1016/j.quascirev.2022.107797

Mondati, G., Spadi, M., Gliozzi, E., Cosentino, D., Cifelli, F., Cavinato, G.P., Tallini, M., Mattei, M., 2021. The tectono-stratigraphic evolution of the Fucino Basin (central Apennines, Italy): new insights from the

geological mapping of its north-eastern margin. J. Maps 17, 87–100. https://doi.org/10.1080/17445647.2021.1880981

Moreno-Amat, E., Rubiales, J.M., Morales-Molino, C., García-Amorena, I., 2017. Incorporating plant fossil data into species distribution models is not straightforward: Pitfalls and possible solutions. Quat. Sci. Rev. 170, 56–68. https://doi.org/10.1016/j.quascirev.2017.06.022

Naafs, B.D.A., Hefter, J., Stein, R., 2013a. Millennial-scale ice rafting events and Hudson Strait Heinrich(-like) Events during the late Pliocene and Pleistocene: a review. Quat. Sci. Rev. 80, 1–28. https://doi.org/10.1016/j.quascirev.2013.08.014

Naafs, B.D.A., Hefter, J., Stein, R., 2013b. Sea surface temperatures and Biomarker abundance in the 0-1 Ma section of IODP Hole Site 306-U1313. https://doi.org/10.1594/PANGAEA.818090

Naafs, B.D.A., Hefter, J., Stein, R., 2014. Dansgaard-Oeschger forcing of sea surface temperature variability in the midlatitude North Atlantic between 500 and 400 ka (MIS 12). Paleoceanography 29, 1024–1030. https://doi.org/10.1002/2014PA002697

Napier, T.J., Hendy, I.L., Hinnov, L.A., Brown, E.T., Shevenell, A., 2018. Subtropical hydroclimate during Termination V (~430-422 ka): Annual records of extreme precipitation, drought, and interannual variability from Santa Barbara Basin. Quat. Sci. Rev. 191, 73–88. https://doi.org/10.1016/j.quascirev.2018.05.003

Nehrbass-Ahles, C., Shin, J., Schmitt, J., Bereiter, B., Joos, F., Schilt, A., Schmidely, L., Silva, L., Teste, G., Grilli, R., Chappellaz, J., Hodell, D., Fischer, H., Stocker, T.F., 2020. Abrupt CO2 release to the atmosphere under glacial and early interglacial climate conditions. Science 369, 1000–1005. https://doi.org/10.1126/science.aay8178

Nielsen, H., Sørensen, I., 1992. Taxonomy and stratigraphy of late-glacial *Pediastrum* taxa from Lysmosen, Denmark — a preliminary study. Rev. Palaeobot. Palynol. 74, 55–75. https://doi.org/10.1016/0034-6667(92)90138-7

Okuda, M., Yasuda, Y., Setoguchi, T., 2001. Middle to Late Pleistocene vegetation history and climatic changes at Lake Kopais, Southeast Greece. Boreas 30, 73–82. https://doi.org/10.1111/j.1502-3885.2001.tb00990.x

Oliveira, D., Desprat, S., Rodrigues, T., Naughton, F., Hodell, D., Trigo, R., Rufino, M., Lopes, C., Abrantes, F., Goni, M.F.S., 2016. The complexity of millennial-scale variability in southwestern Europe during MIS 11. Quat. Res. 86, 373–387. https://doi.org/10.1016/j.yqres.2016.09.002

Overpeck, J.T., Iii, T.W., Prentice, I.C., 1985. Quantitative Interpretation of Fossil Pollen Spectra: Dissimilarity Coefficients and the Method of Modern Analogs. Quat. Res. 23, 87–108. https://doi.org/10.1016/0033-5894(85)90074-2

Paillard, D., 2001. Glacial cycles: Toward a new paradigm. Rev. Geophys. 39, 325–346. https://doi.org/10.1029/2000RG000091

Patacca, E., Scandone, P., 2007. Geology of the Southern Apennines. Boll.- Soc. Geol. Ital. 7, 75–112.

Pereira, A., Monaco, L., Marra, F., Nomade, S., Gaeta, M., Leicher, N., Palladino, D.M., Sottili, G., Guillou, H., Scao, V., Giaccio, B., 2020. Tephrochronology of the central Mediterranean MIS 11c interglacial (~425–395 ka): New constraints from the Vico volcano and Tiber delta, central Italy. Quat. Sci. Rev. 243, 106470. https://doi.org/10.1016/j.quascirev.2020.106470

Peyron, O., Magny, M., Goring, S., Joannin, S., de Beaulieu, J.-L., Brugiapaglia, E., Sadori, L., Garfi, G., Kouli, K., Ioakim, C., Combourieu-Nebout, N., 2013. Contrasting patterns of climatic changes during the Holocene across the Italian Peninsula reconstructed from pollen data. Clim. Past 9, 1233–1252. https://doi.org/10.5194/cp-9-1233-2013

Pidek, I.A., Svitavská-Svobodová, H., Van der Knaap, W.O., Magyari, E., 2013. Pollen percentage thresholds of *Abies alba* based on 13-year annual records of pollen deposition in modified Tauber traps: perspectives of application to fossil situations. Rev. Palaeobot. Palynol. 195, 26–36. https://doi.org/10.1016/j.revpalbo.2013.03.006

Prokopenko, A.A., Bezrukova, E.V., Khursevich, G.K., Solotchina, E.P., Kuzmin, M.I., Tarasov, P.E., 2010. Climate in continental interior Asia during the longest interglacial of the past 500 000 years: the new MIS 11 records from Lake Baikal, SE Siberia. Clim. Past 6, 31–48. https://doi.org/10.5194/cp-6-31-2010

Pross, J., Christanis, K., Fischer, T., Fletcher, W.J., Hardiman, M., Kalaitzidis, S., Knipping, M., Kotthoff, U., Milner, A.M., Muller, U.C., Schmiedl, G., Siavalas, G., Tzedakis, P.C., Wulf, S., 2015. The 1.35-Ma-long terrestrial climate archive of Tenaghi Philippon, northeastern Greece: evolution, exploration, and perspectives for future research. Newsl. Stratigr. 48, 253–276. https://doi.org/10.1127/nos/2015/0063

R Core Team, 2017. R: A Language and Environment for Statistical Computing.

R Core Team, 2021. R: A language and environment for statistical computing. R Foundation for Statistical Computing, Vienna, Austria. https://www.R-project.org. Computing.

Railsback, L.B., Gibbard, P.L., Head, M.J., Voarintsoa, N.R.G., Toucanne, S., 2015. An optimized scheme of lettered marine isotope substages for the last 1.0 million years, and the climatostratigraphic nature of isotope stages and substages. Quat. Sci. Rev. 111, 94–106. https://doi.org/10.1016/j.quascirev.2015.01.012

Raymo, M.E., 1997. The timing of major climate terminations. Paleoceanography 12, 577–585. https://doi.org/10.1029/97PA01169

Regattieri, E., Giaccio, B., Galli, P., Nomade, S., Peronace, E., Messina, P., Sposato, A., Boschi, C., Gemelli, M., 2016. A multi-proxy record of MIS 11–12 deglaciation and glacial MIS 12 instability from the Sulmona basin (central Italy). Quat. Sci. Rev. 132, 129–145. https://doi.org/10.1016/j.quascirev.2015.11.015

Roberts, N., Brayshaw, D., Kuzucuoğlu, C., Perez, R., Sadori, L., 2011. The mid-Holocene climatic transition in the Mediterranean: Causes and consequences. The Holocene 21, 3–13. https://doi.org/10.1177/0959683610388058

Rodrigues, T., Voelker, A.H.L., Grimalt, J.O., Abrantes, F., Naughton, F., 2011. Iberian Margin sea surface temperature during MIS 15 to 9 (580–300 ka): Glacial suborbital variability versus interglacial stability. Paleoceanography 26. https://doi.org/10.1029/2010PA001927

Rodrigues, T., Alonso-García, M., Hodell, D.A., Rufino, M., Naughton, F., Grimalt, J.O., Voelker, A.H.L., Abrantes, F., 2017. A 1-Ma record of sea surface temperature and extreme cooling events in the North Atlantic: A perspective from the Iberian Margin. Quat. Sci. Rev. 172, 118–130. https://doi.org/10.1016/j.quascirev.2017.07.004

Rohling, E.J., Braun, K., Grant, K., Kucera, M., Roberts, A.P., Siddall, M., Trommer, G., 2010. Comparison between Holocene and Marine Isotope Stage-11 sea-level histories. Earth Planet. Sci. Lett. 291, 97–105. https://doi.org/10.1016/j.epsl.2009.12.054

Ruddiman, W.F., 2003. The Anthropogenic Greenhouse Era Began Thousands of Years Ago. Clim. Change 61, 261–293. https://doi.org/10.1023/B:CLIM.0000004577.17928.fa

Ruddiman, W.F., Fuller, D.Q., Kutzbach, J.E., Tzedakis, P.C., Kaplan, J.O., Ellis, E.C., Vavrus, S.J., Roberts, C.N., Fyfe, R., He, F., Lemmen, C., Woodbridge, J., 2016. Late Holocene climate: Natural or anthropogenic? Rev. Geophys. 54, 93–118. https://doi.org/10.1002/2015RG000503

Sassoon, D., Lebreton, V., Combourieu-Nebout, N., Peyron, O., Moncel, M.-H., 2023. Palaeoenvironmental changes in the southwestern Mediterranean (ODP site 976, Alboran sea) during the MIS 12/11 transition and the MIS 11 interglacial and implications for hominin populations. Quat. Sci. Rev. 304, 108010. https://doi.org/10.1016/j.quascirev.2023.108010

Schmidl, A., Kofler, W., Oeggl-Wahlmüller, N., Oeggl, K., 2005. Land Use in the Eastern Alps During the Bronze Age—an Archaeobotanical Case Study of a Hilltop Settlement in the Montafon (western Austria)*. Archaeometry 47, 455–470. https://doi.org/10.1111/j.1475-4754.2005.00213.x

Seppä, H., Birks, H.J.B., Odland, A., Poska, A., Veski, S., 2004. A modern pollen–climate calibration set from northern Europe: developing and testing a tool for palaeoclimatological reconstructions. J. Biogeogr. 31, 251–267. https://doi.org/10.1111/j.1365-2699.2004.00923.x

Seppä, H., Bjune, A.E., Telford, R.J., Birks, H.J.B., Veski, S., 2009. Last nine-thousand years of temperature variability in Northern Europe. Clim. Past 5, 523–535. https://doi.org/10.5194/cp-5-523-2009

Silvestri, L., Saraceni, M., Bongioannini Cerlini, P., 2022. Links between precipitation, circulation weather types and orography in central Italy. Int. J. Climatol. 42, 5807–5825. https://doi.org/10.1002/joc.7563

Simpson, G.L., 2012. Analogue Methods in Palaeolimnology, in: Birks, H.J.B., Lotter, A.F., Juggins, S., Smol, J.P. (Eds.), Tracking Environmental Change Using Lake Sediments: Data Handling and Numerical Techniques. Springer Netherlands, Dordrecht, pp. 495–522. https://doi.org/10.1007/978-94-007-2745-8_15

Simpson, G., Oksanen, J., 2024. Analogue and weighted averaging methods for palaeoecology. R package version 0.17-7, https://cran.r-project.org/package=analogue.

Singh, H., Singh, A.D., Tripathi, R., Singh, P., Verma, K., Voelker, A.H.L., Hodell, D.A., 2023. Centennial-millennial scale ocean-climate variability in the northeastern Atlantic across the last three terminations. Glob. Planet. Change 223, 104100. https://doi.org/10.1016/j.gloplacha.2023.104100

Sinopoli, G., Peyron, O., Masi, A., Holtvoeth, J., Francke, A., Wagner, B., Sadori, L., 2019. Pollen-based temperature and precipitation changes in the Ohrid Basin (western Balkans) between 160 and 70 ka. Clim. Past 15, 53–71. https://doi.org/10.5194/cp-15-53-2019

Spratt, R.M., Lisiecki, L.E., 2015. A Late Pleistocene sea level stack. Discuss. Pap.

Spratt, R.M., Lisiecki, L.E., 2016. A Late Pleistocene sea level stack. Clim. Past 12, 1079–1092. https://doi.org/10.5194/cp-12-1079-2016

Stansell, N.D., Abbott, M.B., Rull, V., Rodbell, D.T., Bezada, M., Montoya, E., 2010. Abrupt Younger Dryas cooling in the northern tropics recorded in lake sediments from the Venezuelan Andes. Earth Planet. Sci. Lett. 293, 154–163. https://doi.org/10.1016/j.epsl.2010.02.040

Svenning, J.-C., 2003. Deterministic Plio-Pleistocene extinctions in the European cool-temperate tree flora. Ecol. Lett. 6, 646–653. https://doi.org/10.1046/j.1461-0248.2003.00477.x

Ter Braak, C., Juggins, S., 1993. Weighted Averaging Partial Least Squares regression (WA-PLS): definition and comparison with other methods for species-environment calibration, in: Multivariate Environmental Statistics. pp. 525–560.

Tomassetti, B., Giorgi, F., Verdecchia, M., Visconti, G., 2003. Regional model simulation of the hydrometeorological effects of the Fucino Lake on the surrounding region. Ann. Geophys. 21, 2219–2232. https://doi.org/10.5194/angeo-21-2219-2003

Tzedakis, P.C., 1993. Long-term tree populations in northwest Greece through multiple Quaternary climatic cycles. Nature 364, 437–440. https://doi.org/10.1038/364437a0

Tzedakis, P.C., Bennett, K.D., 1995. Interglacial vegetation succession: A view from southern Europe. Quat. Sci. Rev. 14, 967–982. https://doi.org/10.1016/0277-3791(95)00042-9

Tzedakis, P.C., Andrieu, V., de Beaulieu, J.-L., Crowhurst, S., Follieri, M., Hooghiemstra, H., Magri, D., Reille, M., Sadori, L., Shackleton, N.J., Wijmstra, T.A., 1997. Comparison of terrestrial and marine records of changing climate of the last 500,000 years. Earth Planet. Sci. Lett. 150, 171–176. https://doi.org/10.1016/S0012-821X(97)00078-2

Tzedakis, P.C., Andrieu, V., de Beaulieu, J.-L., Birks, H.J.B., Crowhurst, S., Follieri, M., Hooghiemstra, H., Magri, D., Reille, M., Sadori, L., Shackleton, N.J., Wijmstra, T.A., 2001. Establishing a terrestrial chronological framework as a basis for biostratigraphical comparisons. Quat. Sci. Rev., European Quaternary Biostratigraphy 20, 1583–1592. https://doi.org/10.1016/S0277-3791(01)00025-7

Tzedakis, P.C., 2007. Seven ambiguities in the Mediterranean palaeoenvironmental narrative. Quat. Sci. Rev. 26, 2042–2066. https://doi.org/10.1016/j.quascirev.2007.03.014

Tzedakis, P.C., Raynaud, D., McManus, J.F., Berger, A., Brovkin, V., Kiefer, T., 2009. Interglacial diversity. Nat. Geosci. 2, 751–755. https://doi.org/10.1038/ngeo660

Tzedakis, P.C., 2010. The MIS 11 / MIS 1 analogy, southern European vegetation, atmospheric methane and the "early anthropogenic hypothesis." Clim. Past 6, 131–144. https://doi.org/10.5194/cp-6-131-2010

Tzedakis, P.C., Crucifix, M., Mitsui, T., Wolff, E.W., 2017. A simple rule to determine which insolation cycles lead to interglacials. Nature 542, 427–432. https://doi.org/10.1038/nature21364

Tzedakis, P.C., Hodell, D.A., Nehrbass-Ahles, C., Mitsui, T., Wolff, E.W., 2022. Marine Isotope Stage 11c: An unusual interglacial. Quat. Sci. Rev. 284, 107493. https://doi.org/10.1016/j.quascirev.2022.107493

Valsecchi, V., Sanchez Goñi, M.F., Londeix, L., 2012. Vegetation dynamics in the Northeastern Mediterranean region during the past 23 000 yr: insights from a new pollen record from the Sea of Marmara. Clim. Past 8, 1941–1956. https://doi.org/10.5194/cp-8-1941-2012

Vavrus, S.J., He, F., Kutzbach, J.E., Ruddiman, W.F., Tzedakis, P.C., 2018. Glacial Inception in Marine Isotope Stage 19: An Orbital Analog for a Natural Holocene Climate. Sci. Rep. 8, 10213. https://doi.org/10.1038/s41598-018-28419-5

Vázquez Riveiros, N., Waelbroeck, C., Skinner, L., Duplessy, J.-C., McManus, J.F., Kandiano, E.S., Bauch, H.A., 2013. The "MIS 11 paradox" and ocean circulation: Role of millennial scale events. Earth Planet. Sci. Lett. 371–372, 258–268. https://doi.org/10.1016/j.epsl.2013.03.036

Vera-Polo, P., Sadori, L., Jiménez-Moreno, G., Masi, A., Giaccio, B., Zanchetta, G., Tzedakis, P.C., Wagner, B., 2024. Climate, vegetation, and environmental change during the MIS 12-MIS 11 glacial-interglacial transition inferred from a high-resolution pollen record from the Fucino Basin of central Italy. Palaeogeogr. Palaeoclimatol. Palaeoecol. 655, 112486. https://doi.org/10.1016/j.palaeo.2024.112486

Voelker, A.H.L., Rodrigues, T., Billups, K., Oppo, D., McManus, J., Stein, R., Hefter, J., Grimalt, J.O., 2010. Variations in mid-latitude North Atlantic surface water properties during the mid-Brunhes (MIS 9–14) and their implications for the thermohaline circulation. Clim. Past 6, 531–552. https://doi.org/10.5194/cp-6-531-2010

Wagner, B., Vogel, H., Francke, A., Friedrich, T., Donders, T., Lacey, J.H., Leng, M.J., Regattieri, E., Sadori, L., Wilke, T., Zanchetta, G., Albrecht, C., Bertini, A., Combourieu-Nebout, N., Cvetkoska, A., Giaccio, B., Grazhdani, A., Hauffe, T., Holtvoeth, J., Joannin, S., Jovanovska, E., Just, J., Kouli, K., Kousis, I., Koutsodendris, A., Krastel, S., Lagos, M., Leicher, N., Levkov, Z., Lindhorst, K., Masi, A., Melles, M., Mercuri, A.M., Nomade, S., Nowaczyk, N., Panagiotopoulos, K., Peyron, O., Reed, J.M., Sagnotti, L., Sinopoli, G., Stelbrink, B., Sulpizio, R., Timmermann, A., Tofilovska, S., Torri, P., Wagner-Cremer, F., Wonik, T., Zhang, X., 2019. Mediterranean winter rainfall in phase with African monsoons during the past 1.36 million years. Nature 573, 256–260. https://doi.org/10.1038/s41586-019-1529-0

Wang, M., Zheng, H., Xie, X., Fan, D., Yang, S., Zhao, Q., Wang, K., 2011. A 600-year flood history in the Yangtze River drainage: Comparison between a subaqueous delta and historical records. Chin. Sci. Bull. 56, 188–195. https://doi.org/10.1007/s11434-010-4212-2

Wei, D., González-Sampériz, P., Gil-Romera, G., Harrison, S.P., Prentice, I.C., 2021. Seasonal temperature and moisture changes in interior semi-arid Spain from the last interglacial to the Late Holocene. Quat. Res. 101, 143–155. https://doi.org/10.1017/qua.2020.108

Wickham, H., 2016. Data Analysis, in: Wickham, H. (Ed.), Ggplot2: Elegant Graphics for Data Analysis. Springer International Publishing, Cham, pp. 189–201. https://doi.org/10.1007/978-3-319-24277-4_9

Wickham, H., Averick, M., Bryan, J., Chang, W., McGowan, L.D., François, R., Grolemund, G., Hayes, A., Henry, L., Hester, J., Kuhn, M., Pedersen, T.L., Miller, E., Bache, S.M., Müller, K., Ooms, J., Robinson, D., Seidel, D.P., Spinu, V., Takahashi, K., Vaughan, D., Wilke, C., Woo, K., Yutani, H., 2019. Welcome to the Tidyverse. J. Open Source Softw. 4, 1686. https://doi.org/10.21105/joss.01686

Wu, L., Wilson, D.J., Wang, R., Yin, X., Chen, Z., Xiao, W., Huang, M., 2020. Evaluating Zr/Rb Ratio From XRF Scanning as an Indicator of Grain-Size Variations of Glaciomarine Sediments in the Southern Ocean. Geochem. Geophys. Geosystems 21, e2020GC009350. https://doi.org/10.1029/2020GC009350

Xiang, L., Huang, X., Huang, C., Chen, X., Wang, H., Chen, J., Hu, Y., Sun, M., Xiao, Y., 2021. *Pediastrum* (Chlorophyceae) assemblages in surface lake sediments in China and western Mongolia and their environmental significance. Rev. Palaeobot. Palynol. 289, 104396. https://doi.org/10.1016/j.revpalbo.2021.104396

Xiang, X.-G., Cao, M., Zhou, Z.-K., 2007. Fossil history and modern distribution of the genus Abies (Pinaceae). Front. For. China 2, 355–365. https://doi.org/10.1007/s11461-007-0058-4

Xu, Q., Xiao, J., Li, Y., Tian, F., Nakagawa, T., 2010. Pollen-Based Quantitative Reconstruction of Holocene Climate Changes in the Daihai Lake Area, Inner Mongolia, China. https://doi.org/10.1175/2009JCLI3155.1

Zhao, Y., Liang, C., Cui, Q., Qin, F., Zheng, Z., Xiao, X., Ma, C., Felde, V.A., Liu, Y., Li, Q., Zhang, Z., Herzschuh, U., Xu, Q., Wei, H., Cai, M., Cao, X., Guo, Z., Birks, H.J.B., 2021. Temperature reconstructions for the last 1.74-Ma on the eastern Tibetan Plateau based on a novel pollen-based quantitative method. Glob. Planet. Change 199, 103433. https://doi.org/10.1016/j.gloplacha.2021.103433

Appendix: Supplementary figures

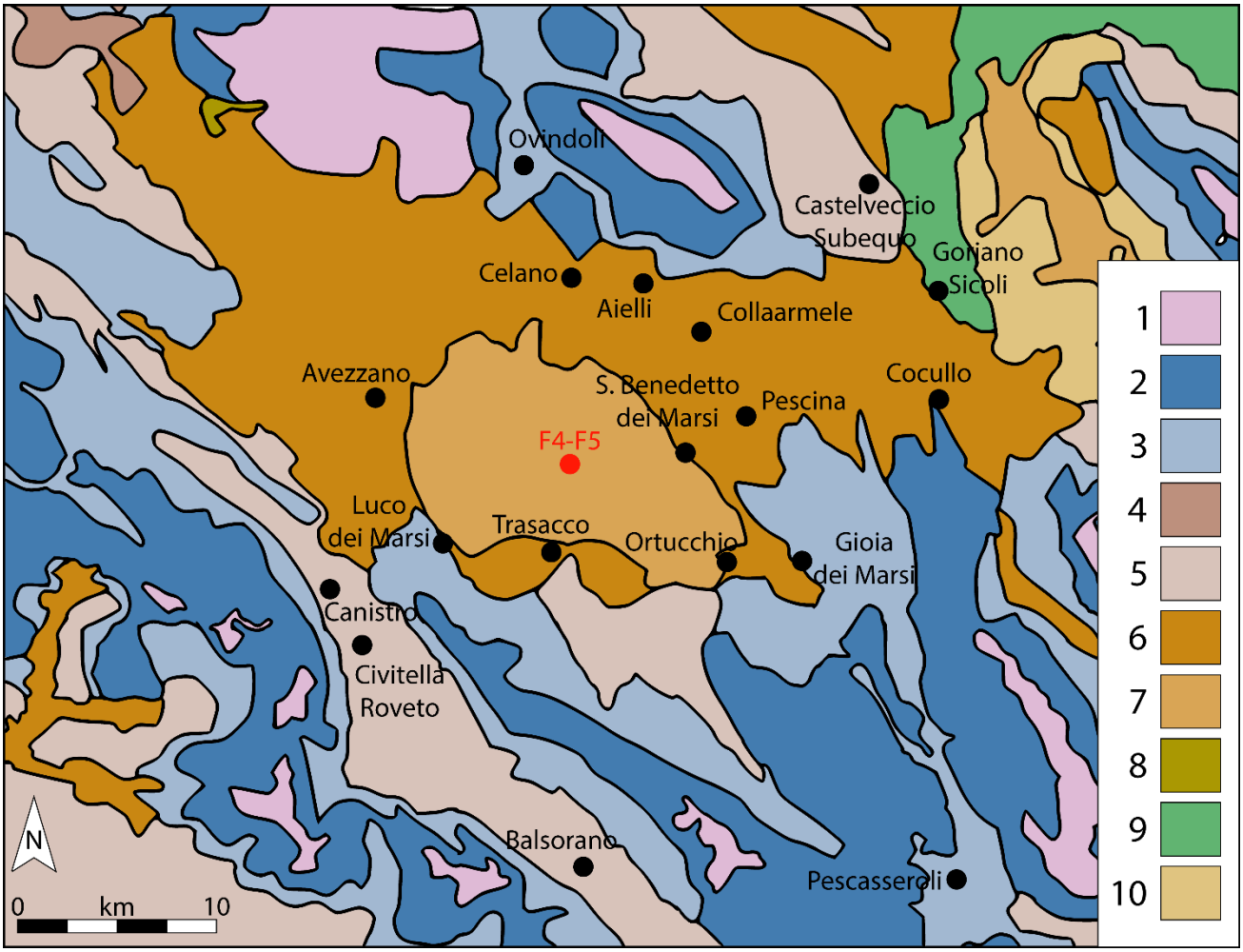

Fig. S1.1.- *Present potential natural vegetational distribution in Fucino Basin from Blasi et al. (2010 and 2017). Temperate cover: (1) Epipactiis atropurpurea-Pinus mugo and Daphne oleoides-Juniperus nana associations; Supratemperate cover sup.: (2) Cardamine kitabelii-Fagus sylvatica, Montropa hypopiys-Fagus sylvatica and Solidago virgaurea-Fagus sylvatica associations; Supratemperate cover inf.: (3) Lathyrus venetus- Fagus sylvatica, Allium pendulinum- Fagus sylvatica, Fraxinus ornus-Fagus sylvatica, Agrostis tenuis-Fagus sylvatica and Anemone apennina-Fagus sylvatica associations; Mesotemperate cover: (4) Carex sylvatica-Quercus cerris, Neottia ovata-Quercus cerris, Aremonia agrimonoides-Quercus cerris, Physospermum verticillatum-Quercus cerris, Thalictrum aquilegiifolium-Quercus cerris, (5) Laburnum anagyroides-Ostrya carpinofolia, Melittis melissophyllum-Ostrya carpinofolia, Sesleria autumnalis-Acer obtusatum, (6) Cytisus sessifolius-Quercus pubescens, (7) Pulmonaria apennina-Carpinus Betulus, Teucrium siculum-Quercus cerris, Salix eleagnos, Salix cinerea, Alnus Incana, (8) Scutellaria columnae-Ostrya carpinofolia, (9) Daphne laureola-Quercus cerris and Carpinus orientalis associations; Transitional mesotemperate cover: (10) Rosa sempervirens-Quercus pubescens and Celamatis flammula-Quercus pubescens. F4-F5 core location in red for geographical reference. Abies alba appears in relict form over 2000 m in those association related with Fagus sylvatica (2 and 3 zones).*

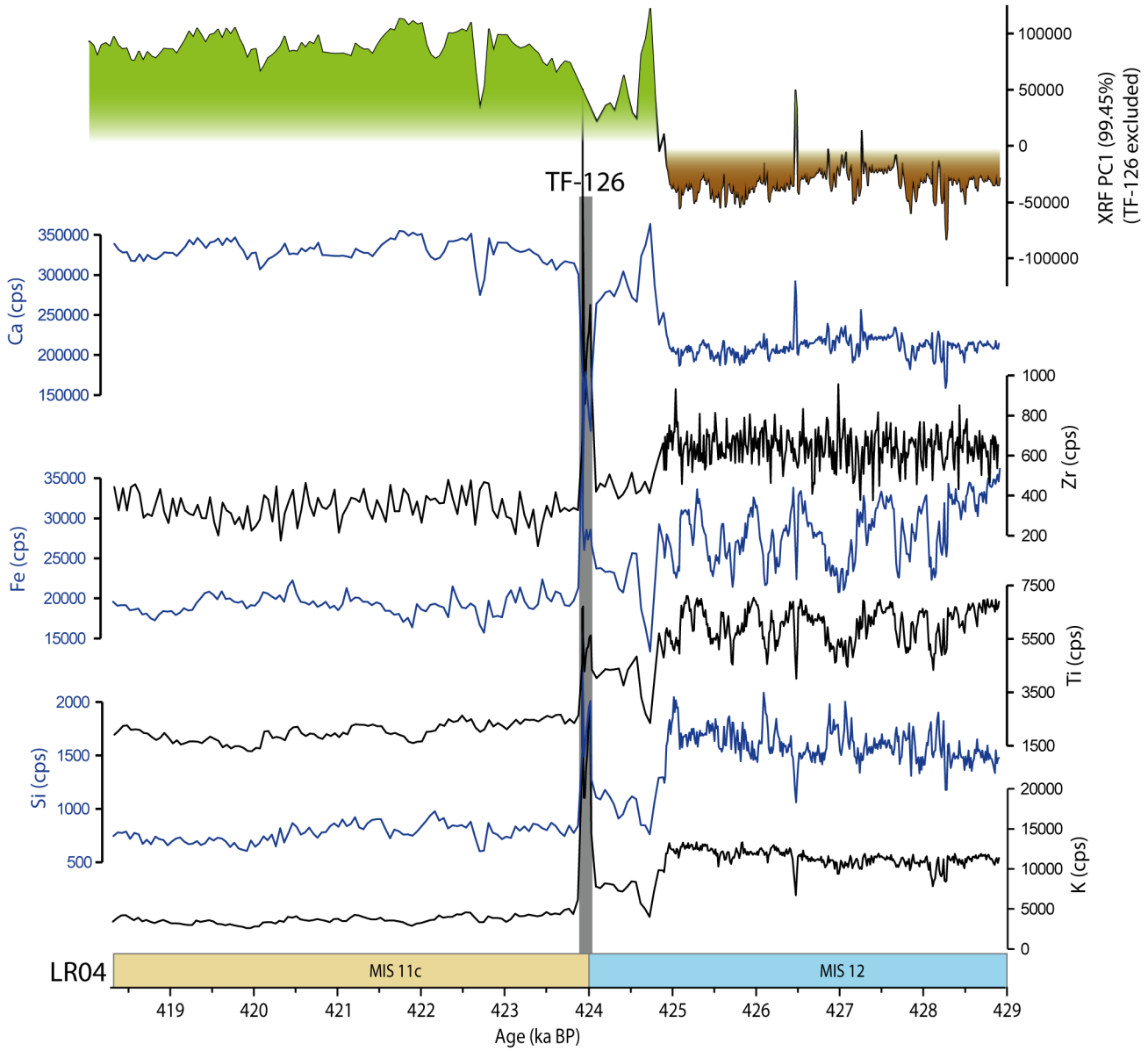

Fig. S1.2.- *XRF PC1 above (Ca: green; Siliciclastic elements: brown; TF-126 (grey box) excluded for the analysis). XRF elements (as counts per second) plotted against age. The boundary between MIS 12 and MIS 11 suggested by Lisiecki and Raymo (2005) (LR04) is shown by the blue and beige boxes at ~424 ka.*

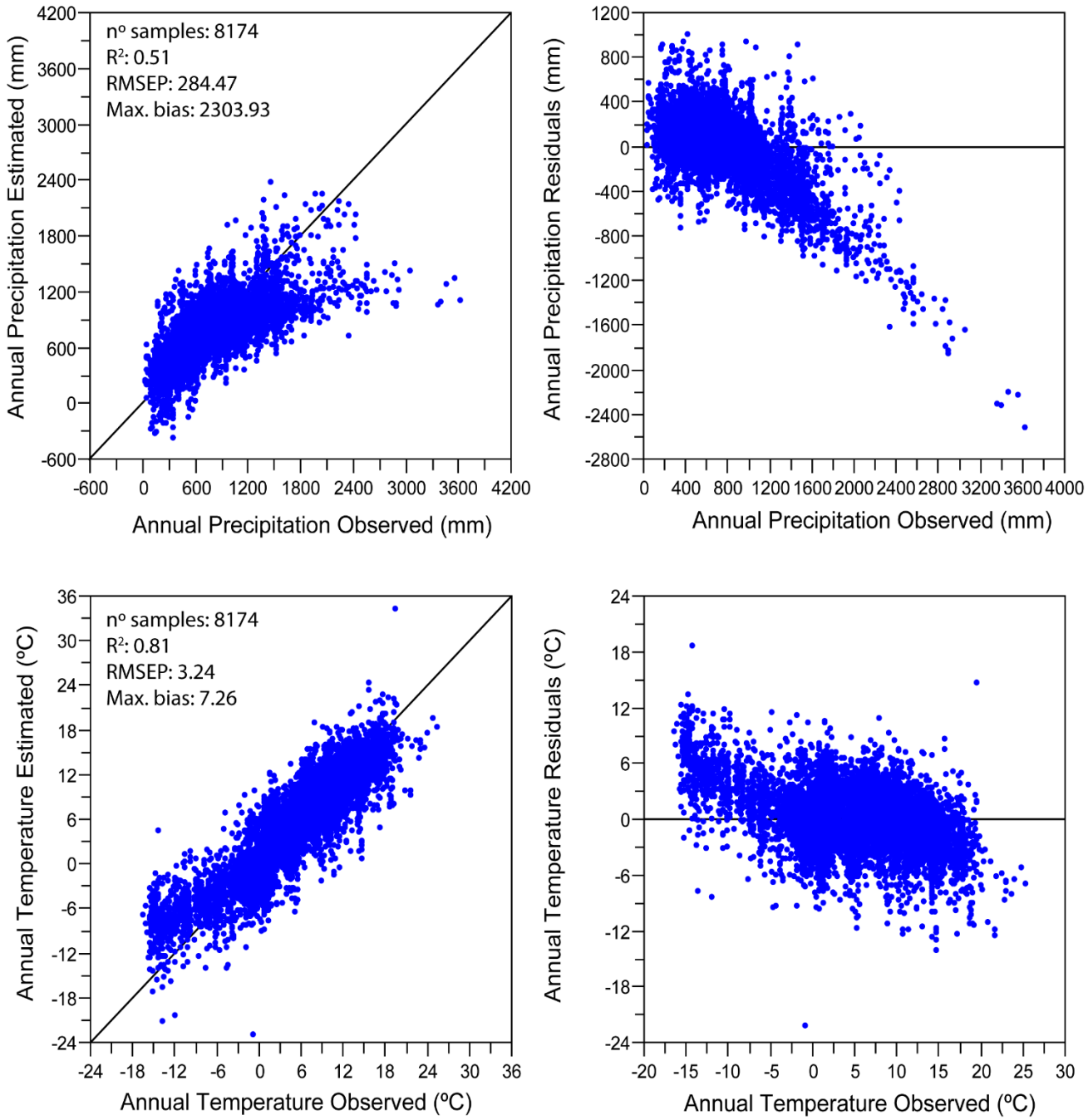

Fig. S1.3.- *Scatter plots of the EMPDv2 (Davis et al., 2020) showing the observed vs estimated of the mean annual precipitation (above) and the mean annual temperature (below) from WorldClim v2.1 database (Fick and Hijmans, 2017). The WA-PLS method is also shown, including the number of samples (nº samples), coefficient of determination (R^2), root-mean square error of prediction (RMSEP) and maximum bias (Max. bias).*

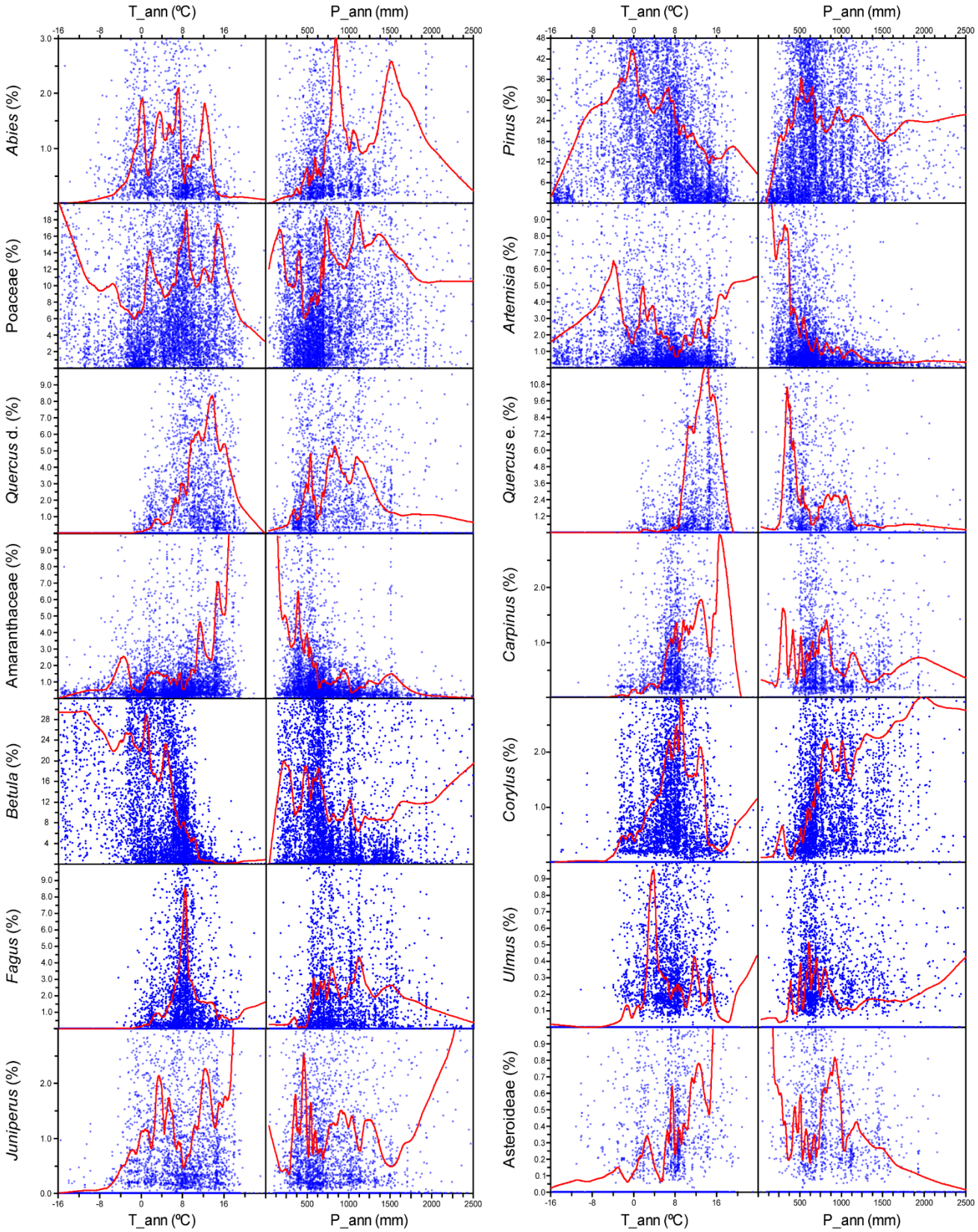

Fig. S1.4.- *Abundances (in percentages) of the main species identified in the Fucino pollen record from the EMPDv2 with respect to the present mean annual temperature (T_ann) and mean annual precipitation (P_ann) from WorldClim v2.1 database (Fick and Hijmans, 2017). Blue dots represent sites in the EMPDv2 (Davis et al., 2020). Red lines show the locally estimated scatterplot smoothing (LOESS) (span 0.08) of the percentages for each tree and herb taxon.*

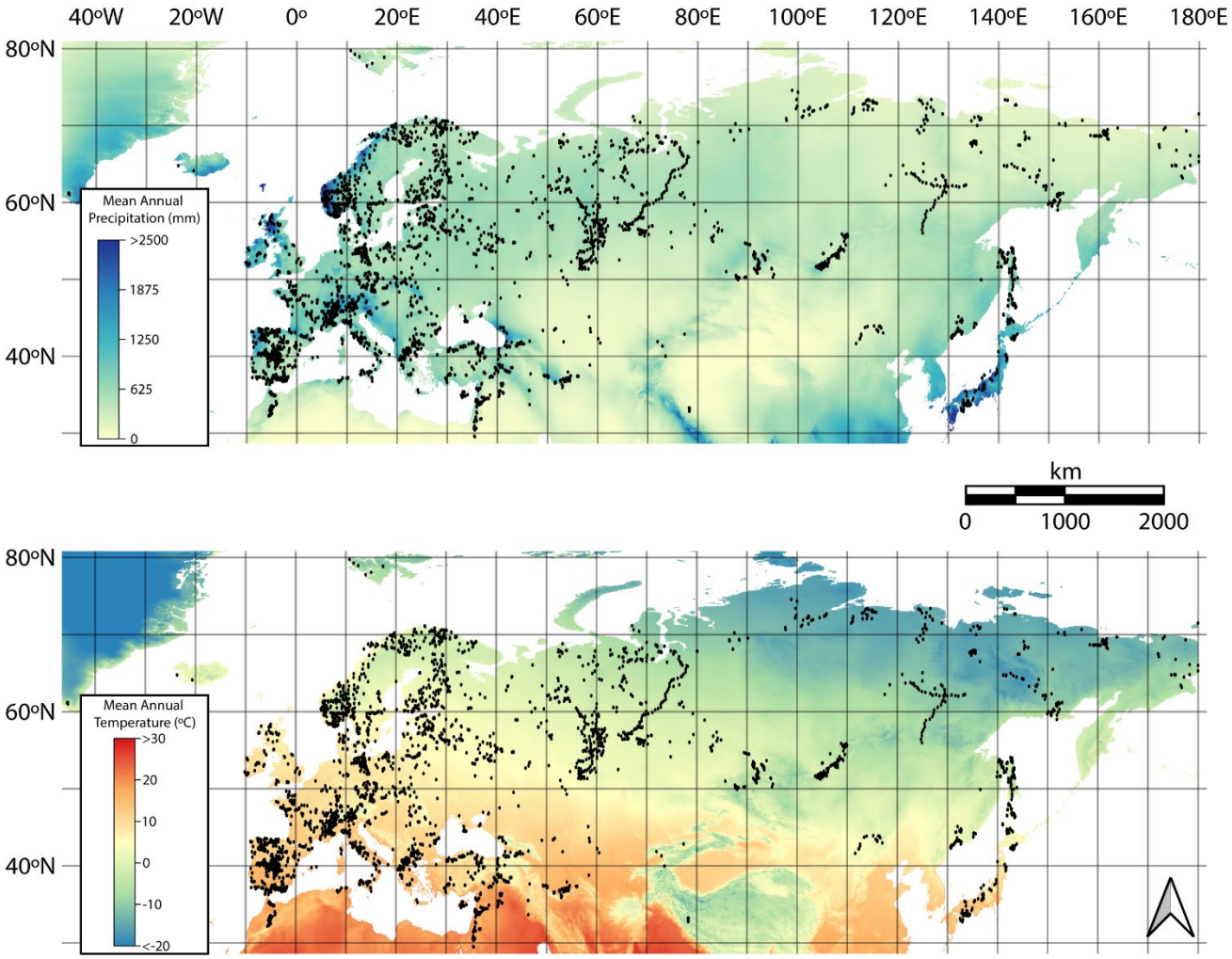

Fig. S1.5.- *Map showing the raster layer of the mean annual precipitation (above) and the mean annual temperature (below) from the WorldClim v2.1 (Fick and Hijmans, 2017) database. Each dot represents a data point from the EMPDv2 that was used for the paleoclimatic reconstruction (Davis et al., 2020).*

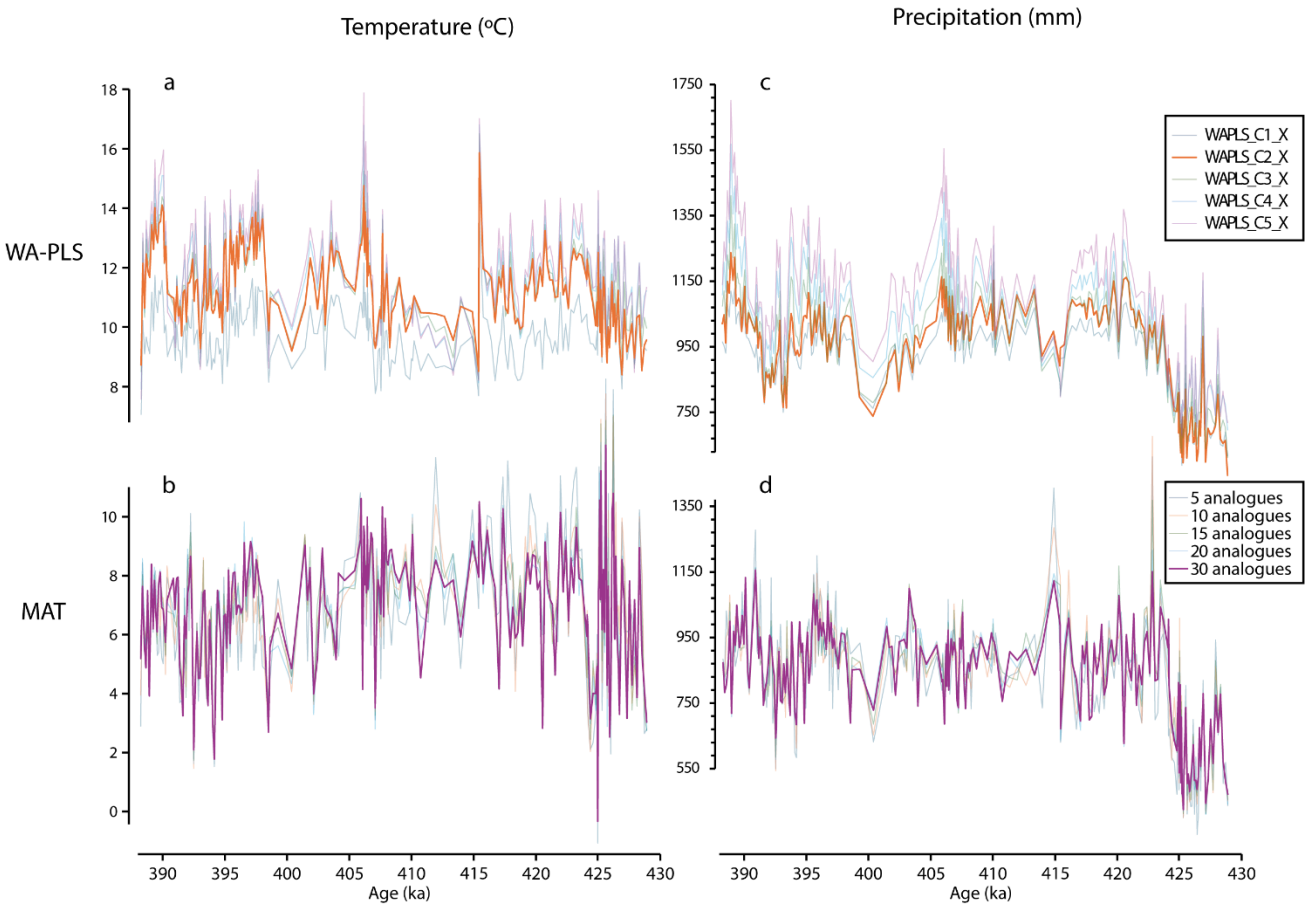

Fig. S3.1.- *Comparison between annual temperature (a and b) and precipitation (c and d) reconstructions for Fucino pollen record using WA-PLS and MAT. On a and c plots are shown the 5 possibly reconstructions estimated from WA-PLS, highlighting the second component for each one. On b and d are represented the MAT reconstructions choosing 5, 10, 20 and 30 closest analogues samples.*

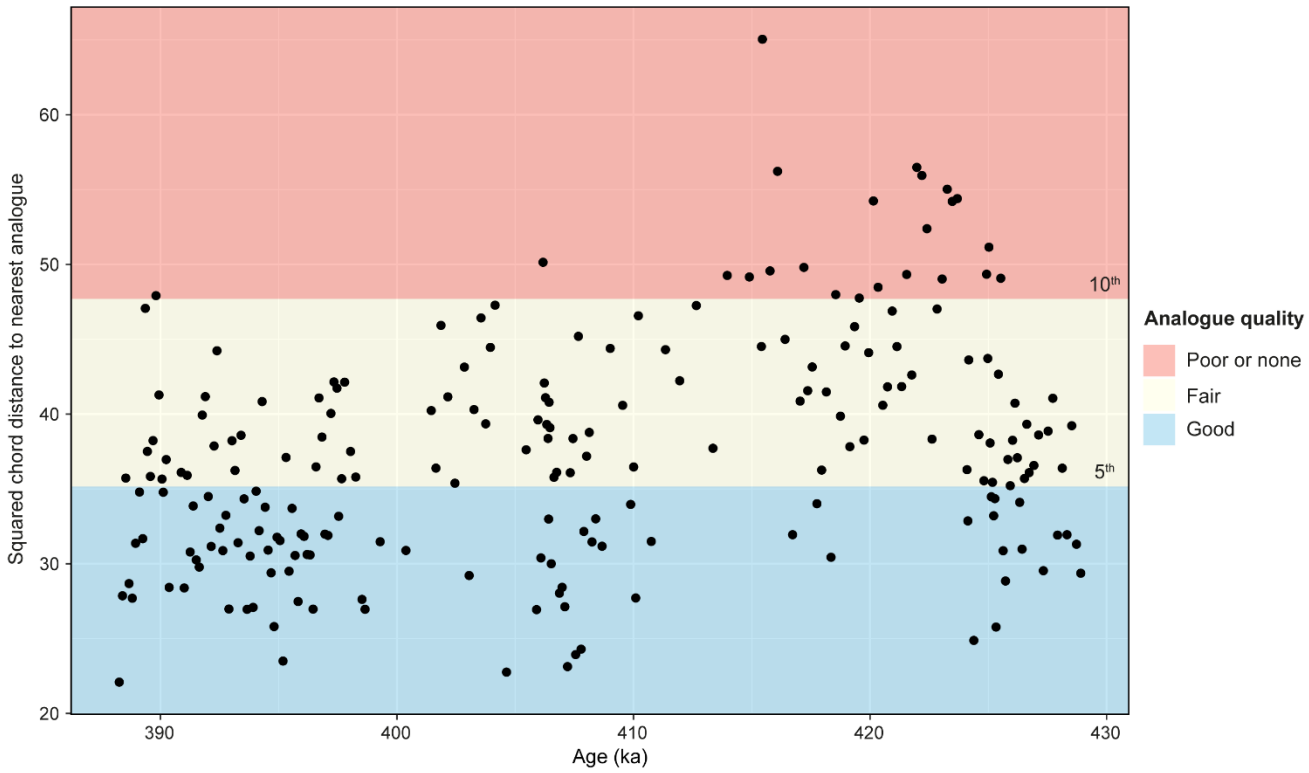

Fig. S3.2.- *The reliability test of the Fucino pollen record based on the analogue quality of the goodness-of-fit analysis, using the EMPDv2 from Davis et al. (2020). Blue, yellow and red shades indicate good-, fair- and poor-analogues, respectively.*

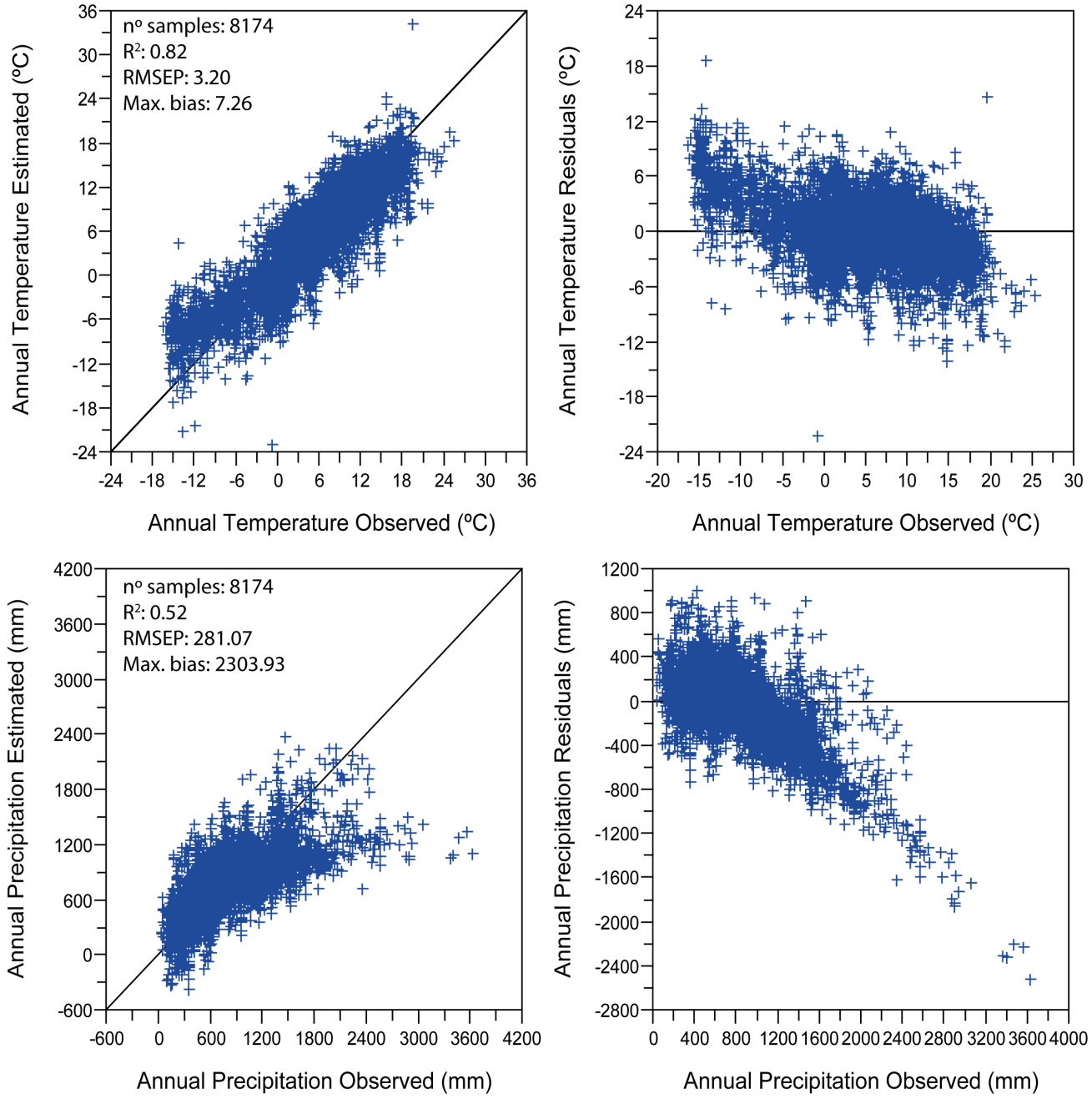

Fig. S3.3.- *Scatter plots of the EMPDv2 (Davis et al., 2020) showing the observed vs estimated of the mean annual precipitation (above) and the mean annual temperature (below) from WorldClim v2.1 database (Fick and Hijmans, 2017). The WA-PLS method is also shown, including the number of samples (n° samples), coefficient of determination (R2), root-mean square error of prediction (RMSEP) and maximum bias (Max. bias).*

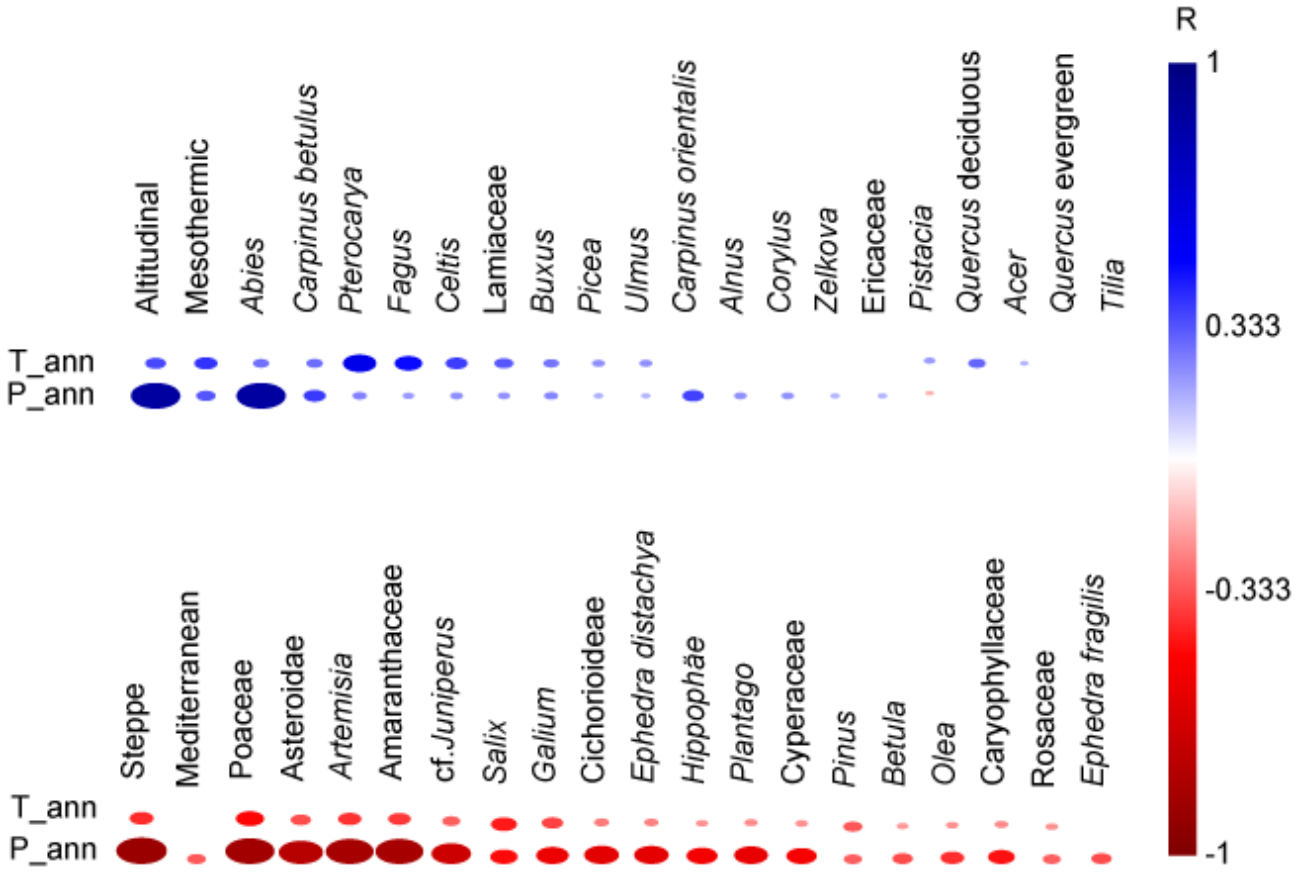

Fig. S3.4.- *Correlation plot between the reconstructed Tann and Pann and the pollen groups and pollen taxa. Blue indicates a positive correlation (warmer and humid). Red indicates a negative correlation (colder and drier). The size of the spheres represents how statistical significance (p) has the data.*